Synthetic deconvolution of an auxin-dependent transcriptional code

Raquel Martin-Arevalillo, Bruno Guillotin, Jonas Schön, Alice Hugues, Marie-France Gerentes, Jeremy Lucas, Emmanuel Thevenon, Graeme Vissers, Mohammed Mohammed Ateequr, Carlos Galvan-Ampudia, et al.

Synthetic deconvolution of an auxin-dependent transcriptional code

Raquel Martin-Arevalillo[1,2,7,8], Bruno Guillotin[4,5,8], Jonas Schön[2], Alice Hugues[1], Marie-France Gerentes[1], Kun Tang[2], Jérémy Lucas[6], Emmanuel Thévenon[6], Marianne Dreuillet[6], Graeme Vissers[4]; Mohammed Mohammed Ateequr[5]; Carlos S. Galvan-Ampudia[1], Guillaume Cerutti[1], Jonathan Legrand[1], Coralie Cance[6], Annick Dubois[1], François Parcy[6], Kenneth D. Birnbaum[4,5,9], Matias D. Zurbriggen[2,3,9], Renaud Dumas[6,9], François Roudier[1*] and Teva Vernoux[1,10*]

[1] Laboratoire Reproduction et Développement des Plantes, Univ Lyon, ENS de Lyon, CNRS, INRAE, INRIA, F-69342, Lyon, France

[2] Institute of Synthetic Biology, University of Düsseldorf, 40225 Düsseldorf, Germany

[3] CEPLAS – Cluster of Excellence on Plant Sciences, University of Düsseldorf, 40225 Düsseldorf, Germany

[4] Center for Genomics and Systems Biology, New York University, New York, NY, USA

[5] Center for Genomics and Systems Biology, New York University Abu Dhabi, Abu Dhabi, United Arab Emirate

[6] Laboratoire Physiologie Cellulaire et Végétale, Université Grenoble Alpes, CNRS, CEA, INRAE, IRIG-DBSCI-LPCV, 17 avenue des martyrs, F-38054, Grenoble, France

[7]Current address: Laboratoire de Recherche en Sciences Végétales, Université Toulouse, CNRS, INP, Castanet-Tolosan, France.

[8,9]These authors contributed equally

[10]Lead contact

[*]Correspondence: teva.vernoux@ens-lyon.fr, francois.roudier@ens-lyon.fr

SUMMARY

How developmental signals program gene expression in space and time is still poorly understood. Here, we addressed this question for the plant master regulator, auxin. Transcriptional responses to auxin rely on a large multigenic transcription factor family, the auxin response factors (ARFs). We deconvoluted the complexity of ARF-regulated transcription using auxin-inducible synthetic promoters built from *cis*-element pair configurations differentially bound by ARFs. We demonstrate using cellular systems that ARF transcriptional properties are not only intrinsic but also depend on the *cis*-element pair configurations they bind to, thus identifying a bi-layer ARF/*cis*-element transcriptional code. Auxin-inducible synthetic promoters were expressed differentially *in planta* showing at single cell resolution how this bi-layer code patterns transcriptional responses to auxin. Combining *cis*-element pair configurations in synthetic promoters created distinct patterns, demonstrating

the combinatorial power of the auxin bi-layer code in generating diverse gene expression patterns that are not simply a direct translation of auxin distribution.

KEYWORDS (10max)

TF, DNA binding, transcriptional code, expression pattern, specificity, ARF, auxin, synthetic deconvolution

INTRODUCTION

A key function of developmental signals is to establish a tight spatiotemporal regulation of gene expression during development. The plant hormone auxin is one such developmental signal. Auxin function throughout plant development depends on when, where and at which concentration it is acting[1], but how a simple signal like auxin triggers distinct spatio-temporally resolved transcriptomic responses remains cryptic.

The answer to this question might lie in the properties of the auxin signaling pathway regulating transcription, the Nuclear Auxin Pathway (NAP), consisting in the TRANSPORT INHIBITOR RESPONSE1/AUXIN-SIGNALING F-BOX (TIR1/AFB) co-receptor, the Auxin/Indole-3-Acetic Acid (Aux/IAA) repressor and the Auxin Response Factor (ARF) transcription factors (TFs) families. ARFs, bound to regulatory regions of auxin responsive genes, can be repressed through protein-protein interactions with Aux/IAAs. A TIR/AFB-Aux/IAA-auxin complex triggers Aux/IAAs ubiquitination and degradation, releasing ARFs repression and allowing gene regulation[1] (Figure 1A). During plant evolution, gene duplication events generated multigenic families of the NAP effectors with diversified biochemical properties[2–5]. This diversity led to hypothesize the existence of a spatio-temporally resolved “auxin code” where combinations of different NAP effectors resulting from their differential expression specifically program the expression of auxin target genes as a function of auxin concentration[6]. ARFs are expected to play a central role in this regulatory system by establishing an ARF-dependent transcriptional code, but this has not yet been thoroughly tested.

ARFs originated in charophyte green algae and diversified in land plants from only few members in bryophytes to large families in Angiosperms[5,7], with *e.g.* 23 ARFs in *Arabidopsis thaliana* and thus a high combinatorial potential. ARFs belong to three different clades, A, B and C (hereafter, A, B and C-ARFs)[8,9]. They share a modular structure consisting of a N-terminal DNA Binding Domain (DBD), a C-terminal Phox/Bem1 (PB1) protein-protein interaction domain (that also contributes to regulate DNA affinity[10]) and an intrinsically disordered region (IDR) in between, named the Middle Region (MR)[11] (Figure 1A). Due to their MR, A-ARFs work primarily as transcriptional activators whereas B-ARFs are repressors[12]. The composition of the MR led to classify C-ARFs as repressors as well, although their contribution to auxin signaling is unclear[13,14] (Figure 1A). ARFs also have different mechanisms

of action linked to their PB1. The model of auxin transcriptional regulation described above applies A-ARFs, which PB1 allows interaction with most Aux/IAAs. By contrast, B- and C-ARF PB1s confer a limited capacity to interact with Aux/IAAs[15]. B-ARFs have been proposed to compete with A-ARFs for binding on regulatory sequences of auxin-regulated genes, a hypothesis supported by analyses of reduced complexity NAPs in bryophytes[14,16] (Figure 1A). However, recent analyses of ARF binding specificities *in vitro* suggest a much more complex ARF-dependent transcriptional code, relying on ARFs acting in trans but also on *cis*-regulations. ARFs bind as dimers to pairs of consensus (T/G)GTCnn *cis*-elements called Auxin Responsive Elements (AuxREs)[17-20]. Different AuxRE pair configurations can be recognized: Inverted, Everted or Direct Repeats (IRn, ERn, DRn), where "n" represents the number of nucleotides between the two AuxREs (Figure 1B). DNA Affinity Purification Sequencing (DAP-seq) experiments in Arabidopsis and Maize showed that A- and B-ARFs have distinct preferences for different AuxRE pair configurations *in vitro*, with only certain configurations being bound by both clades[19,21,22] (see below). Competition between A- and B-ARFs might thus occur only on a subset of auxin-regulated genes. How this contributes to explain specificity in transcriptional regulation remains unknown.

Here, we used a synthetic-biology driven approach to decipher the ARF-dependent transcriptional code and its contribution to specificity in gene expression. To deconvolute the transcriptional code in Arabidopsis, we simplified the A-, B- and C-ARF target gene landscape to four synthetic promoters built from AuxRE pair configurations identified as ARF preferential binding sites. Combining biochemistry, synthetic biology approaches, single-cell RNA sequencing (scRNA-seq) and *in planta* studies, we show in biological systems of increasing complexity that these four *cis*-element configurations are differentially bound by ARFs and by combinations of ARFs from different clades. We also demonstrate that ARF transcriptional properties are not simply intrinsic to the protein but are also modified by AuxRE pairs they bind to, establishing a bi-layer ARF/AuxRE code. The four AuxRE-based synthetic promoters led to very different expression in Arabidopsis roots, showing at single cell resolution how this bi-layer code patterns transcriptional responses to auxin. We further demonstrate that specific AuxRE pair configurations contribute to establish expression patterns of endogenous auxin responsive genes. Finally, we show that endogenous promoters can use a more complex syntax with combinations of AuxRE pair configurations, that when reproduced in synthetic reporters, generate a range of distinct auxin-dependent expression patterns in Arabidopsis roots. Taken together, our work shows how an ARF-dependent transcriptional code based on an ARF/AuxRE bi-layer control system translates auxin information into different patterns of expression during plant development.

RESULTS

A-, B- and C-ARFs have different preferences for *cis*-element pair configurations *in vitro*

DAP-seq experiments have shown that, while A-ARFs can bind IR, ER and DR AuxRE pair configurations with varying spacings (IR7/8 and 17/18, ER2/3 and 12/13, DR4/5 and 14/15, with the highest enrichment for ER12/13 and the lowest for DR14/15), B-ARFs bind preferentially IR7/8[19,21,22]. For C-ARFs, re-analysis of DAP-seq data obtained with Arabidopsis C-ARF16[22] could not retrieve any target AuxRE motif (Figure S1A). We used DAP-seq with Arabidopsis C-ARF10. We obtained 1819 C-ARF10-bound regions robustly found in 3 replicates (Figure S1B). As for A- and B-ARFs[19,21,22], the DNA motif most represented in the best-covered peaks for C-ARF10 was the TGTCGG DNA sequence (Figure 1C; Figure S1C). Studying the overrepresentation of IRs/ERs/DRs in C-ARF10-bound regions, we identified a preferential binding to ER12/13 (the highest enrichment) and DR4, suggesting yet different preferences for AuxRE pair configurations of C-ARFs (Figure 1D). EMSA using a representative ARF for each clade (A-ARF5, B-ARF1 and C-ARF10) confirmed the binding preferences of the different ARF clades to oligonucleotides containing a single AuxRE pair (Figure 1E; Figure S1D). Binding preferences were maintained across a range of ARF concentrations, even at the highest ARF concentration tested, indicating that the results are not biased by a potential saturation of the binding of a subset of ARFs. EMSA further suggested a weaker binding of A-ARF5 to DR5 and an even weaker one to DR15 compared to IR8 and ER13 (Figure 1E; Figure S1D). It also showed that C-ARF10 weakly binds DR15 and IR8. In summary, *in vitro* binding assays predict four AuxRE pair configurations preferentially bound by ARFs from different clades: IR7/8 by A/B-ARFs, ER12/13 by A/C-ARFs, DR4/5 and more weakly DR14/15 by A-ARFs (Figure 1F). Our results extend to C-ARFs the evidence that ARFs have clade-specific preferences for AuxRE pair configurations. Thus, the ARF-dependent transcriptional code potentially relies on the three clades of ARFs competing for binding differently depending on the *cis*-element configurations present in target gene promoters

A-, B and C-ARFs have distinct preferences for synthetic promoters constructed from different *cis*-element pairs both *in vitro* and *in vivo*

Inspired by the *DR5* auxin transcriptional reporter constructed over 20 years ago from *DR5* repeats[12,18,23-25], we applied reductionist principles to reduce the complexity of the ARF binding landscape and to test ARF binding specificity *in vivo*. We designed four synthetic promoters with three repeats of an IR8, ER13, DR5 or DR15 AuxRE pair - *i.e.* configurations preferentially targeted by ARFs *in vitro* -, followed by a minimal core promoter (Figure 2A; Table S1). We used the TGTCGG AuxRE sequence shown to be bound by B-ARF1 and A-ARF5[26] with the highest affinity and to increase sensitivity to auxin in synthetic promoters[25]. The remaining nucleotides in each promoter were chosen to limit the occurrence of non-desired AuxREs and we used MEME to confirm the absence of high-affinity canonical binding sites for other TFs

(Table S1). We named the four synthetic promoters *hIR8*, *hER13*, *hDR5* and *hDR15*, where h stands for high-affinity (Figure 2A).

To characterize the promoters, we used again EMSA to test B-ARF1, A-ARF5 and C-ARF10 binding affinities but this time to oligonucleotides containing two or three AuxRE pairs repeats, as in synthetic promoters. ARF binding was now detected on all oligonucleotides, even at the lowest ARF concentration, but ARFs still showed clade-specific preferential binding to different AuxRE pair configurations (Figure 2B-D; Figure S1.D). Compared to oligonucleotides with a single AuxRE pair (Figures 1E-F), binding specificities were modified, mainly for A-ARF5: IR8 was still bound preferentially by B-ARF1, ER13 by C-ARF10 but also to a lesser extent by A-ARF5 and B-ARF1, DR5 by A-ARF5 and DR15 more weakly by all ARFs (Figures 2B-D). Here again, ARF binding specificity could be seen across a range of ARF concentrations and even at the highest ARF concentration tested, where binding was close to saturation (Figures 2B-C; Figure S1.D). These results confirm that ARFs have clade-specific binding preferences for AuxRE pairs. They further indicate that ARF binding specificity can be modified by the number of adjacent AuxRE pairs in a sequence, suggesting a cooperative effect, possibly through ARF dimer interactions *e.g.* through the PB1 domain[10].

We then used a synthetic biology strategy to test ARF binding preferences with a higher number of ARFs, in a cellular context. Previous work showed that ARFs binding not only requires the DBD, but also the PB1 domain that contributes to affinity [10]. Sequences required for transcriptional activity are located in the MR [12,27,28]. To uncouple binding from transcriptional regulation capacity and ensure identical robust transcriptional activation capacities to ARFs from different clades, we constructed chimeric ARFs with their MR substituted by A-ARF5 MR and a VP16 activation domain added to the C-terminus (Figure 2E). We chose representatives from each clade: B-ARF1/2/3, A-ARF5-8/19 and C-ARF10/16. The capacity of chimeric ARFs to regulate the *hIR8*, *hER13*, *hDR5* or *hDR15* promoter driving a secreted alkaline phosphatase (SEAP) reporter gene was tested in an orthogonal cell system, Chinese Hamster Ovary K1 (CHO-K1) cells (Figure 2E). This strategy limits biases coming from ARF activator/repressor functions and interference from other plant components. Differences in the activity of the reporter gene are then expected to be a proxy for differences in ARF binding capacity to the promoters due to their different DBDs and PB1s.

Consistently with the EMSA results (Figures 2B-D), all chimeric ARFs bound and transactivated all reporters, yet with significant differences supporting differential binding to the promoters (Figure 2F). However, the assay might underestimate the chimeric A-ARF19 binding activity due to a lower protein production in CHO-K1 cells (Figure S1E). Also, the very low activity systematically observed with chimeric C-ARF16 could be due to degradation of the protein (Figure S1E). Even with these limitations, our results show that, on average, chimeric A-ARFs induced the strongest activity on all reporters compared to B- and C-ARFs, although

the induction was more similar across clades for *hIR8* (Figure 2F). Importantly, chimeric A-ARFs induced reporters with some quantitative differences, notably a higher induction of *hER13*. Differences in reporter activation capacity were observed between chimeric A-ARFs (notably a lower activation for A-ARF8), that were mostly consistent for all promoters. Our results suggest that A-ARFs have strong binding capacities for all promoters. By contrast, chimeric B- and C-ARF reporter induction was strong with *hIR8* and *hER13*, and only slightly above the control for *hDR5* and *hDR15*, suggesting a higher binding capacity to *hIR8* and *hER13* (Figure 2F). Using a selection of chimeric ARFs and reporter plasmids, we demonstrated that increasing the relative quantity of chimeric ARF plasmids had no significant impact on the binding trends observed (Figure S1F). Specificities in ARF binding between clades in our assay are thus unlikely biased by saturation of the binding of some of the chimeric ARFs.

Our results indicate consistent specificities of ARF binding between clades *in vitro* and in the CHO-K1 heterologous cellular context on sequences containing two or three AuxRE pairs: A-ARFs bind all 4 configurations; B-ARFs and C-ARFs bind preferentially IR8 and ER13 (Figures 2D,G). The limited differences between the results obtained *in vitro* and in CHO-K1 cells could be due to small changes of binding properties *in vivo*. Also, IDR can contribute to regulate TF binding[29]. The differences between the two assays could thus also be due to a contribution of the MR with the full-length ARFs used in EMSA. In addition, our results suggest that variations in binding affinity exist within clades due to differences in biochemical properties of at least the DBDs and PB1 domains. Altogether, our finding supports a scenario where the ARF-dependent transcriptional code relies on ARFs with a range of binding affinities and on the fact that A-ARFs bind all AuxRE pair configurations tested, while B- and C-ARFs compete for this binding preferentially on IR8 and ER13. We further show that cooperative ARF binding on adjacent AuxRE pair modifies ARF binding preferences. The capacity of an ARF to bind a promoter is thus also dependent on the number of AuxRE pairs present, which also contributes to the ARF-dependent transcriptional code.

ARFs differentially regulate synthetic promoters constructed from different *cis*-element pairs in plant cells

To further study whether and how A-, B- and C-ARFs preferences for AuxRE pair configurations contribute to auxin-dependent transcriptional regulation in plants, we moved to protoplasts, isolated plant cells which enable quantitatively assaying multiple ARF/AuxRE combinations simultaneously. Here, we used full-length ARFs, with their intrinsic activator or repressor function, and expressed them constitutively in a plant cell environment where auxin signaling components are already present and regulation of synthetic reporter activity by auxin can be studied. In contrast to CHO-K1 cells, when we investigated ARF production in

protoplasts after transfection using ARF-firefly luciferase (FF) translational fusions, we found important differences between ARFs (Figure S2A). Thus, regulatory activities cannot be compared between different ARFs, not only because ARF regulatory activities are influenced by ARF regulatory potential and binding capacity, but also because the proteins accumulate differentially in protoplasts. Thus, activity comparisons in protoplasts can only be done with confidence for a given ARF between synthetic reporters.

ARF-encoding plasmids were co-transfected in protoplasts (Figure 3A), in absence or presence of auxin, with a synthetic reporter plasmid, harboring one of the synthetic promoters driving FF expression and a constitutively expressed Renilla luciferase (REN) used as internal normalization element. All synthetic reporters were induced by auxin either alone or when co-transfected with ARFs (Figure 3B; Figure S2B). *hER8* and *hIR13* promoter variants of in which every other AuxREs was mutated were expressed at a very low basal expression and either not or poorly induced upon co-transfection with A-ARF19, even in the presence of auxin (Figure S2C). In addition, dexamethasone-inducible ARFs triggered rapid reporter activation upon induction, coherently with the expected direct transcriptional regulation by ARFs (Figure S2D). Thus, all synthetic reporters are *bona fide* auxin-inducible reporters in plant cells and *AuxRE* pair elements in the promoters control a specific and most likely direct regulation by ARFs.

As expected, on average, A- and B-ARFs induced and repressed the reporters, respectively, but with quantitative differences between reporters for a given ARF and with an increase activation capacity for most A-ARFs after auxin treatment (Figure 3B; Figure S2B). For C-ARFs, we observed an *hER13* induction that increased after auxin treatment. Also *hIR8* was induced by C-ARF10 with or without auxin, and *hDR15* by C-ARF16 after auxin treatment (Figure 3B; Figure S2B). In line with the identification of putative activation domains in C-ARFs [28], C-ARFs could thus act as activators of transcription of synthetic reporters in response to auxin, and might not act only as repressors[12]. Taken together, our results indicate that ARFs differentially regulate transcription of the different reporters. As for CHO-K1 cells, increasing the relative quantity of the transfected ARF plasmid in protoplasts had no major impact on the regulation trends observed for a selection of ARF and promoters, indicating that our results are unlikely biased by saturation of ARF binding due overexpression of ARFs (Figure S2E).

When considering a given ARF, differences in activity between reporters could be expected to reflect primarily differences in binding capacities. However, in many cases, differences in transcriptional regulation with reporters could not simply be explained by our analysis of ARF binding properties (Figures 2C-G). For instance, binding analyses indicate comparable A-ARF5 binding to *hER13* and *hDR5* (Figures 2C, F) but activation of *hER13* by A-ARF5 was an order of magnitude higher than for *hDR5* in protoplasts (Figure 3B). More generally, a higher activation was observed for all A-ARFs with *hER13* compared to other reporters (Figure 3B,C),

which is not fully expected from our binding assays (Figure 2C,F). The strongest repression by B-ARF2 was observed with *hDR15,* while the binding analyses suggest that B-ARF2 bind poorly to this promoter. Binding analyses also suggested comparable binding on *hIR8* and *hER13* both for B-ARF1 and 2 (Figure 2C, F), and yet repression in absence of auxin by both B-ARFs was observed only for *hIR8* (Figure 3B, Figure S2B). Also, the non-canonical B-ARF3 induced *hIR8 and hER13* but repressed *hDR15* (Figure 3B,C).

This set of results shows that ARFs regulate transcription differentially depending on the AuxRE pair configurations they bind to. It further suggests a much more complex *in planta* regulation determined both by the affinity of ARFs for a given AuxRE pair configuration, and by an effect of this configuration on the regulatory properties of ARFs. Thus, ARF transcriptional effects and their auxin regulation are not solely intrinsic to ARFs but are also under the regulation of *cis*-elements they bind to in promoters.

Combining ARFs from different clades modifies their transcriptional activity

We then sought to ask how interaction between ARFs contributes to the ARF-dependent transcriptional code and the role of AuxRE pair configurations in these interactions, be it competition as currently assumed or more complex synergies. Again, we used the simplified protoplast system to analyze regulation of the four synthetic promoters by combinations of ARFs (Figure 3D). We used two sets of A-, B- and C-ARFs: A-ARF19/B-ARF1/C-ARF16 (Figure 3E) and A-ARF6/B-ARF 2/C-ARF10 (Figure 3F). We also used a lower amount of reporter plasmids to ensure a robust dynamic range of reporter activation, making the results with single ARF controls not directly comparable to the one shown in Figure 3B. Consistent with a competitive interaction between A and B-ARFs, B-ARF2 co-transfection decreased *hIR8*, *hER13* and *hDR15* induction compared to A-ARF6 alone (Figure 3E). Similarly, B-ARF1 decreased A-ARF19 induction of *hIR8* (Figure 3F). However, several results also suggest unexpected synergistic action between ARFs from different clades. On *hDR5*, B-ARFs either strongly increased (B-ARF1; Figure 3F) or did not interfere with (B-ARF2; Figure 3E) activation by A-ARFs. Strong synergies were also seen for combinations of A- and C-ARFs for the induction of *hER13* (both combinations), of *hIR8* (with A-ARF1 and C-ARF16) and of *hDR5* (with A-ARF2 and C-ARF10) (Figure 3E,F). Thus, transcriptional regulation by multiple ARFs is not simply determined by competitions between ARFs, with either repressive or inductive activity, on the promoter of target genes as proposed in bryophytes[14,16]. Rather, combining ARFs can alter their activating vs. repressive effects, depending on the *cis*-elements targeted, even leading B-ARFs to contribute to transcriptional activation. Although the molecular mechanisms involved are unknown, A-ARF5 and B-ARF3 have been suggested to be able to act both as activators and repressors [30,31]. Transcriptional activation domains have also recently been identified in B-ARFs, including Arabidopsis B-ARF1, 2 and 3 [28]. Binding

configurations of both A- and B-ARFs on target *cis*-elements could then allow for a change in B-ARF activity from repressor to activator, due to unknown ARF interactions or to accessory proteins, explaining our observations with A-ARF6 and B-ARF2. Together with our results with single ARFs in protoplasts (Figures 3A-C), this suggests a scenario where transcriptional regulation of a given gene by ARFs results from both an effect in *trans* of the combination of ARFs present in a cell and an effect in *cis* from the AuxRE pairs configurations found in the gene promoter. AuxRE pairs will not only select which ARFs bind to the promoter but also influence the transcriptional properties of these ARFs, depending on whether they belong to a single or to different clades, thus generating a complex and extended ARF/AuxRE bi-layer combinatorial regulatory code.

AuxRE pairs provide spatial specificity to synthetic reporters *in planta*

If ARFs simply relay auxin concentration, as currently assumed, all synthetic promoters should lead to similar expression within plant tissues. However, if our hypothesis of an ARF/AuxRE code is correct, reporters driven by our synthetic promoters could have contrasting expression patterns. Thus, we generated Arabidopsis lines transformed with the four synthetic transcriptional reporters controlling expression of mTurquoise2 (mTQ). The four reporters consistently drove distinct expression patterns in roots (Figure 4A; Figure S3). *hIR8* led to a weak expression in the upper lateral root cap (LRC) and in epidermal cells. *hER13* was expressed in the quiescent center (QC), initial cells and upper tier of the columella and had a weak expression in the vasculature. As previously reported for other DR5-based reporters[25,32], *hDR5* was strongly expressed in the vasculature, the QC, and most of the columella. Unlike other reporters, *hDR15* showed no expression in the root tip but weak expression was detected in epidermal cells in the differentiation zone. Co-expression of the four synthetic promoters driving distinct fluorescent proteins from a single insertion sequence recapitulated the differences in expression patterns seen in the individual synthetic reporter lines (although *hDR15* expression could not be detected in these plants; Figure 4B, Figure S3). After auxin treatment, all promoters showed an increase in expression confirming that they are auxin-inducible transcriptional reporters (Figures 4A,B).

These results demonstrate that AuxRE pairs provide spatial specificity to transcription, confirming the importance of *cis*-motifs in setting spatial patterns of auxin responses. They further substantiate a bi-layer processing of the auxin signal involving both ARF in *trans* and AuxRE pair configurations in *cis*. For a cell expressing a given repertoire of ARFs, depending on the AuxRE pair configuration targeted, ARFs might or not translate the signal into gene expression, resulting in expression patterns that do not simply reflect auxin distribution in the tissue but that are the interpretation of the auxin signal by both the ARF and the promoter *cis*-element configuration control layers.

Single cell analysis identifies candidate ARF networks controlling synthetic reporter expression

To identify ARFs involved in establishing synthetic reporter expression patterns in the root, we next used scRNA-seq with the 4 reporter lines with (1µM IAA, 16 h) or without (No IAA) exogenous auxin treatment. 24.8% Differentially Expressed Genes (DEGs) were detected between No IAA and IAA datasets, highlighting the significant transcriptional response to auxin (Table S3).

After dataset integration[33], we assigned cell type identities using published markers and built UMAP representations (Figure 4C). We mapped mTQ mRNAs expressed from the synthetic promoters onto each UMAP. We validated the cellular domains detected by confocal imaging for *hIR8*, *hER13* and *hDR5* with or without IAA treatment (Figure 4D). Whilst *hDR15*-driven mTQ expression was not detected in the root tip by confocal imaging under control conditions, we detected *mTQ* mRNA in LRC cells in the scRNA-seq dataset in both conditions, as well as in epidermal cells and additional cell types upon auxin treatment (Figure 4D). While we do not have a clear explanation for this difference, it could result from a post-transcriptional effect affecting protein production. Our scRNA-seq results thus confirm that each synthetic promoter establishes a different cellular expression pattern in response to auxin.

We then analyzed the expression profiles of the 12 *ARFs* robustly detected in the control and IAA datasets (all A- and *C-ARFs* and *B-ARF1-3* and *9,* Figure S4). In control conditions, A-*ARFs* showed cell type-specific expressions, except A-*ARF7* that was uniformly expressed. B-*ARF3* and *9* were expressed in a cell type-specific manner, while B-*ARF1* and *2* showed a broad expression pattern. All C-*ARFs* showed discrete expression patterns. All detected *ARFs* were differentially expressed upon auxin treatment with an increased or broader expression in UMAPs (Figure S4). This shows that all these *ARFs* are regulated (directly or indirectly) by auxin and that this regulation might be a significant, yet underestimated, component of the auxin signaling pathway dynamics as only a few *ARFs* have been suggested to be regulated by auxin so far[34].

We observed significant overlaps between expression of reporters and *ARFs* (Figure S5A). To identify candidate ARFs regulating reporter expression, we first calculated pairwise correlations between each reporter and each *ARF* expression in all cells (Figure 5A; Table S3). Consistent with the results in our protoplast assays, positive correlations with reporter expressions were mostly found for A and C-*ARFs* with specific correlations for each reporter: *hIR8* with C-*ARF16*, *hER13* with C-*ARF10*, *hDR5* with C-*ARF10* and *17*, and *hDR15* with all three C-*ARFs*. Similarly, *hER13* and *hDR5* correlated with A-*ARF5*, *6* and *8* expressions, whereas *hIR8* only correlated positively with A-*ARF19* and *hDR15* only with A-*ARF5*, which was the main A-ARF inducing *hDR15* in the protoplast assay. These two reporters also showed

negative correlations with several A-*ARFs*. Amongst B-*ARFs*, B-*ARF9* positively correlated with *hIR8* and *hDR5* and negatively with *hDR15* expression, whilst B-*ARF1* expression correlated negatively with *hDR5*.

To further identify ARF combinations potentially controlling reporter expression, we computed odds ratios to correlate the expression of pairs of *ARFs* with the expression of the reporters. This analysis predicted numerous ARF pairs, within and between clades, the expression of which correlate with that of each reporter, supporting the interclade combinatorial potential observed in protoplasts (Figure 5A; Figure S5B; Table S3). Again, we found that each reporter correlated specifically with certain ARF pairs: *hIR8* expression was positively correlated mostly with A+B combinations whereas A+A and A+C or A+A, A+B and A+C combinations correlated with *hER13* and *hDR5* expression, respectively. *hDR15* expression was positively correlated to A+C pairs but the network also predicted multiple negative correlations with A+A and A+B pairs. Additionally, we used a machine learning algorithm to generate a random forest model of combinatorial regulation of ARFs on reporter expression across the full cell atlas. This approach confirmed several of the reporter-*ARF* and reporter-*ARF* pair associations (positive or negative) predicted by correlation tests (Figure 5B). The random forest model also predicted distinct regulatory modules of B-*ARF* and B+C-*ARFs*, suggesting that the combinatorial effect of these clades on reporter transcription is not linearly linked to their co-expression with them (Figure S5C; Table S3).

The complementary approaches we used, robustly suggest that different ARF combinations drive the expression of each synthetic reporter, in line with the idea that AuxRE pairs select which ARFs bind to a promoter. The putative networks we identified also suggest several properties of ARFs in the regulation of the reporters *in planta*. Since the four networks are constituted by both specific and common elements, they likely reflect both the specificity of ARFs for the four reporters and corroborate the potential of ARF interclade combinations in regulating reporter expression observed in cellular systems (Figure 2, 3). Also, all networks present a two-level structure in which most ARF pairs contain at least one ARF that alone is positively correlated with the reporter. Examples of this are the uniformly expressed ARFs B-*ARF1* and *2* and A-*ARF7* that appear in the networks mostly as associated with another *ARF* (Figure 5A). Regulation of the reporters by these ARFs could be then restricted to the domains of co-expression with their paired ARF. This situation could reflect specific *cis-trans* interactions, as seen using combinations of ARFs in protoplast assays (Figure 3D,E), and further supports a regulation by an ARF/AuxRE bi-layer control system.

ARFs control the expression pattern of auxin-regulated synthetic reporters *in planta*

To assess the functional relevance of the ARF networks predicted from scRNA-seq data, we introduced the four synthetic reporter lines in *arf* single mutants. The expression level and/or

pattern of reporters was affected in several mutants for ARFs with different predicted regulatory potential in our network analysis (Figure 5C-E, Figure S6).

Significant changes in reporter patterns were first seen in several mutants for ARFs whose expression directly correlates with reporter expression in our scRNA-seq data (Figure 5, Figure S6). We indeed observed an almost complete loss of expression of *hIR8* in *arf19* and *hER13* in *arf6*, a decrease of the *hDR5* signal together with a change in the apical-basal gradient of expression in *arf8* and *arf19*, and a strong change in the *hDR5* apical-basal expression gradient in *arf6* without a change in the maximal expression level (Figure 5C-E, Figure S6). Note that these changes cannot simply result from alterations in the organization of the root in mutants as only the *arf5/monopteros* mutant shows a root phenotype amongst *arf* single mutants[35]. Regarding *arf5*, changes in *hER13* and *hDR5* expression patterns were also detected in this mutant: both reporters were ectopically detected in epidermal cells and not in inner cell-types as in the wild type (Figure S6A). Additionally, in 30-50% of the *arf5* roots analyzed, no signal was detected for the three reporters (data not shown). Similar to wild-type, no expression was detected for *hDR15* reporter in root tips of any of the *arf* mutant tested (*arf1-3*, *8*, *19* and *10*, data not shown) except for *arf5*, in which expression was detected in epidermal cells of all roots analyzed (Figure S6). Thus, the *arf5* mutation leads either to loss of reporter expression or to ectopic reporter expression, which unlikely result only from perturbed root tip organization in the mutant. In most instances, these results suggest that ARFs identified as directly correlating with reporter expression in our scRNA-seq data are involved in direct ARF-promoter regulation and can control both the level of expression and the expression patterns of the reporters.

We also observed changes in reporter expression and/or patterns in mutants for *ARFs* associated to reporters as paired to another *ARF* in our network analysis (Figure 5A,B). This was the case for *hIR8* in *arf10* that changed both in expression level and pattern (with an expression starting further away from the root tip in the root cap/epidermis) or *hER13* in *arf7 and 19* (Figure 5C-E; Figure S6B,C). We observed also a decrease in reporter expression levels in mutants for ARFs negatively associated to the reporter (*arf6* for *hIR8*, *arf16* for *hER13* and *arf19* for *hDR5*; Figure 5E, Figure S6), which could result from an indirect effect of *ARF* deficiency modifying global auxin responses and affecting the regulation of other *ARFs*. These observations provide further functional validation to the ARF networks identified from our scRNA-seq data.

Our genetic analysis also supports the functional relevance of the ARF/AuxRE bi-layer code, as mutations in *ARFs* common to two networks did not always have the same effect depending on the AuxRE configuration of the reporter. For instance, for mutants in ARFs common to *hER13* and *hDR5* ARF networks, *arf8* affects *hDR5* but not *hER13* and *vice versa* for *arf7*,

while *arf6* affects both reporters but with different effects (Figure 5C-E, Figure S6). A given ARF can thus play different regulatory functions depending on the reporter that it targets.
Altogether, these results provide direct genetic evidence to the ARF networks we identified. They also further substantiate the importance of distinct regulatory circuits in establishing the spatial specificity of auxin responses *in planta* based on multi-tiered *cis-trans* relationships between ARF combinations and AuxRE pairs.

AuxRE pair configurations contribute to set spatial patterns *in planta*

We next used our scRNA-seq data to evaluate whether the AuxRE pair configurations we studied using synthetic promoters also contribute to set expression patterns of endogenous auxin responsive genes (ARG). Given the discrepancies observed between imaging and scRNA-seq for *hDR15*, we did not use the DR15 configuration here. We first predicted IR8, ER13 and DR5 motifs within the Arabidopsis genome in the -500 bp upstream transcription start sites (TSS), where AuxRE occurrence is the highest[36]. Next, we selected genes with IR8, ER13 and/or DR5 AuxRE pairs in this region that were differentially regulated by auxin in our scRNA-seq data (Figure 6A). Most identified genes had either IR8, ER13 or DR5 AuxRE pairs in their -500 bp promoter (Figure 6A). Around 20% had combinations of IR8/ER13, IR8/DR5 or ER13/DR5 motifs (Figure 7A). Out of the ones with only one AuxRE pair configuration, 5-10% had 2 or 3 binding motifs and never more (Figure 6A; Table S4). Altogether this suggests that auxin regulation arises primarily from one or few AuxRE pairs of a given configuration in promoters of target genes.
Although some of these genes had a spatial pattern similar to the synthetic reporters, the vast majority of them showed patterns different from the reporters, most likely due to regulation by additional TFs besides ARFs. To investigate the contribution of specific AuxRE pair configurations to gene expression, we focused on genes with only one AuxRE pair configuration in their proximal promoter. We separated them into those with 2 or 3 AuxRE pairs (x2 or x3 IR8, ER13, DR5) or just one (x1 IR8, ER13, DR5) (Figure 6A; Table S4). We calculated an average expression of genes binned into these 6 categories that we projected on the root cell atlas for both “No IAA” and “IAA” conditions (Figure 6B-D; Figure S7A). To assess significant differences, we performed spatial cross-correlation[37] between gene categories within each cell type (Table S4). Average expression of x2 IR8, x2 ER13 or x2/x3 DR5 genes showed distinct patterns with statistically significant differences in multiple cell types (Figure 6B; Table S4), while the averaged expression from genes having only one AuxRE pair, x1 IR8, x1 ER13 and x1 DR5, showed few differences (Figure 6C; Table S4). However, the subset of genes with single AuxRE pair for which at least one of the AuxREs was the high affinity TGTCGG motif (x1 IR8-TGTCGG, x1 ER13-TGTCGG, x1 DR5-TGTCGG), also presented contrasted expression patterns (Figure 6D; Table S4).

We could observe noticeable similarities between average patterns for genes with 2 or 3 AuxRE pairs and synthetic reporter patterns. The x2 IR8 gene average pattern showed no expression in the QC and initial cells and expression in atrichoblasts as the *hIR8* reporter. The x2 ER13 or x2 DR5 gene average patterns showed expression in the QC, initial cells, and in the vasculature, *i.e.* in tissues where the corresponding synthetic reporters are most highly expressed (Figure 6B). Similarly, genes with only one AuxRE pair but with one TGTCGG sequence showed stronger averaged expression in tissues where the synthetic reporters are expressed: atrichoblasts for IR8, vasculature for ER13 and QC/initials and vasculature for DR5 (Figure 6D).

Taken together, our analysis suggest that AuxRE pair configurations, number and sequence contribute to defining the expression pattern of ARGs, indicating that the ARF/AuxRE code revealed by our biochemistry experiments and our reductionist approaches in cellular systems operates to regulate expression of endogenous genes.

AuxRE pairs combinatorially set spatial expression patterns

Amongst the ARGs for which we identified two (or more) different AuxRE pair configurations in the proximal promoter (Figure 6A), AuxRE pairs were either spread in the promoter (we call this adjacent here for simplicity) or overlapping, with a half site shared between two AuxRE pairs (Figure 7A). We thus analyzed the contribution of two combined AuxRE pair configurations to the expression of ARGs, focusing on IR8/ER13 and IR8/DR5 combinations (Figure 7A; Table S4). Average expression patterns of genes whose promoters contain such combinations were strikingly different (Figure 7B, Figure S7B). Genes with IR8/ER13 and IR8/DR5 combinations in the same configuration (adjacent or overlapped) in their promoter presented partially opposite expression patterns. Genes with adjacent and overlapping configurations for the same combination in their promoter also presented different average expression patterns, statistically different in multiple cell types (Figure 7B).

This suggests a combinatorial contribution of different AuxRE pairs to setting the expression pattern of ARGs. Promoters of the ARGs ARR7, PINOID BINDING PROTEIN (PBP1) and IAA11[38–41] harbor combinations of different AuxRE pairs. Mutating a single AuxRE pair altered gene expression patterns and response to auxin, leading to an increased or decreased expression in a cell-dependent manner (Figure S7C-F, S8A), an observation in line with a combinatorial contribution of AuxRE pairs. To explore further how different AuxRE pairs combinatorial regulation of expression pattern of ARGs, we generated a collection of additional synthetic promoters with three copies of overlapping of adjacent configurations of IR8/ER13 or IR8/DR5 motifs as found in endogenous promoters (called *hIR8/hER13* and *hIR8/hDR5*; Figure 7C). We also generated juxtaposed *hIR8/hER13* and *hIR8/hDR5* synthetic reporters. As opposed to adjacent configurations, for which we intercalated the different AuxRE pairs,

juxtaposed reporters were built from stitching consecutively *hIR8* and *hER13*, or *hIR8* and *hDR5* sequences. Finally, we also generated *hIR8/hDR15* synthetic reporters in the three configurations (Figure 7C; Table S5). These combinations of AuxRE configurations led in some cases to an expression pattern in the root identical to the one obtained with only one of the AuxRE pair configuration used, suggesting dominant effects (*e.g.* a *hDR5*-like pattern for juxtaposed *hIR8/hDR5*), or to an additive pattern (e.g. for the overlapped *hIR8*/*hDR5* reporter that is expressed in both the *hDR5* and *hIR8* domains), and also to several distinct patterns of expression compared with the single-motif reporters (e.g. overlapped and adjacent hIR8/hER13 or *hIR8*/*hDR15*; Figure 7C, S8B). Strikingly, adjacent *hIR8/hER13* and *hIR8/hDR5* synthetic reporters had mirror expression patterns (Figure 7C, S8B) similarly to average expression of adjacent 'IR8+ER13' and 'IR8+DR5' gene categories (Figure 7B). These results show that not only different combinations of AuxRE pair configurations result in different expression patterns but also that the topology of their arrangement further expands the palette of expression patterns that can be obtained from combining IR8/ER13/DR5/DR15 configurations, even leading to entirely distinct expression patterns. Thus, combinations of AuxRE pair configurations provide further regulatory power to the ARF/AuxRE code for controlling the spatial expression of auxin target genes.

Discussion

Understanding how information from a developmental signal is processed into a multiplicity of cellular and developmental responses in space and time is key to understand development. Here, we have identified the general operating principles of a powerful combinatorial regulatory system acting downstream of auxin to regulate transcription patterns in plants.

Transcription in response to auxin is mediated by ARF TFs from three clades, A, B and C [42]. ARF dimers bind pairs of *cis*-elements, the AuxREs, in IR, ER or DR orientations. Using both published[19,21,22] and DAP-seq data from our study, as well as EMSA assays, we identified interclade specificity in the binding to specific AuxRE pairs configurations, namely IR8, ER13, DR5 and DR15. We also showed that the number of AuxRE pairs of a given configuration present in a sequence can modify ARF binding specificity, possibly due to cooperativity between ARF dimers. This allowed us to design synthetic promoters potentially targeted by different ARFs in order to decipher the principles explaining transcriptional specificity in response to auxin. We show that the synthetic promoters we designed can be complementarily studied using biochemical approaches, orthogonal systems and isolated plant cells (protoplasts) using both chimeric and wild-type ARFs to analyze the specificity and regulatory potential of ARFs, instructing us on their mode of action *in planta*. scRNA-seq then provided an unmatched spatial resolution to identify the regulatory networks at play and to analyze transcriptional regulation at the genomic scale. scRNA-seq using plants expressing synthetic

reporters facilitated the identification of regulatory networks by including a synthetic locus uniquely targeted by one family of TFs, here the ARFs, versus the co-regulation by multiple TFs occurring on endogenous promoters. We validated our methodology for the identification of regulatory ARF modules using genetics. As transcriptional regulation relies on TF families for many other plant hormones, a similar strategy could be used to interrogate whether other signaling pathways operate according to similar principles. DAP-seq data have become available for many TFs and our strategy could thus be used also for TF families beyond the ones involved in plant hormone signaling pathways[22]. Our work thus establishes a blueprint for the use of synthetic promoters to decipher the complex regulations that control specificity in transcriptional responses, notably in response to developmental signals.

We show that synthetic reporters constructed with promoters harboring IR8, ER13, DR5 or DR15 motifs are auxin-inducible and generate different expression patterns in the root. Also, these AuxRE pair configurations when present in promoters of auxin-regulated genes contributes to generate specific expression patterns. The fact that ARF TF family are differentially expressed in plant tissues[15,43,44] had led to the proposal that distinct modules of co-expressed ARFs could code different transcriptional responses, notably due to different ratios of A-ARFs and B-ARFs competing for binding on target promoters. A combination of correlation, combinatorial models and machine learning analysis of scRNA-seq data together with genetics allowed us to decipher the ARF-dependent transcriptional code at single-cell resolution in the root by identifying ARF networks controlling the specificity of the expression of the *hIR8*, *hER13* and *hDR5* synthetic promoters. However, the composition of these networks and our assays in mammalian cells, protoplasts and plants indicate that the regulatory potential of ARF networks in a cell does not simply result from competition between ARFs with activator or repressor activity. We show that complex functional interactions between ARFs of different clades can lead to antagonistic or synergistic effects on transcription that cannot be predicted simply from the clade to which an ARF belongs. This could result from the formation of ARF heterodimers, and evidence exists for heterodimerization between ARFs from all different clades[15,45,46] or by indirect interactions mediated by other transcriptional regulators. We further found, both in isolated cells and in the root, that AuxRE pair configurations influence activity of ARFs and that combining different AuxRE pair configurations in synthetic promoters can create distinct expression patterns compared to synthetic promoters constructed from a single AuxRE pair configuration. Thus, specificity in transcription in response to auxin is encoded both in *trans* by combinations of ARF TFs, and in *cis* by AuxRE pair configurations they bind to, establishing a bi-layer control system that can generate a wide diversity of gene expression patterns from the spatial auxin distribution in the Arabidopsis root. This work thus elucidated the principles of how AuxREs and ARFs define a *cis-trans* transcriptional code, providing a model explaining how the same auxin signal triggers

distinct transcriptional responses across different cell types. How *cis*-elements influence *trans* regulations is unknown. One possibility is that AuxRE pairs could change the way an ARF dimer is formed and/or contact the transcriptional machinery, thus influencing the ARF transcriptional activity. The operating principles of the auxin code we have identified might be also modulated by interactions of ARFs and DNA with other TFs and proteins regulating transcription and chromatin state that could vary depending on AuxREs.

Finally, *DR5* synthetic reporters have been instrumental in the last 20 years to analyze the auxin responses and function during plant development. However, the synthetic reporters characterized here are all regulated by auxin and revealed a much wider diversity of auxin-dependent patterns. While *DR5* expression is more closely related to auxin distribution in the root[32], the reporter lines we generated show spatial expression patterns that significantly differ and that are not a direct translation of auxin distribution within the root. This illustrates the non-linear processing capacities of the bi-layer control system we identified. *DR5*-driven transcription thus likely reports only a subset of auxin transcriptional responses and *DR5* reporters should be used with knowledge of this limitation. Finally, our work streamlines the design of synthetic promoters to control expression patterns of plant genes using plant-specific *cis*-elements. We show that combinations of AuxRE configurations can indeed be used to engineer synthetic spatial patterns in the Arabidopsis root, expanding the toolkit available using orthogonal transcriptional regulators[47,48].

Limitations of the study

Although we provide solid evidence that a *trans*/*cis* bi-layer control system patterns auxin-dependent gene expression, how this system precisely operates and whether it involves additional actors (such as other proteins or chromatin configurations) remain to be identified. We anticipate that the tools and data generated in this work will be key toward these aims.

RESOURCE AVAILABILITY

Lead contact

Further information and requests for resources and reagents should be directed to and will be fulfilled by the lead contact, Teva Vernoux (teva.vernoux@ens-lyon.fr).

Materials availability

Unique materials generated in this study will be available from the lead contact upon request.

Data and code availability

- DAP-seq and scRNA-seq data have been deposited at GEO as GSE237176 and GSE241573 respectively and are publicly available as of the date of publication.
- Microscopy data have been deposited at Zenodo as 10.5281/zenodo.14924818 and are publicly available as of the date of publication.

- All original codes have been deposited at GitHub and are publicly available at https://github.com/Bioinfo-LPCV-RDF/TF_genomic_analysis, https://gitbio.ens-lyon.fr/ahugues/chromauxi, https://github.com/BrunoGuillotin/ScRNAseq_Correlation_with_Random.git and https://github.com/govissers/ARF_Binding_2023.git as of the date of publication.

ACKNOWLEDGMENTS

K.D.B, F.R. and T.V. dedicate this work to the memory of their mentor Philip N. Benfey. We thank M. Semon for advice on scRNA-seq analyses; J. Friml and V. Willemsen for *arf10/16* mutant seeds; M. Boudoscq for advice on protoplast protein extraction; X. Lai for advice on DAP-seq; K. Boubekeur for help with EMSA; the PLATIM facility (SFR Biosciences, UMS3444/CNRS, US8/Inserm, ENS de Lyon, UCBL) for assistance with microscopy; R. Schönle and S. Kuschel for technical assistance. This work was supported by a short-term fellowship from the Company of Biologists to R.M.-A.; a long-term fellowship from the Human Frontiers of Science (LT000972/2018-L) to B.G.; the Deutsche Foschungsgemeinschaft (DFG) German Research Foundation under the Germany´s Excellence Strategy (CEPLAS-EXC-2048 project no. 390686111) to M.D.Z.; NEXTPlant (Project ID 391465903/GRK 2466) to J.S. and M.D.Z.; the University of Düsseldorf to R.M.-A. and M.D.Z.; the ChromAuxi project from the Agence Nationale de la Recherche (ANR-18-CE12-0014-02) to T.V., F.R., R.D. and F.P.; the European Union, ERC TEMPO Project 101095380 to T.V.. Views and opinions expressed are however those of the authors only and do not necessarily reflect those of the European Union or the European Research Council Executive Agency (ERCEA). Neither the European Union nor the granting authority can be held responsible for them.

AUTHORS CONTRIBUTION

R.M.-A., B.G., M.D.Z., R.D, F.P, F.R. and T.V, designed the project and experiments. R.M.-A. and B.G. performed experiments and analyzed scRNA-seq data and motifs predictions. M.-F.G., J.S., E.T., R.D., C.C, K.T. and A.M. performed experiments. A.H. performed odd ratio tests and V.G the machine learning. J.L. analyzed DAP-seq data and motifs predictions. A.D. helped with results interpretation, C.G.A with confocal microscopy, G.C. with quantitative image analysis and J.L. with statistical analysis. R.M.-A., B.G., F.R. and T.V. wrote the paper with input from all authors. K.D.B., M.D.Z., F.P., R.D, F.R. and T.V. supervised the study. All authors read and approved the manuscript.

DECLARATION OF INTERESTS

The authors declare no competing interests.

FIGURE LEGENDS

Figure 1. ARF preferential binding motifs *in vitro*

(A) ARF modular domain structure and activity. DBD: DNA-binding domain; PB1: Phox/BEM1 domain; MR: middle region. A, B and C-ARFs possible mechanisms of action: A-ARFs activate auxin-dependent transcription through Aux/IAA degradation; B-ARFs repress transcription by competition; C-ARF mechanism of action remains unknown.

(B) IR, ER and DR configurations. Arrows: AuxRE motifs; n: spacing between two AuxREs.

(C) Most represented motif found in the 600 best C-ARF10 DAP-seq peaks.

(D) IR, ER and DR over-representation in C-ARF10 DAP-seq bound regions compared to a random distribution. Score thresholds: levels of stringency, going from strict (-8) to relaxed (-10).

(E) B-ARF1, A-ARF5 and C-ARF10 EMSA with IR8, ER13, DR5 and DR15 at different ARF concentrations. SS: single AuxRE (negative control). +/- signs: presence/absence of ARF protein. Bottom panels: quantifications of the percentage of DNA bound.

(F) ARF preferences for AuxRE pairs configurations based on published DAP-seq data[19,21,22], C-ARF10 DAP-seq data (left) and EMSA (right). See also Figure S1.

Figure 2. ARFs differential binding to AuxRE pair repeats in mammalian cells.

(A) Synthetic promoter design: 3 repeats of IR8, ER13, DR5 or DR15 followed by a core minimal promoter control the expression of a reporter gene.

(B and C) EMSA using B-ARF1, A-ARF5 and C-ARF10 with oligonucleotides containing 2 (x2) or 3 (x3) IR8, ER13, DR5 or DR15 repeats at different protein concentrations. SS: single AuxRE (negative control). +/- signs: presence/absence of ARF protein. Panels under gels: quantifications of the percentage of DNA bound.

(D) ARF DNA binding preferences based on EMSA (B,C).

(E) Principle of chimeric ARF activity assay in CHO-K1 cells.

(F) Synthetic reporter expression (SEAP: human secreted alkaline phosphatase) in CHO-K1 cells transfected with or without (Mock) chimeric ARFs. 3 replicates were done with 4 technical replicates. Bars show average values. Replicate 1/2/3: blue/pink/yellow dots respectively. Heatmaps: ARF/Mock fold-change. A cell is colored only if differences between Mock and ARF are significant (t-test for biological replicates and Fisher's method for Combining *p*-values). Significant differences are indicated by letters (ANOVA-Tukey, *p*-values <0.05). Raw data and statistical analysis results: Table S2.

(G) ARF DNA binding preferences for different AuxRE pairs repeats based on CHO-K1 cell assays (E,F).

See also Figure S1.

Figure 3. Differential regulation of synthetic reporters by ARFs or pairs of ARFs in plant protoplasts

(A and D) Protoplasts assays with a single ARF (A) or pair of ARFs (D).

(B) Synthetic reporter expression with or without (Mock) ARF before (No IAA) and after an IAA treatment (1µM, 6h). FF: firefly luciferase, REN: renilla luciferase. A scaled-up graph is shown for *hIR8*, *hDR5* and *hDR15*. Asterisks: significant differences between ARF and Mock (*t*-test).

(C) Summary of ARF regulation of different AuxRE pairs.

(E) Synthetic reporter expression with or without (Mock) a single ARF or an ARF pair (A+B or A+C). Asterisks: significant differences between A+B or A+C conditions and A-ARF alone (*t*-test).

B,E: 3 replicates were done with 4 technical replicates each. Replicate 1/2/3: blue/pink/yellow dots respectively. For each replicate, data were normalized to the Mock sample. Bars show average normalized values. Heatmaps: ARF/Mock fold-change. A cell is colored only if differences between Mock and ARF are significant (t-test for biological replicates and Fisher's method for Combining *p*-values). Green/purple indicate activation/repression. Raw data and statistical analysis: Table S2.

See also Figure S2.

Figure 4. AuxRE pairs provide spatial specificity to synthetic reporters *in planta*

(A and B) Expression (single plane) of *hIR8*, *hER13*, *hDR5* or *hDR15* driving mTQ (blue) (A), or of *hIR8*::*mTQ*, *hER13::Venus*, *hDR5::mCherry* and *hDR15::LSMOrange* (mTQ: blue; Venus: yellow ;mCherry: purple; LSMOrange could not be detected) in the root. (B). Roots were treated with mock or exogenous (1µM IAA, 16 h). Cell walls were marked with PI (red in A; grey in B). White arrows: cells expressing *hIR8* in the lateral root cap (LRC). Insets: z-stack max projections showing expression of *hIR8* in the LRC and *hDR15* in the differentiation zone. N=5-10 roots per line.

(C) Root structure and single cell atlas reconstructed from *hIR8*, *hER13*, *hDR5* and *hDR15* scRNA-seq datasets (no IAA). The same colors are used to mark cell-types on root and Seurat clustering.

(D) *mTQ* expression driven by *hIR8*, *hER13*, *hDR5* or *hDR15* promoters mapped on the root single cell atlas from (C).

See also Figure S3.

Figure 5. ARF combinations control expression of auxin-regulated synthetic reporters *in planta*

(A) ARF Networks correlated to each reporter in scRNA-seq data predicted by co-expression correlation (ARF) and odd-ratio analysis (ARF pair). Numbers in circles indicate the corresponding ARF. Light grey circles: B-ARFs; dark-grey circles: A-ARFs; black circles: C-ARFs. Blue-circles: *arf* mutants show altered reporter expression. Green/purple lines: positive/negative correlations respectively.
(B) Common predictions between correlation networks from (A) and the ones predicted using machine learning.
(C) *hIR8::mTQ*, *hER13::mTQ* or *hDR5::mTQ* expression (single plane) in *arf* mutant roots. Insets: z-stack max projections of *hIR8* roots. Blue: mTQ. Red: Cell walls marked with PI. Wt: wild-type.
(D) *hDR5* expression profile along the root in wild-type and *arf6*. The mTQ2 signal was quantified in dashed areas in (C). QC: quiescent center.
(E) Global expression of reporters in *arf* mutant roots. Asterisks: significant changes compared to wild-type (ANOVA-Tukey test, *p*-value < 0.05). N=10-20 roots per line.
See also Figure S5 and S6.

Figure 6. AuxRE pairs contribute to set spatial patterns *in planta*
(A) Identification of genes with *IR8*, *ER13* or *DR5* motifs in their promoters. Single/two/three motifs: x1/x2/x3 respectively. Single motif with a TGTCGG consensus sequence: x1-TGTCGG. n: number of genes. TSS: transcription start site. DEG: differentially expressed genes.
(B to D) Averaged expression per cell of gene groups in (A) projected on the root single cell atlas (Figure 4C). The normalized 2.5-10 scale is shown. Circles: cell types with statistically significant differences (spatial cross-correlation tests followed by randomization, *p*-value>0.05) between IR8 vs ER13 and IR8 vs DR5 (Table S4). Numbers: cell types as in Figure 4.
See also Figure S7.

Figure 7. AuxRE pairs combinatorially set spatial expression patterns
(A) Identification of genes with IR8/ER13 or IR8/DR5 combinations amongst the genes with IR8 motifs from Figure 6. Combined motifs are either overlapped or adjacent as represented. n: number of genes in each category.
(B) Averaged expression per cell for gene groups in (A) projected on the root single cell atlas (Figure 4C). Dashed circles: cell types where differences were statistically significant (spatial cross-correlation tests followed by randomization, *p*-value>0.05) (see Table S4). Tests done on overlapped vs adjacent categories. Numbers: cell types as in Figure 4C.
(C) *hIR8/hER13::mTQ*, *hIR8/hDR5::mTQ* or *hIR8/hDR15::mTQ* reporter design and expression (single plane) in roots. Blue: mTQ. Red: Cell walls marked with PI. N= 5-10 roots per line.

See also Figure S7 and S8.

STAR METHODS

EXPERIMENTAL MODEL AND STUDY PARTICIPANT DETAILS

Cell lines

Chinese Hamster ovary (CHO-K1, DSMZ ACC110) cells were cultivated in HAM's F12 medium with 10% (v/v) fetal bovine serum (FBS) and 1% (v/v) penicillin/streptomycin at 37°C with 5% CO_2.

Plant materials and growth conditions

For protoplasts extraction and transfection Columbia (Col-0) ecotype *A. thaliana* seedlings were grown on SCA medium (0.32 % (wt/vol) Gamborg's B5 basal salt powder with vitamins (bioWORLD), 4 mM $MgSO_4 \cdot 7H_2O$, 43.8 mM sucrose and 0.8% (wt/vol) phytoagar in H_2O, pH 5.8, autoclaved with a 22 °C, 16-h light – 8-h dark cycle [49].

For plants transformation and reproduction Col-0 *A. thaliana* plants were grown on soil at 20°C long-day conditions (16 h light/8 h darkness).

For roots confocal imaging and scRNA-seq experiments, *A. thaliana* transgenic lines and mutants were grown on half-strength Murashige and Skoog (MS) medium supplemented with 1% sucrose and 1% agar at 20°C long-day conditions (16 h light/8 h darkness).

METHOD DETAILS

Plasmids construction

All primers used for plasmids construction are listed in Table S6. All plasmid information used in CHO-K1 cells and protoplasts is documented and curated in the GMOCU platform (DOI: https://doi.org/10.1002/adbi.202300529).

Plasmid for ARF10 production in bacteria

Maltose Binding Protein (MBP)-ARF10 was amplified from *ARF10* coding sequence in pHM-GWA containing MBP tag, using primers ARF10-FL-MBP-fwd and ARF10-FL-MBP-rev and cloned by Gibson Assembly into pPSG-IBA162 (Nter-FLAG-Tag and Cter-Twin-Strep-Tag) previously digested by Esp3I, to generate plasmid pCC015. A second cloning step was performed to remove the gateway linker using Gibson Assembly. Two fragments were amplified from pCC015 using oCC020/oCC027 and oCC028/oCC029 primers and cloned into pCC015 previously digested by NheI/XmaI to generate plasmid pCC027.

ARF plasmids for CHO-K1 transfection

ARF plasmids were built as chimeric ARFs where the MR of each ARF was substituted by ARF5 MR and a C-terminal VP16 domain was added. In a first step, ARF DBDs and ARF5 MR were amplified from cDNA ARF plasmids and assembled into a pJA032 destination

plasmid containing a VP16 activation domain. Second, ARF PB1 domains were amplified from cDNA ARF plasmid and inserted into the previously assembled DBD+ARF5MR+VP16 constructs. Both cloning steps were carried out using AQUA cloning technology[50].

ARF plasmids for protoplasts transfection

ARF plasmids for protoplasts transfections were built by triple LR reactions performed with Gateway® recombination technology on the 35S promoter, ARF cDNAs and the tUB10 terminator in the destination vector pDESTR4-R3. For this, ARF cDNA was amplified and cloned in pENTR vectors for the LR reaction. For ARF-GR constructs, GR was introduced into pDESTR4-R3 ARF plasmids using AQUA cloning technology. For the ARF expression dynamics experiments, firefly luciferase fused with a 3xFLAG was cloned C-terminally to each ARF in pDESTR4-R3 via the AQUA cloning method [51].

Synthetic reporters cloning

Synthetic promoter sequences were constructed as synthetic DNA (Thermofisher). DNA sequences for all these synthetic promoters can be found in Table S1 and Table S5. attB4 and attB1 sequences were added flanking the synthetic promoter sequence in each case for cloning into pDNR441 and further LR reactions.

For CHO-K1 cells transfection or protoplast transformation, synthetic reporter plasmids were built by amplification of the synthetic promoters from the synthetic DNA plasmids and insertion upstream SEAP or Firefly reporter genes, respectively, in destination plasmids using AQUA cloning technology[51] (CHO-K1 cells) or LR reactions (protoplasts) performed with Gateway® recombination technology (IR/DR/ER:Firefly:tnos). In a second cloning step, 35S:Renilla was cloned downstream Firefly to be used as control for transfection in protoplasts measurements.

For plants transformations hIR8/hER13/hDR5/hDR15 synthetic reporters were built by triple LR reactions performed with Gateway recombination technology using the corresponding synthetic reporter plasmid, the fluorescent marker mTurquoise2 fused to SV40 Nuclear Localisation Signal and mTurquoise2-t35S in the destination vector pK7m34GW with kanamycin resistance as a selectable marker.

Synthetic promoter plasmid for co-expression of the 4 reporters was built by Golden Gate cloning combining Basta and FastRed in planta selection markers, followed by the hIR8 promoter driving expression of mTQ fused to N7 nuclear localisation signal and the nopaline synthase terminator (T-nos), followed by the hER13 promoter driving expression of mVenus fused to N7 nuclear localisation signal and the T-nos terminator, followed by the hDR5 promoter driving expression of mCherry fused to N7 nuclear localisation signal and the T-nos terminator, followed by the hDR15 promoter driving expression of mOrange fused to N7 nuclear localisation signal and the T-nos terminator.

IR8+ER13/IR8+DR5/IR8+DR15 synthetic promoter plasmids were built by triple LR reactions performed with Gateway recombination technology using the corresponding promoter plasmid

(synthetic DNA, Thermofisher), the fluorescent marker mTQ fused to NLS Nuclear Localisation Signal and the t35S terminator in the destination vector pLok180 with fastred as a selectable marker.

ARF10 production

ARF10 was overproduced in *Escherichia coli* Rosetta 2 strain. After transformation with plasmid pCC027, bacteria cultures were grown with carbenicillin and chloramphenicol at 37˚C until they achieved an OD600nm of 0.6. Protein expression was induced with isopropyl-β-D-1-thyogalactopiranoside (IPTG) at a final concentration of 0.4 mM at 18˚C overnight. Bacteria cultures were centrifuged. The pellet corresponding to 2% of one liter of *E. coli* culture medium was resuspended and sonicated in 3 ml of a buffer containing 20mM Tris-HCl pH 8.0, 1mM DTT, Pierce antiprotease (1 tablet for 50 ml) and DNAse (7 U). After centrifugation, 5 µl and 1.5 ml of the supernatant (protein concentration of 1 mg/ml) were used for EMSA and Amp-DAP-seq experiments, respectively.

EMSA DNA binding tests

The DNA probes corresponding to the DNA binding sites IR7, ER3, ER13, DR5, DR15 and SS were artificially designed (ThermoFisher). The oligonucleotides for the forward strand were designed with an overhanging G in the 5' position to allow DNA labelling (Table S6). Once the oligonucleotides had been annealed (in 50 mM Tris-HCl pH8.0 and 150 mM NaCl), labelling was carried out with a final concentration of 200 nM of oligonucleotides for 1 h at 37°C with Cy5-dCTP (0.4 µM) and the large fragment (Klenow) of DNA polymerase I in NEB2 buffer (New England Biolabs). The enzyme was then inactivated by incubation for 10 minutes at 65°C. The oligonucleotides were stored at 4°C in the dark. 2% native agarose gels prepared with 0.5X TBE buffer were previously run in 0.5X TBE buffer at 90 V for 90 min at 4˚C. 5 µl of protein (equivalent to a final concentration of 0.5 µM ARF10) was mixed with labelled DNA (final concentration 10 nM), salmon sperm competitor DNA (final concentration 0.02 mg/ml) in a final volume of 20 µL of buffer containing 20 mM HEPES-KOH pH 7.9, 50 mM KCl, 100 mM Tris-HCl pH 8.0 and 2.5% glycerol. Samples were incubated in the dark for 30 min at 4˚C, loaded into the gels and run for 1 hr at 90 V at 4˚C in 0.5x TBE. DNA-protein interactions were visualized with a Cy5 exposure filter (ImageQuant800, GE Healthcare).

DAP-seq

Each DAP-seq replicate was performed using 1.5 ml of soluble fraction equivalent to 10 ml of a 1L culture of ARF10 overproducing *E. coli* Rosetta 2. After centrifugation (3000g, 30 min), the pellet was resuspended in 1.5 ml of buffer (Tris-HCl 10 mM pH 8.0, PBS 1x, NP40 0.0005%, DNase 3u, MgCl2 2mM, DTT 5 mM, Antiprotease EDTA free ThermoFisher 1x) and

sonicated for 3 min (Branson Sonifier, output control 3, duty cycle50%). After centrifugation (15 000 g, 30 min), the soluble supernatant is mixed with 20 µl of Anti-FLAG M2 Magnetic Beads (Sigma-Aldrich) and incubated for 1 h at 4 °C on a rotating wheel. Beads were then immobilized and washed 4 times with 100 µL of DAP buffer (PBS1X, 5mM TCEP, 0,0005% NP40), moved to a new tube and washed once again. DAP-seq input libraries (50 ng)[52] were then added, and protein-DNA mixes were incubated for 1.5 h at 4 °C on a rotating wheel. Beads were immobilized and washed 5 times with 100 µl DAP buffer, moved to a new tube and washed 2 more times. Finally, beads were mixed with 30 µl of elution buffer (10 mM Tris-HCl pH 8.5) and heated for 10 min at 90 °C. IP-ed DNA fragments contained in the elution were amplified by PCR according to published protocol[53] with Illumina TruSeq primers. PCR products were purified using AMPure XP magnetic beads (Beckman Coulter) following manufacturer's instructions. Library molar concentrations were determined by qPCR using NEBNext Library Quant Kit for Illumina (NEB). Libraries were then pooled with equal molarity. Sequencing was done on Illumina HiSeq (Genewiz). Three replicates of this experiment were performed.

DAP-seq analysis

The analysis was performed on the 3 ARF10 DAP-seq replicates. Reads processing and peak calling of ARF10 DAP-seq data were performed as previously described in Lai et al., 2020 [54]. The reads quality were assessed using FastQC (v0.11.7; https://www.bioinformatics.babraham.ac.uk/projects/fastqc/) and adapters were removed by NGmerge[55]. Mapping procedure was performed using Bowtie2 (v2.3.4.1)[56], against the TAIR10 *A.thaliana* reference genome (www.arabidopsis.org). Mapped Reads were then filtered by mapping quality (above 30), by multimapping (reads with single location kept) and a maximum of 2 mismatches were accepted. Duplicates were removed using MACS2 filtered-up[57] (v2.2.7.1; no duplicates authorized). Peakcalling was performed using MACS2 callpeak on each replicate. The resulting peaks were filtered where the input DAP-seq got a high coverage value. Consensus peaks among all the replicates were computed using MSPC[58]. Consensus peaks were then resized at 200 bp centered around the average maximum of the peak.

AuxRE pair configurations enrichment analysis

The best 600 consensus peaks, according to coverage, were used for de novo enrichment motif search using MEME[59] (motif size restricted to 8-10 bp, 5 motifs generated). The prevalent motif found (AuxRE TGTCNN) was then converted to PWM and its predictive power was assessed by ROC, using all but the 600 best peaks versus an equal number of unbound regions, selected randomly but with the same nucleotide length, GC content and type of localization (promoter, UTR, exon, intron or intergenic).

IR, ER, DR enrichment analysis was performed using all consensus peaks. A penalty score was first computed using the PWM by a scanning window python script (Key Resources Table), a threshold of penalty was defined and used to define TF binding sites (TFBS). Then, the relative positions of the detected TFBS were used to compute all possible distances and configurations (IR, ER or DR) present in the set of peaks. Enrichment was computed on all possible configurations by calculating a Z-score. This analysis was repeated with different specificity and sensitivity using three different thresholds, -8, -9 and -10[19]. The latter method was also used to predict all possible AuxRE pairs configurations in the synthetic promoters to validate their design (Table S1) and was adapted for the prediction of IR8, ER13 and DR5 AuxRE pairs done for Figure 6 and 7 using double PWM (see "Averaged gene expression of IR, ER, DR-genes" methods section). The prediction of other TF binding sites was done using MEME software as described in Ma *et al.*[60].

CHO-K1 assays

Cell preparation and reporter expression analysis

50,000 Chinese Hamster Ovary cells (CHO-K1, DSMZ ACC 110) in 500 µl HAM's F12 medium were seeded per well in 24-well plates (Corning) 24 h before transfection. 0,75 µg DNA per well were diluted in 50 µl of OptiMEM and mixed with a PEI/OptiMEM mix [2.5 µl PEI solution (1 mg/ml) in 50 µl OptiMEM] [61]. The ratio between target plasmid and ARF plasmid was 1:1 (0,375 µg each) except for ARF: hIR8 co-transfections, which was done with a 5-fold excess (0.125 µg of IR8 reporter plasmid and 0.625 µg of ARF plasmids) to reduce hIR8 basal level of expression. When comparing saturation levels, the ratios of 1:1 (0.375 µg each), 1:10 (0.075 µg of reporter plasmid and 0.75 µg of ARF plasmids) and 1:50 (0.015 µg of reporter plasmid and 0.75 µg of ARF plasmids) were used. 100 µl of transfection mix was added to each well in a drop-wise manner. Medium was exchanged after 4 h and 200 µl supernatant was taken after 20 h of incubation at 37°C for subsequent SEAP reporter measurement as described in Müller 2014 [62].

Western Blot analysis in CHO-K1 cells

The levels of ARF proteins tagged with HA-tag were determined by SDS-PAGE and immunoblotting. CHOK1 cells were lysed in RIPA buffer (100 mM NaCl, 20 mM TRIS pH 7.5, 1% NP40, 1 mM PMSF, 9.5 mM NaF, 1mM DTT and 1 tablet protease inhibitor per 10 ml) 24 h post transfection and the cell suspension was drawn through a fine syringe (ø 0.40 x 20 mm) to break the cells. After 15 min incubation and centrifugation (15,000 *g* at 4°C for 10 min) the supernatant was stored at -20°C. Total protein amount for normalization was determined with *RC DC* Protein Assay (Bio Rad). Before loading the SDS-PAGE gel (10% gel) the cell extract was heated at 95°C for 10 min in SDS sample buffer (125 mM TRIS pH 6.8, 5% SDS, 43.5% glycerol, 100 mM DTT, 0.02% bromophenol blue, 20% mercaptoethanol). The protoplasts

were thoroughly centrifuged (1,000 *g* for 3 min) and directly diluted in SDS sample buffer and heated at 95°C for 10 min before loading to the SDS-PAGE gel. The SDS-PAGE was run at 150 V for about 1,5 h. The following transfer of proteins from the SDS-PAGE gel to a PVDF membrane was done semi-dry at 54 mA for ~70 min. The PVDF membrane was incubated overnight in blocking solution (5% milk powder in 1x TBS + 0.1% Tween 20) at 4°C. Afterwards, the membrane was decorated with primary antibody in working concentration (1:1,000 AB [for protoplasts] or 1:20,000 [for CHOK1 cell extract] of Anti-HA-Peroxidase [Roche] or 1:2,000 of Anti-Plant-Actin [Agrisera]/ Anti-Mammalian-Actin antibody [Sigma-Aldrich], 5% milk powder in 1x TBS) and incubated for 1,5 h. The secondary antibody for Actin was Anti-Rabbit IgG HRP-linked Antibody diluted in 5% milk powder in 1x TBS and incubated for 1,5 h. Proteins were visually confirmed by chemoluminescence (WesternBright, Biozym Biotech) in an Amersham imager 600.

Protoplast assays

Cell preparation and reporter expression analysis in protoplasts

Protoplasts were isolated from *A. thaliana* seedlings grown on SCA medium (0.32 % (wt/vol) Gamborg's B5 basal salt powder with vitamins (bioWORLD), 4 mM MgSO4·7H2O, 43.8 mM sucrose and 0.8% (wt/vol) phytoagar in H2O, pH 5.8, autoclaved with a 22 °C, 16-h light – 8-h dark cycle (Samodelov 2016). After 2 weeks the leaves were carefully sliced with a scalpel and incubated in darkness at 22 °C overnight in MMC solution (10 mM MES, 40 mM CaCl2·H2O, 467 mM mannitol, pH 5.8, sterile filtered) containing 0.5% cellulase Onozuka R10 and macerozyme R10 (SERVA Electrophoresis). After ~18h, the lysate was carefully mixed, passed through a 70 µm pore size sieve and subsequently centrifuged at low speed. After medium removal the protoplasts were transferred to a MSC solution (10 mM MES, 0.4 M sucrose, 20 mM MgCl2·6H2O, 467 mM mannitol, pH 5.8, sterile filtered) and overlaid with MMM solution (15 mM MgCl2, 5 mM MES, 467 mM mannitol, pH 5.8, sterile filtered) for phase separation. After centrifugation the protoplasts were collected at the interphase and transferred to W5 solution (2 mM MES, 154 mM NaCl, 125 mM CaCl2·2H2O, 5 mM KCl, 5 mM glucose, pH 5.8, sterile filtered) and diluted to 1,000,000 protoplasts per 100 µl after counting. The plasmids were transferred by polyethylene-glycol-mediated transformation. Mixtures of the different plasmids to a final amount of 30 µg DNA were used to transform 1,000,000 protoplasts in non-treated 6-well plates by dropwise addition of a PEG solution (4 g PEG4000, 2.5 ml of 800 mM mannitol, 1 ml of 1 M CaCl2 and 3 ml H2O). Reporter and single ARF plasmids were co-transfected in a 4-fold excess (20 µg reporter plasmid and 5 µg ARF plasmid), while for protoplast transfections with ARF pairs, reporter:ARF plasmid amounts were optimized to reduce variation in renilla luciferase values that might come from differences in the efficiency of the transfection. For ARF6/2/10 and ARF19/1/26 combinations, protoplasts were co-

transfected in a 2-fold excess (5 µg reporter plasmid and 10 µg ARF plasmids). When comparing saturation levels, ratios of 4:1 (20 µg reporter and 5 µg ARF plasmids), 1:2.5 (7.2 µg reporter and 17.8 µg ARF plasmids) and 1:10 (2.3 µg reporter and 22.7 µg ARF plasmids) were used. After 8-min incubation, 120 µl MMM and 1,240 µl W5, with 10% FBS, 64.52 µg µl−1 ampicillin, were added to get a final volume of 1.6 ml protoplast suspension. The protoplasts were kept in darkness for ~24 h at 22°C (modified from Ochoa-Fernandez et al.[63]). Four technical replicates of 80 µl protoplast suspensions (approximately 50,000 protoplasts) were pipetted into two separate 96-well white flat-bottom plates (Costar) for parallel determination of activity of both luciferases. Addition of 20 µl of either FLuc substrate (0.47 mM d-luciferin (Biosynth AG), 20 mM tricine, 2.67 mM MgSO4·7H2O, 0.1 mM EDTA·2H2O, 33.3 mM dithiothreitol, 0.52 mM adenosine 5′-triphosphate, 0.27 mM acetyl– coenzyme A, 5 mM NaOH, 264 µM MgCO3·5H2O, in H2O, pH 8) or renilla luciferase substrate (0.472 mM coelenterazine stock solution in methanol, diluted directly before use, 1:15 in PBS) was performed prior to luminescence determination in a plate reader (determination of 20-min kinetics, integration time 0.1 s)[63]. Three biological replicates of each experiment were done.

ARF-FF fusions kinetics

Isolated protoplasts were transformed with plasmids containing the respective ARFs fused to a Firefly luciferase under control of a constitutive 35S promoter (as described earlier). For each transformation (500,000 protoplasts) with 5 µg of ARF-FF fusion plasmids were used. Shortly after transformation the protoplasts were collected by centrifugation at 100 *g* for 5min and resuspend in 1.6 ml W5 buffer (2 mM MES, 154 mM NaCl, 125 mM $CaCl_2$•H_2O, 5 mM KCl, 5 mM glucose, pH5.8, sterile filtered) addition with 5% FBS(PAN-biotech) and 1.2 mM D-luciferin and 100 µg/ml ampicillin. Each setup was distributed into 4 wells of a 96 well plate as technical replicates and sealed with an optically clear film. Firefly-luminescence was determined in a microplate reader every 30 min (0.1 s integration time) for the time indicated.

ARF-GR driven firefly luciferase expression dynamics

To analyze ARF-GR regulation of expression of reporters after Dex treatment, protoplasts were isolated and transformed as described previously. For each transformation (500,000 protoplasts), 20 µg of reporter with 5 µg of ARF-GR fusion were used. As a control, 20 µg reporter was mixed with either 5 µg ARF or 5 µg empty backbone plasmid. After transformation, protoplasts were processed as above. Each independent transformation was divided over 8 wells (approximately 60,000 protoplasts, 200 µl per well) and transferred to 96-well white flat-bottom plates (Costar). The plates were sealed with an optically clear film (Sarstedt) and the luminescence recorded in a Berthold Centro XS3 LB960 microplate reader every 30 mi (0.1 s integration time). After 4 h, 10 µM dexamethasone (Sigma) was added to each of the 4 replicate wells (from a 10mM stock in EtOH); for mock, the same amount of ethanol (0.2 µl per well) was added.

Plants transformation

All transgenic lines were generated in the Columbia (Col-0) ecotype of *A. thaliana*. Transgenic plants were generated using the floral dip method[64]. Plants were grown on soil at 20°C long-day conditions (16 h light/8 h darkness) till flowering. 50µl *Agrobacterium tumefaciens* GV3101 strain were transfected with synthetic reporter plasmids by electroporation and incubated on LB plates for 2 days at 28°C. Next, one Agrobacterium colony was resuspended in 50µl water, plated on YEB medium and incubated overnight at 28°C. Bacteria were collected by scraping the plate and resuspended in transformation medium ($MgCl_2$ 10mM, sucrose 5%, silwet 0.03%). Arabidopsis flowers were dipped in 200ml of transformation medium for 20-30 seconds. For each construct we selected 2-4 independent homozygous lines and verified by confocal microscopy that the expression of the reporter was similar.

Confocal microscopy

Plants were grown on half-strength Murashige and Skoog (MS) medium supplemented with 1% sucrose and 1% agar at 20°C long-day conditions (16 h light/8 h darkness). Experiments were done on 7 days old seedlings. IAA treatment was done by transferring plants to a new plate supplemented with IAA 1 µM for 16 h. Roots were dyed with propidium iodide at 1µg/ml. Confocal laser scanning microscopy was carried out with Zeiss LSM 980AS2 spectral microscope and Zeiss LSM700 microscopes. Acquisitions were always performed using the same settings (PMT voltage, laser power and detection wavelengths).

ScRNA-seq

Plants were grown in the same conditions as for confocal microscopy experiments. 7 days Arabidopsis roots were cut 700 µm above the meristem and placed in an enzyme solution optimized for Arabidopsis (Mannitol 8%, 400 mM, MES 20 mM, KCl 20 mM, $CaCl_2$ 40 mM, pH 5.8 with Tris, BSA 100 µg/ml, 1.2% cellulase “Onozuka” R10, 0.4% macerozyme R-10 (both Yakult Pharmaceutical Industry CO.). Protoplasts were then filtered through a 20-µm cell strainer and transferred to microcentrifuge tubes for centrifugation.

Protoplasts were centrifuged for 3 mins at 500 *g* and the pellets were washed and resuspended in washing solution twice (Mannitol 8%, MES 20 mM, KCl 20 mM, $CaCl_2$ 10 mM, pH 5.8 with Tris, and BSA 100 µg/ml) and used immediately for single-cell RNAseq.

An aliquot of protoplasts was stained with trypan blue (0.2% final) and checked on a hemocytometer under the microscope to determine cell viability and concentration before loading into the 10x Chromium.

For each experiment, 16,000 cells were loaded in a Single Cell B Chip (10x Genomics). Single-cell libraries were then prepared using the Chromium Single Cell 3´ library kit V3, following manufacturer instructions. Libraries were sequenced with Novaseq 6000 chip SP V2.5 (4

libraries per chip). Raw scRNA-seq data was analyzed by Cell Ranger 5.0.1 (10x Genomics) to generate gene-cell matrices. Gene reads were aligned to the Arabidopsis TAIR10.38. A replicate corresponds to one independent single cell sample from a specific line (DR5, DR15, ER8, IR13) in a specific condition (control vs auxin) on a specific day. Replicates are considered as biological replicates, no technical replicates have been done, ie: two single cell run from the same cell prep. DR5 3 replicates in control and 3 in auxin conditions (CTR 1518, 993,1523 cells, IAA 2339,3604, 2215 cells), DR15 one replicate in control, one in auxin conditions (CTR 1775, IAA 2941 cells), ER8 one replicate in control, one in auxin conditions (CTR 2359, IAA 3491 cells) and IR13 two replicates in control, two in auxin conditions (CTR 1919, 977, IAA, 4231, 5004 cells).

Datasets were integrated and cells mapped using the Seurat package v3.0[33] as follows: first, genes with counts in fewer than three cells were excluded from the analysis. Second, low-quality cells were removed using threshold minimum Unique Molecular Identifier (UMI) 5000, minimum gene 1000, maximum UMI 300000 and maximum gene 12000 per cell. Clustering of cells done by log-normalized raw counts and the 2000 most variable genes were identified for each replicate using the "vst" method in Seurat. Next, we used the *FindIntegrationAnchors* function to identify anchors between the fourteen replicate datasets, using 20 dimensions. A new profile with an integrated expression matrix containing cells from all experiments was produced with the *IntegrateData* function. For dimensionality reduction, the integrated expression matrix was scaled (linear transformed) using the *ScaleData* function, and Principal Component analysis (PCA) performed. The top 30 principal components were selected. Cells or nuclei were clustered using a K-nearest neighbor (KNN) graph, which is based on the Euclidean distance in PCA space. The *FindNeighbors* and *FindClusters* function with a resolution of 0.5 was applied. Next, non-linear dimensional reduction was performed using the UMAP algorithm with the top 30 PCs. Differentially expressed genes were calculated using the *Findmarkers* function in the default settings.

ARFs network generation from scRNAseq data

Correlation test

Correlation between each reporter and each *ARF* expression was done on R using the cor function comparing all the cells of each dataset expressing the reporters with all the expressed genes. Then to test if a given correlation was significant, the same number of cells was randomly distributed in the dataset 1000 times and the correlation analysis was repeated. For each gene the *p*-Value is the FDR of the correlation being higher or lower than the 1000 random distribution.

Odds ratio test

The raw UMI matrix of cells vs expressed genes (except mitochondria and chloroplast genes) was scaled using SCTransform v2[65] and the resulting corrected UMI matrix was then binarized. A gene was simply considered to be expressed (1) if at least 1 UMI was detected in a given cell or declared unexpressed (0) otherwise.

The co-expression of either a single *ARF* or *ARF* pairs with each reporter was tested by computing the associated odds ratio.

The odds ratio for any ARF_k and the reporter is defined as follows:

$$OR(k) = \frac{p(A(k) = 1 \,\&\, R = 1) \times p(A(k) = 0 \,\&\, R = 0)}{p(A(k) = 0 \,\&\, R = 1) \times p(A(k) = 1 \,\&\, R = 0)}$$

where:

A(k) is the event "ARF_k is expressed in a cell"

R is the event "The mTQ reporter is expressed in a cell"

The same reasoning is now applied to A(i,j). The odds ratio for a given pair ARF_i & ARF_j and the reporter is defined as:

$$OR(i,j) = \frac{p(A(i,i) = 1 \,\&\, R = 1) \times p(A(i,j) = 0 \,\&\, R = 0)}{p(A(i,j) = 0 \,\&\, R = 1) \times p(A(i,j) = 1 \,\&\, R = 0)}$$

where:

A(i,j) is the event "ARF_i and ARF_j are expressed in a cell" (A(i) *inter* A(j))

R is the event "The mTQ reporter is expressed in a cell"

For both a single *ARF* and an ARF pair, if the events A and R are independent, then the associated odds ratio is expected to be equal to 1. On the contrary, if ARF_i and ARF_j are more likely to be co-expressed in a cell that expresses the reporter than in a cell that does not (or the other way round, the odds ratio being symmetrical), the odds ratio will be higher than 1. Reciprocally, if one event reduces the odds of the other one, the odds ratio is lower than 1.

To test the statistical significance of the odds ratio, we proceeded to a randomization test to compute a null distribution of odds ratios. The binarized expression vector of the ARF (or the *ARF-ARF* pair) of interest was permuted and the odds ratio between the permuted expression vector and the expression vector of the reporter was computed with 10^6 resampling steps. The null distribution was used to assess the probability that the true odds ratio is significantly higher than expected by chance. We kept putative associations for which the true odds ratio was higher (lower) than the 90th (10th) percentile of the null distribution.

Random forest models

Random forest models were constructed using the integrated single-cell dataset encompassing all four reporters as follows. First, average mTQ expression for each reporter was calculated across clusters in control or auxin conditions. Thus, each of the 40 clusters was given an average expression of each reporter. If a given reporter was not significantly expressed in at least four clusters (LogFoldChange > 0 and adjusted *p*-value < 0.01), then the random forest did not contain enough reporter positive clusters to learn and predict, and would

therefore perform very poorly (data not shown). In that case each cluster in which the reporter was expressed would be sub-clustered using the Louvain algorithm with a resolution of 0.5 (same resolution used for the cluster calling using Seurat integration). Then, the average gene expression of each ARF gene was calculated across clusters using every cell from every replicate in the dataset to improve power. For each reporter, this resulted in a matrix of average reporter expression and average ARF expression across clusters.

For each ARF-ARF gene pairs, interactions were modeled as follows: ARF-X coexpression with ARF-Y was modeled as (ARF-X*ARF-Y). This resulted in a total of three submatrices for each reporter: coexpression (ARF-ARF), independent (ARF-Reporter), and combined (independent plus coexpression).

For each reporter dataset, testing sets were built on each of these matrices by successive random sampling of 25% of clusters until at least three clusters significantly expressed mTQ. The remaining 75% of clusters were used for training. Random forest models predicting mTQ expression matrices were trained for each reporter dataset and each expression matrix and assessed for precision and recall. Parameters were assessed for importance with the varImp function in the randomForest package, which ranks parameters by their average percent increase in mean-squared error of out-of-bag data for each tree in the forest. Meaning, percent of influence of this ARF or ARF-ARF toward improving model performance. The model was run 5 times and for each ARF the percent of influence was averaged and standard deviation calculated. Only the predictions for which the average of the 5 repetitions was higher than the standard deviation between the repetitions were considered.

Averaged gene expression of IR, ER, DR-genes

To predict IR8, ER13 and DR5 sites, we created double PWM, using two A-ARF5 PWM [19] in the corresponding IR8, ER13 and DR5 configurations. Positions in between the two PWMs were filled with zeros to have no influence on the final score. Each PWM was used to scan the Arabidopsis genome with a threshold of -20 for the AuxRE pair. Predicted IR8, ER13 and DR5 were intersected with Arabidopsis promoter regions (500 bp before TSS) obtaining 3 lists of genes with IR8, ER13 and DR5 predicted sites in their 500 bp promoters. We further selected only those sites with a score > -12 for each AuxRE. Altogether, predicted IR8, ER13 and DR5 motifs in the final lists have a total score for the AuxRE pair >-20 and >-12 for each AuxRE. We validated these lists by a computation of conformation enrichment (as described for DAP-seq analysis).

We filtered IR8, ER13 and DR5 lists with those genes DE in our scRNA-seq IAA dataset (Table S3) and divided them into x1, x1-TGTCGG, or x2 and x3 or IR8/ER13 and IR8/DR5 categories. For each gene category, the total averaged expression was calculated for each cell. To identify difference of expression for each cell type a bivariate spatial cross-correlation using local

Moran's-I (LISA)[37] with 1000 simulations for calculating permutation distribution under the null hypothesis of no spatial autocorrelation was performed. A pValue > 0.05 means that the two gene category do not spatially cross correlate for this cell type (Table S4).

QUANTIFICATION AND STATISTICAL ANALYSIS

CHO-K1 experiments

For each CHO-K1 transfection experiment three biological replicates were performed with 4 technical replicates each. For statistical analysis, the three biological replicates were pulled together and treated simultaneously. *t*-tests were performed to determine statistical differences between Mock (reporter) transfections and ARF (reporter + ARF) transfections *(p*-value <0.05). Multiple comparisons (ANOVA-Tukey tests, *p*-value <0.05) were also performed to determine differences between two ARF transfection events (Table S2)

Protoplast experiments

For each protoplast transfection experiment three biological replicates were performed with 4 technical replicates each. Contrary to CHO-K1 cells, for which the expression of the four reporters was similar and close to 0, in protoplasts, the expression of the four reporters was very different, likely due to their regulation by endogenous factors in plant cells. For this reason, protoplast transfection data were normalized to each reporter value. Normalized data from the three biological replicates were pulled together and treated simultaneously. T-tests were performed to determine statistical differences between Mock (reporter) transfections and ARF (reporter + ARF) transfections (*p*-value <0.05). For each ARF we also compared their differential regulation of the four reporters (Table S2).

Reporter quantification in arf background

For reporter lines crossed with *arf* mutants, quantification of the fluorescent protein signal was done using Fiji. ANOVA-Tukey tests were performed to assess significant differences in the mutant backgrounds (p-value <0,05). For each line 10-20 roots were imaged. Reporter lines in *mpS319/arf5* background were not included in this analysis due to the difficulty to quantify and compare the mutant roots that are deeply affected in their development. For this mutant we performed a descriptive analysis of the reporter signal.

Nuclei signal quantification

For the transcriptional lines with ARR7 and PBP11endogenous promoters, nuclei were automatically detected in root confocal images as local maxima in a Gaussian scale-space, using standard deviations varying from 0.8µm to 3.2µm. A binary mask of the root region was extracted by Gaussian smoothing (σ=8µm), thresholding (Otsu method), 2D hole-filling, and largest 3D connected component extraction. Detected nuclei lying further than 5µm from this root region were not retained for the analysis. The fluorescence intensities of mTQ2 and

mCherry (noted TQ and CHE respectively) were then quantified for each retained nucleus as a Gaussian-weighted average of the voxel intensities around the detected points (σ=1µm) to compute a value Log2(TQ/CHE) for each nucleus of the considered root. For each line 8-10 roots were imaged.

These computations were realized using a custom Python script (Key Resources Table) relying on the Tissue Image ToolKit package (https://mosaic.gitlabpages.inria.fr/timagetk/).

SUPPLEMENTAL INFORMATION LEGENDS

Figure S1. Binding motifs and binding properties of ARFs, related to Figures 1 and 2. **A.** Reanalysis of motifs most frequently found in peaks detected in the C-ARF16 DAP-seq data generated by O'Malley et al.[66] . No AuxRE-type motifs were found in this sample. **B**. Comparison of coverages under C-ARF10 consensus peaks for the three DAP-seq replicates. C-ARF10 bound regions were defined as peaks common to the three replicates. **C**. ROC (Receiver Operating Characteristic) curve generated using the DNA motif found for C-ARF10. Bound sequences correspond to the set of peaks detected for C-ARF10, while unbound sequences are generated from the *A. thaliana* genome (see methods). The area under the curve (AUC) indicates the prediction quality associated with the motif. AUC value equal to 0.856 indicates that the model is highly predictive. **D.** Replicate of the EMSAs shown in Figure 1E and Figure 2. **E**. Westerns for HA-tagged ARF detection in CHO-K1 transfected cells **F**. Expression of the synthetic reporters (SEAP) in CHO-K1 cells transfected with each synthetic reporter (Mock) and synthetic reporter + chimeric ARFs 1, 2, 5, 19, 10 and 16. The experiment was performed at three ARF:reporter plasmids ratios: 1:1 (as used in Figure 2F), 10:1 and 50:1, thus keeping constant ARF plasmid and reducing the reporter plasmid used for transfection. The three ratios show similar profiles suggesting that the conditions used are not saturating. 2-3 replicates of the experiment were performed with 3 technical replicates each, which values are represented in the graphs as blue (replicate 1), pink (replicate 2) and yellow (replicate 3) dots. Asterisks indicate significant differences between ARF and Mock (t-test for each biological replicate plus Fisher's Method for Combining *p*-Values). Significant differences between ARF samples are indicated by letters (ANOVA-Tukey, *p*-value <0.05). Data and statistical analysis results available in Table S2.

Figure S2. Transcriptional regulation by ARFs in protoplasts, related to Figure 3. A. **A**. Expression dynamics of ARFs protein amounts in transfected protoplasts. ARF-Firefly (FF) fused versions were used to quantify the levels of each ARF in protoplasts. ARFs accumulate at different amounts in protoplasts. The maximum of accumulation takes place at 8h. **B**. IAA/No IAA fold-change. Note that here, in order to point out the differences between both conditions, the non-normalized data were used to calculate IAA/No IAA fold-change, contrary to the results

shown in Figure 3 and Figure S2, for which all data were normalized to each Mock value. **C**. Expression of the synthetic reporters (FF/REN) hIR8 and hER13 or its mutated versions (hIR8mut and hER13mut) in protoplasts transfected with ARF19. Asterisks indicate significant differences between the reporter and the reporter + ARF19 (t-test, p-value <0.05). The mutations deeply diminish or abolish the activation of the reporter by ARF19 and its auxin responsiveness. **D**. Dynamics of the expression of hER13 and hDR15 reporters (FF) in protoplasts co-transfected with ARF2, 5 or 8 and the corresponding ARF-GR versions induced by DEX treatment. EtOH corresponds to the control condition for the DEX-induction. **E.** Data for the expressions of synthetic reporters after a 6h IAA (1µM) treatment in protoplasts shown in Figure 3. **F**. Expression of the synthetic reporters (FF/REN) in protoplasts transfected with each synthetic reporter (Mock) and synthetic reporter + ARFs 5, 8 and 19. The experiment was performed at three ARF:reporter plasmids ratios: 1:4 (used in Figure 3), 2.5:1 and 10:1. The three experiments show similar profiles suggesting that the conditions used are not saturating. 2 replicates of the experiment were performed with 4 technical replicates each, which values are represented in the graphs as blue (replicate 1) and pink (replicate 2) dots. Asterisk indicates significant differences between ARF and Mock (t-test for each biological replicate plus Fisher's Method for Combining P-Values). Data and statistical analysis results available in Table S2.

Figure S3. **Synthetic reporter expression patterns, related to Figure 4.** Expression pattern for *hIR8*, *hER13*, *hDR5*, *hDR15* and *hIR8*::*mTQ-hER13::Venus-hDR5::mCherry-hDR15::LSMOrange* reporters in the roots of independent transgenic lines than the ones shown in Figure 4.

Figure S4. ARF expression at the single cell scale, related to Figures 4 and 5. UMPAs show *ARF* expressions on the root single cell atlas (Figure 4C) in No IAA and IAA conditions (in purple, cells expressing *ARFs*). The table shows the cell-types where each *ARF* is expressed. Colored cells (B-ARFs in light grey, A-ARFs in dark grey and C-ARFs in black) indicate that the ARF is expressed in the corresponding cell type. A gene was considered to be expressed if its expression in a cell-type was higher than the median of the expression of all Arabidopsis genes in that cell type.

Figure S5. Predictions of ARF and ARF pair candidates regulating synthetic promoters, related to Figures 4 and 5. A. Examples of co-expression of the reporters (in orange) and *ARFs* (in purple) are shown. Levels of co-expression between both are shown in each cell with a gradient of colors where pink is the highest co-expression and grey the lowest. **B**. % of the number of A+B, A+C, A+A, B+C, B+B and C+C pairs of ARFs correlated to reporter expression relative to the total ARF pairs correlations found by the odd-ratio test for each reporter. **C**. Machine learning predictions. Edges on top of the tables indicate ARFs predicted as reporter regulators by themselves while colored cells in the tables indicate ARFs pairs predicted as

reporter regulators. B-ARFs in light grey, A-ARFs in dark grey and C-ARFs in black. Machine learning predictions were repeated 5 times. We took into account only predictions for which the average of the 5 repetitions was higher than the standard deviation of the repetitions.

Figure S6. Synthetic reporter expression in *arf* mutants, related to Figure 5. A. Confocal images of all synthetic reporters in *arf* mutants background tested. Wild-type controls are shown on the left. For all *hIR8* and for *arf5* roots, max projections of z-stacks are shown for better visualization of the reporter signal since it was detected mostly in epidermal cells. In all other cases, single-plane images in the middle of the root are shown. White arrows point at cells expressing *hER13* or *hDR5* reporters in *arf5* mutant background. Asterisks indicate mutants where reporter expression was altered. **B-D**. Analysis of changes in the pattern of expression of *hIR8*, *hER13* and *hDR5* reporters in *arf* mutant backgrounds. This experiment was done in *arf* mutants for which we had previously determined a decrease in reporter expression. (B) For *hIR8*, the reporter expression starts further from the root tip in *arf6* and *arf10* mutants. Arrows in (B): first cells showing expression of the reporter away from the QC. This effect was not quantified in *arf19* as hIR8 was not expressed in a vast majority of roots in this mutant. The graph on the right shows the average of the distance between the root tip and the first cell where mTQ2 signal was detected. Asterisks indicate significant differences between *arf* backgrounds and wt (hIR8) (t-test, *p*-value <0.05). (C) For hER13, we measured the mTQ2 signal profile longitudinally from the quiescent center (QC) to the root tip (dashed lined square). Three peaks of mTQ2 signal were detected in the wild-type (wt), corresponding to mTQ2 expression in the QC cells and the two columella initials cell rows (c.i.1 and c.i.2). The maximum of expression corresponds to c.i.2. In *arf19*, the same pattern is observed but with lower levels of mTQ2 expression. In *arf16*, for 5 out of 13 roots, a change in the pattern of expression was observed, with a maximum of expression in the QC and c.i.1. hER13 expression was not quantified in *arf6* as it was not expressed in most roots analyzed. (D) For *hDR5*, we proceeded similarly to the analysis done on *hER13* lines, but, since the hDR5 expression is more extended, for the mTQ2 quantification we took into account the full length of the root. Several peaks of mTQ2 signal were detected with the intensity of the signal progressively increasing when approaching the root tip, with a maximum in the QC. The signal rapidly decays in the columella. A similar pattern is observed in *arf8* and *arf19* with a lower signal, indicating that in these mutants, contrary to what was observed for *arf6* (Figure 5C-D), *hDR5* expression decreases but the spatial pattern remains the same.

Figure S7. AuxRE pair configuration, number and sequence affect gene expression, related to Figures 6 and 7. A-B. Averaged expressions of the different gene categories from Figures 6 and 7 showing also the IAA-treated condition. UMAPs show the averaged expression per cell of genes with either more than one (x2 or x3) *IR8*, *ER13* or *DR5* , with only one (x1) *IR8*, *ER13* or *DR5*, with x1 *IR8*, *ER13* or *DR5* with at least one TGTCGG AuxRE (E), or with

IR8/*ER13* and *IR8*/*DR5* (F) in overlapped and adjacent configurations. **C-F**. Importance of AuxREs in the expression of auxin responsive genes for *ARR7*, *PBP1* and *IAA11*. For *ARR7* and *PBP1*, constructs where their wild-type (wt) promoter controls the expression of mTQ2 and the mutated promoter the expression of mCherry (the red cross indicates the AuxRE element mutated in each case) were used (C). For *IAA11*, wt and mutated promoter transcriptional reporter lines published in Freire-Rios et al. 2020[41] were used. For each promoter the predicted AuxRE pairs are shown. (D-F): Confocal images of *ARR7*, *PBP1* and *IAA11*. For each line, single-plane images in the middle of the root and max projections of z-stacks are shown. To measure the differences induced by the mutations in *ARR7* and *PBP1* promoters, we quantified mTQ2 and mCherry signals in nuclei and represented the Log2(TQ/CHE) in the projection of the root. This analysis shows for both lines, that the mutation in the promoter induces complex changes in the expression, suggesting that the mutation in the promoters can induce either a decrease or an increase in the expression in a cell-dependent manner. Quantifications are shown on the right of each figure, with n indicating the number of roots analyzed and colours the mTQ2/mCherry ratio variations. For IAA11 lines, GFP expression was quantified independently in IAA11 transcriptional line and in the mutated promoter line. In this case the mutation induces a strong decrease in the signal. Quantifications of the total GFP signal in the root (on max-projections) are shown on the right. Statistical differences (t-test, *p*-value <0.05) between lines and conditions are indicated by an asterisk.

Figure S8. **Expression of fluorescent proteins from promoters with AuxRE pairs combinations, related to Figures 7 and S7. A,B.** Independent transgenic lines for analysis of expression driven by (A) either *ARR7*, *PBP1* or *IAA11* promoters with a mutated AuxRE as in Figure S7C-F or (B) synthetic promoters with combined AuxRE as in Figure 7C.

Table S2. Data and statistical analysis for CHO-K1 and protoplast experiments, related to Figures 2 and 3. Data for CHO-K1 experiments correspond to SEAP values; for protoplast experiments, values in the tables correspond to FF/REN values normalized to the Mock condition in each replicate. For protoplasts ARF-GR kinetic experiments, values in the table correspond to FF measurements along time.

Table S3. scRNA-seq data analyses, related to Figures 4 and 5. Differentially expressed genes (DEG) in scRNA-seq upon IAA treatment in the first two tabs. For each cell type DEG were identified by the Wilcoxon Rank Sum test between Mock condition and auxin treatment. All replicates across the four reporters were used for this test. The first tab represents the raw data. The second tab represents the summary of DEG across all cell types, only the fold-change is represented. ARFs network predictions using correlation, odd-ratios and machine learning analyses (Relates to Figure 5). The results for these analyses are in 4 separate tabs: Correlation ARF-R (reporter), odd ratio ARFpair-R, Machine learning ARF-R and Machine

learning ARFpair-R. Correlation ARF-R tab: Correlations between ARFs and reporters expression. For each reporter, the total correlation with each ARF(Tot_Cor) and the significancy (*p*-value<0.05) of this correlation calculated by the randomization test (Rand Tot_cor) are indicated. Cells are colored for significant positive (green) or negative (red) correlations. Odd ratio ARF pair-R tab: For each reporter, the three first columns correspond to the odds ratio of the ARF pair and the reporter, the 10th percentile and the 90th percentile of the reference distribution. The last column equals 1 or -1 if the true odds ratio is greater than the 90th percentile and lower than the 10th percentile, respectively. Otherwise, it equals 0. Machine learning tabs: "overall" columns indicate the prediction values for the 5 iterations of the random forest model for each ARF or ARF pair. IMP_AVG is the average of the 5 values. IMP_SD is the standard deviation of the 5 values. IMP_SE is the error of the prediction. ARF or ARF pairs were considered as possible regulators of reporter expression if IMP_AVG<IMP_SD.

Table S4. Expression of genes with *IR8*, *ER13*, *DR5* and combinations of these in scRNAseq, related to Figures 6 and 7. Relates to Figures 6 and 7. The different gene sets identified as explained in figures 6, 7 and Figure S7 and the spatial cross-correlation statistical analysis can be found in different excel tabs. In each tab: ATG for each gene, chromosome, start and stop of the -500bp TSS region used for the AuxRE pairs predictions, scores and position of the two AuxREs composing the *IR8*, *ER13* and *DR5* elements and sequence of the AuxRE pair (with an extra 2bp at the beginning and the end of the sequence: an example is shown for the first gene in tab '>1 IR8', where the two AuxREs of the *IR8* motif are colored in blue and flanked by 2bp on each side). Note that for gene categories >1, =1 , =1 –TGTCGG the information in the tabs correspond only to the *IR8*, *ER13* and *DR5* motifs whereas for gene categories IR8+ ER13 and IR8+DR5 (adjacent or overlapping) information is shown for the two AuxRE pairs configurations. The Spatial Cross-correlation statistical analysis was conducted to compare each category of genes having a AuxRE motif. The *p*-value above 0.05 represents the non-correlation and the differential behavior of the gene category compared.

Table S6. List of primers used, related to STAR methods.

REFERENCES

1. Leyser, O. (2018). Auxin Signaling. Plant Physiol. *176*, 465–479. https://doi.org/10.1104/pp.17.00765.

2. Calderón Villalobos, L.I.A., Lee, S., De Oliveira, C., Ivetac, A., Brandt, W., Armitage, L., Sheard, L.B., Tan, X., Parry, G., Mao, H., et al. (2012). A combinatorial TIR1/AFB–Aux/IAA co-receptor system for differential sensing of auxin. Nat Chem Biol *8*, 477–485. https://doi.org/10.1038/nchembio.926.

3. Havens, K.A., Guseman, J.M., Jang, S.S., Pierre-Jerome, E., Bolten, N., Klavins, E., and Nemhauser, J.L. (2012). A Synthetic Approach Reveals Extensive Tunability of Auxin Signaling. Plant Physiology *160*, 135–142. https://doi.org/10.1104/pp.112.202184.

4. Moss, B.L., Mao, H., Guseman, J.M., Hinds, T.R., Hellmuth, A., Kovenock, M., Noorassa, A., Lanctot, A., Villalobos, L.I.A.C., Zheng, N., et al. (2015). Rate Motifs Tune Auxin/Indole-3-Acetic Acid Degradation Dynamics. Plant Physiol. *169*, 803–813. https://doi.org/10.1104/pp.15.00587.
5. Mutte, S.K., Kato, H., Rothfels, C., Melkonian, M., Wong, G.K.-S., and Weijers, D. (2018). Origin and evolution of the nuclear auxin response system. eLife *7*, e33399. https://doi.org/10.7554/eLife.33399.
6. Paque, S., and Weijers, D. (2016). Q&A: Auxin: the plant molecule that influences almost anything. BMC Biol *14*, 67. https://doi.org/10.1186/s12915-016-0291-0.
7. Martin-Arevalillo, R., Thévenon, E., Jégu, F., Vinos-Poyo, T., Vernoux, T., Parcy, F., and Dumas, R. (2019). Evolution of the Auxin Response Factors from charophyte ancestors. PLoS Genet *15*, e1008400. https://doi.org/10.1371/journal.pgen.1008400.
8. Hagen, G., and Guilfoyle, T. (2002). Auxin-responsive gene expression: genes, promoters and regulatory factors. In Auxin Molecular Biology, C. Perrot-Rechenmann and G. Hagen, eds. (Springer Netherlands), pp. 373–385. https://doi.org/10.1007/978-94-010-0377-3_9.
9. Finet, C., Berne-Dedieu, A., Scutt, C.P., and Marlétaz, F. (2013). Evolution of the ARF Gene Family in Land Plants: Old Domains, New Tricks. Molecular Biology and Evolution *30*, 45–56. https://doi.org/10.1093/molbev/mss220.
10. Fontana, M., Roosjen, M., Crespo García, I., Van Den Berg, W., Malfois, M., Boer, R., Weijers, D., and Hohlbein, J. (2023). Cooperative action of separate interaction domains promotes high-affinity DNA binding of *Arabidopsis thaliana* ARF transcription factors. Proc. Natl. Acad. Sci. U.S.A. *120*, e2219916120. https://doi.org/10.1073/pnas.2219916120.
11. Cancé, C., Martin-Arevalillo, R., Boubekeur, K., and Dumas, R. (2022). Auxin response factors are keys to the many auxin doors. New Phytologist *235*, 402–419. https://doi.org/10.1111/nph.18159.
12. Tiwari, S.B., Hagen, G., and Guilfoyle, T. (2003). The Roles of Auxin Response Factor Domains in Auxin-Responsive Transcription. Plant Cell *15*, 533–543. https://doi.org/10.1105/tpc.008417.
13. Flores-Sandoval, E., Eklund, D.M., Hong, S., Alvarez, J.P., Fisher, T.J., Lampugnani, E.R., Golz, J.F., Vázquez-Lobo, A., Dierschke, T., Lin, S., et al. (2018). Class C ARF s evolved before the origin of land plants and antagonize differentiation and developmental transitions in *Marchantia polymorpha*. New Phytol *218*, 1612–1630. https://doi.org/10.1111/nph.15090.
14. Kato, H., Mutte, S.K., Suzuki, H., Crespo, I., Das, S., Radoeva, T., Fontana, M., Yoshitake, Y., Hainiwa, E., van den Berg, W., et al. (2020). Design principles of a minimal auxin response system. Nat. Plants *6*, 473–482. https://doi.org/10.1038/s41477-020-0662-y.
15. Vernoux, T., Brunoud, G., Farcot, E., Morin, V., Van den Daele, H., Legrand, J., Oliva, M., Das, P., Larrieu, A., Wells, D., et al. (2011). The auxin signalling network translates dynamic input into robust patterning at the shoot apex. Mol Syst Biol *7*, 508. https://doi.org/10.1038/msb.2011.39.
16. Lavy, M., Prigge, M.J., Tao, S., Shain, S., Kuo, A., Kirchsteiger, K., and Estelle, M. (2016). Constitutive auxin response in Physcomitrella reveals complex interactions between Aux/IAA and ARF proteins. eLife *5*, e13325. https://doi.org/10.7554/eLife.13325.
17. Ulmasov, T., Liu, Z.-B., Hagen, G., and Guilfoyle', T.J. Composite Structure of Auxin Response Elements.
18. Ulmasov, T., Hagen, G., and Guilfoyle, T.J. (1997). ARF1, a Transcription Factor That Binds to Auxin Response Elements. Science *276*, 1865–1868. https://doi.org/10.1126/science.276.5320.1865.

19. Stigliani, A., Martin-Arevalillo, R., Lucas, J., Bessy, A., Vinos-Poyo, T., Mironova, V., Vernoux, T., Dumas, R., and Parcy, F. (2019). Capturing Auxin Response Factors Syntax Using DNA Binding Models. Molecular Plant *12*, 822–832. https://doi.org/10.1016/j.molp.2018.09.010.
20. Pierre-Jerome, E., Moss, B.L., Lanctot, A., Hageman, A., and Nemhauser, J.L. (2016). Functional analysis of molecular interactions in synthetic auxin response circuits. Proc. Natl. Acad. Sci. U.S.A. *113*, 11354–11359. https://doi.org/10.1073/pnas.1604379113.
21. Galli, M., Khakhar, A., Lu, Z., Chen, Z., Sen, S., Joshi, T., Nemhauser, J.L., Schmitz, R.J., and Gallavotti, A. (2018). The DNA binding landscape of the maize AUXIN RESPONSE FACTOR family. Nat Commun *9*, 4526. https://doi.org/10.1038/s41467-018-06977-6.
22. O'Malley, R.C., Huang, S.C., Song, L., Lewsey, M.G., Bartlett, A., Nery, J.R., Galli, M., Gallavotti, A., and Ecker, J.R. (2016). Cistrome and Epicistrome Features Shape the Regulatory DNA Landscape. Cell *165*, 1280–1292. https://doi.org/10.1016/j.cell.2016.04.038.
23. Ulmasov, T., Murfett, J., Hagen, G., and Guilfoyle, T.J. (1997). Aux/lAA Proteins Repress Expression of Reporter Genes Containing Natural and Highly Active Synthetic Auxin Response Elements. The Plant Cell, 1963-1971,.
24. Sabatini, S., Beis, D., Wolkenfelt, H., Murfett, J., Guilfoyle, T., Malamy, J., Benfey, P., Leyser, O., Bechtold, N., Weisbeek, P., et al. (1999). An Auxin-Dependent Distal Organizer of Pattern and Polarity in the Arabidopsis Root. Cell *99*, 463–472. https://doi.org/10.1016/S0092-8674(00)81535-4.
25. Liao, C.-Y., Smet, W., Brunoud, G., Yoshida, S., Vernoux, T., and Weijers, D. (2015). Reporters for sensitive and quantitative measurement of auxin response. Nature Methods *12*, 207–210. https://doi.org/10.1038/nmeth.3279.
26. Boer, D.R., Freire-Rios, A., van den Berg, W.A.M., Saaki, T., Manfield, I.W., Kepinski, S., López-Vidrieo, I., Franco-Zorrilla, J.M., de Vries, S.C., Solano, R., et al. (2014). Structural Basis for DNA Binding Specificity by the Auxin-Dependent ARF Transcription Factors. Cell *156*, 577–589. https://doi.org/10.1016/j.cell.2013.12.027.
27. Ulmasov, T., Hagen, G., and Guilfoyle, T.J. (1999). Activation and repression of transcription by auxin-response factors. Proc. Natl. Acad. Sci. U.S.A. *96*, 5844–5849. https://doi.org/10.1073/pnas.96.10.5844.
28. Morffy, N., Van Den Broeck, L., Miller, C., Emenecker, R.J., Bryant, J.A., Lee, T.M., Sageman-Furnas, K., Wilkinson, E.G., Pathak, S., Kotha, S.R., et al. (2024). Identification of plant transcriptional activation domains. Nature *632*, 166–173. https://doi.org/10.1038/s41586-024-07707-3.
29. Már, M., Nitsenko, K., and Heidarsson, P.O. (2023). Multifunctional Intrinsically Disordered Regions in Transcription Factors. Chemistry A European J *29*, e202203369. https://doi.org/10.1002/chem.202203369.
30. Zhao, Z., Andersen, S.U., Ljung, K., Dolezal, K., Miotk, A., Schultheiss, S.J., and Lohmann, J.U. (2010). Hormonal control of the shoot stem-cell niche. Nature *465*, 1089–1092. https://doi.org/10.1038/nature09126.
31. Simonini, S., Bencivenga, S., Trick, M., and Østergaard, L. (2017). Auxin-Induced Modulation of ETTIN Activity Orchestrates Gene Expression in Arabidopsis. Plant Cell *29*, 1864–1882. https://doi.org/10.1105/tpc.17.00389.
32. Brunoud, G., Wells, D.M., Oliva, M., Larrieu, A., Mirabet, V., Burrow, A.H., Beeckman, T., Kepinski, S., Traas, J., Bennett, M.J., et al. (2012). A novel sensor to map auxin response and distribution at high spatio-temporal resolution. Nature *482*, 103–106. https://doi.org/10.1038/nature10791.

33. Hao, Y., Hao, S., Andersen-Nissen, E., Mauck, W.M., Zheng, S., Butler, A., Lee, M.J., Wilk, A.J., Darby, C., Zager, M., et al. (2021). Integrated analysis of multimodal single-cell data. Cell *184*, 3573-3587.e29. https://doi.org/10.1016/j.cell.2021.04.048.
34. Chandler, J.W. (2016). Auxin response factors: Auxin response factors. Plant, Cell & Environment *39*, 1014–1028. https://doi.org/10.1111/pce.12662.
35. Okushima, Y., Overvoorde, P.J., Arima, K., Alonso, J.M., Chan, A., Chang, C., Ecker, J.R., Hughes, B., Lui, A., Nguyen, D., et al. (2005). Functional Genomic Analysis of the *AUXIN RESPONSE FACTOR* Gene Family Members in *Arabidopsis thaliana* : Unique and Overlapping Functions of *ARF7* and *ARF19*. The Plant Cell *17*, 444–463. https://doi.org/10.1105/tpc.104.028316.
36. Mironova, V.V., Omelyanchuk, N.A., Wiebe, D.S., and Levitsky, V.G. (2014). Computational analysis of auxin responsive elements in the Arabidopsis thaliana L. genome. BMC Genomics *15*, S4. https://doi.org/10.1186/1471-2164-15-S12-S4.
37. Chen, Y. (2015). A New Methodology of Spatial Cross-Correlation Analysis. PLoS ONE *10*, e0126158. https://doi.org/10.1371/journal.pone.0126158.
38. Novikova, D.D., Omelyanchuk, N., Korosteleva, A., Albrecht, C., Lavrekha, V.V., Weijers, D., and Mironova, V. (2024). Mechanism of auxin-dependent gene regulation through composite auxin response elements. Preprint at Plant Biology, https://doi.org/10.1101/2024.07.16.603724 https://doi.org/10.1101/2024.07.16.603724.
39. Müller, B., and Sheen, J. (2008). Cytokinin and auxin interaction in root stem-cell specification during early embryogenesis. Nature *453*, 1094–1097. https://doi.org/10.1038/nature06943.
40. Benjamins, R., Ampudia, C.S.G., Hooykaas, P.J.J., and Offringa, R. (2003). PINOID-Mediated Signaling Involves Calcium-Binding Proteins. Plant Physiology *132*, 1623–1630. https://doi.org/10.1104/pp.103.019943.
41. Freire-Rios, A., Tanaka, K., Crespo, I., Van Der Wijk, E., Sizentsova, Y., Levitsky, V., Lindhoud, S., Fontana, M., Hohlbein, J., Boer, D.R., et al. (2020). Architecture of DNA elements mediating ARF transcription factor binding and auxin-responsive gene expression in *Arabidopsis*. Proc. Natl. Acad. Sci. U.S.A. *117*, 24557–24566. https://doi.org/10.1073/pnas.2009554117.
42. Finet, C., Berne-Dedieu, A., Scutt, C.P., and Marlétaz, F. (2013). Evolution of the ARF Gene Family in Land Plants: Old Domains, New Tricks. Molecular Biology and Evolution *30*, 45–56. https://doi.org/10.1093/molbev/mss220.
43. Truskina, J., Han, J., Chrysanthou, E., Galvan-Ampudia, C.S., Lainé, S., Brunoud, G., Macé, J., Bellows, S., Legrand, J., Bågman, A.-M., et al. (2021). A network of transcriptional repressors modulates auxin responses. Nature *589*, 116–119. https://doi.org/10.1038/s41586-020-2940-2.
44. Rademacher, E.H., Möller, B., Lokerse, A.S., Llavata-Peris, C.I., van den Berg, W., and Weijers, D. (2011). A cellular expression map of the Arabidopsis AUXIN RESPONSE FACTOR gene family: A cellular expression map of ARF gene expression. The Plant Journal *68*, 597–606. https://doi.org/10.1111/j.1365-313X.2011.04710.x.
45. Ouellet, F., Overvoorde, P.J., and Theologis, A. IAA17/AXR3: Biochemical Insight into an Auxin Mutant Phenotype.
46. Li, J.-F., Bush, J., Xiong, Y., Li, L., and McCormack, M. (2011). Large-Scale Protein-Protein Interaction Analysis in Arabidopsis Mesophyll Protoplasts by Split Firefly Luciferase Complementation. PLoS ONE *6*, e27364. https://doi.org/10.1371/journal.pone.0027364.
47. Brophy, J.A.N., Magallon, K.J., Duan, L., Zhong, V., Ramachandran, P., Kniazev, K., and Dinneny, J.R. (2022). Synthetic genetic circuits as a means of reprogramming plant roots. Science *377*, 747–751. https://doi.org/10.1126/science.abo4326.

48. Belcher, M.S., Vuu, K.M., Zhou, A., Mansoori, N., Agosto Ramos, A., Thompson, M.G., Scheller, H.V., Loqué, D., and Shih, P.M. (2020). Design of orthogonal regulatory systems for modulating gene expression in plants. Nat Chem Biol, 857–865.
49. Ochoa-Fernandez, R., Abel, N.B., Wieland, F.-G., Schlegel, J., Koch, L.-A., Miller, J.B., Engesser, R., Giuriani, G., Brandl, S.M., Timmer, J., et al. (2020). Optogenetic control of gene expression in plants in the presence of ambient white light. Nat Methods *17*, 717–725. https://doi.org/10.1038/s41592-020-0868-y.
50. Beyer, H.M., Gonschorek, P., Samodelov, S.L., Meier, M., Weber, W., and Zurbriggen, M.D. (2015). AQUA Cloning: A Versatile and Simple Enzyme-Free Cloning Approach. PLoS ONE *10*, e0137652. https://doi.org/10.1371/journal.pone.0137652.
51. Beyer, H.M., Gonschorek, P., Samodelov, S.L., Meier, M., Weber, W., and Zurbriggen, M.D. (2015). AQUA Cloning: A Versatile and Simple Enzyme-Free Cloning Approach. PLoS ONE *10*, e0137652. https://doi.org/10.1371/journal.pone.0137652.
52. Lai, X., Blanc-Mathieu, R., GrandVuillemin, L., Huang, Y., Stigliani, A., Lucas, J., Thévenon, E., Loue-Manifel, J., Turchi, L., Daher, H., et al. (2021). The LEAFY floral regulator displays pioneer transcription factor properties. Molecular Plant *14*, 829–837. https://doi.org/10.1016/j.molp.2021.03.004.
53. Bartlett, A., O'Malley, R.C., Huang, S.C., Galli, M., Nery, J.R., Gallavotti, A., and Ecker, J.R. (2017). Mapping genome-wide transcription-factor binding sites using DAP-seq. Nat Protoc *12*, 1659–1672. https://doi.org/10.1038/nprot.2017.055.
54. Lai, X., Stigliani, A., Lucas, J., Hugouvieux, V., Parcy, F., and Zubieta, C. (2020). Genome-wide binding of SEPALLATA3 and AGAMOUS complexes determined by sequential DNA-affinity purification sequencing. Nucleic Acids Research *48*, 9637–9648. https://doi.org/10.1093/nar/gkaa729.
55. Gaspar, J.M. (2018). NGmerge: merging paired-end reads via novel empirically-derived models of sequencing errors. BMC Bioinformatics *19*, 536. https://doi.org/10.1186/s12859-018-2579-2.
56. Langmead, B., and Salzberg, S.L. (2012). Fast gapped-read alignment with Bowtie 2. Nature Methods *9*, 357–359. https://doi.org/10.1038/nmeth.1923.
57. Zhang, Y., Liu, T., Meyer, C.A., Eeckhoute, J., Johnson, D.S., Bernstein, B.E., Nusbaum, C., Myers, R.M., Brown, M., Li, W., et al. (2008). Model-based Analysis of ChIP-Seq (MACS). Genome Biol *9*, R137. https://doi.org/10.1186/gb-2008-9-9-r137.
58. Jalili, V., Matteucci, M., Masseroli, M., and Morelli, M.J. (2015). Using combined evidence from replicates to evaluate ChIP-seq peaks. Bioinformatics *31*, 2761–2769. https://doi.org/10.1093/bioinformatics/btv293.
59. Bailey, T.L., Johnson, J., Grant, C.E., and Noble, W.S. (2015). The MEME Suite. Nucleic Acids Res *43*, W39–W49. https://doi.org/10.1093/nar/gkv416.
60. Ma, W., Noble, W.S., and Bailey, T.L. (2014). Motif-based analysis of large nucleotide data sets using MEME-ChIP. Nat Protoc *9*, 1428–1450. https://doi.org/10.1038/nprot.2014.083.
61. Blomeier, T., Fischbach, P., Koch, L., Andres, J., Miñambres, M., Beyer, H.M., and Zurbriggen, M.D. (2021). Blue Light-Operated CRISPR/Cas13b-Mediated mRNA Knockdown (Lockdown). Advanced Biology *5*, 2000307. https://doi.org/10.1002/adbi.202000307.
62. Müller, K., Zurbriggen, M.D., and Weber, W. (2014). Control of gene expression using a red- and far-red light–responsive bi-stable toggle switch. Nat Protoc *9*, 622–632. https://doi.org/10.1038/nprot.2014.038.
63. Ochoa-Fernandez, R., Abel, N.B., Wieland, F.-G., Schlegel, J., Koch, L.-A., Miller, J.B., Engesser, R., Giuriani, G., Brandl, S.M., Timmer, J., et al. (2020). Optogenetic control

of gene expression in plants in the presence of ambient white light. Nature Methods *17*, 717–725. https://doi.org/10.1038/s41592-020-0868-y.
64. Clough, S.J., and Bent, A.F. (1998). Floral dip a simplified method for Agrobacterium -mediated transformation of Arabidopsis thaliana.
65. Hafemeister, C., and Satija, R. (2019). Normalization and variance stabilization of single-cell RNA-seq data using regularized negative binomial regression. Genome Biol *20*, 296. https://doi.org/10.1186/s13059-019-1874-1.
66. O'Malley, R.C., Huang, S.C., Song, L., Lewsey, M.G., Bartlett, A., Nery, J.R., Galli, M., Gallavotti, A., and Ecker, J.R. (2016). Cistrome and Epicistrome Features Shape the Regulatory DNA Landscape. Cell *165*, 1280–1292. https://doi.org/10.1016/j.cell.2016.04.038.
67. Nagpal, P, Ellis, C.M., Weber, H., Ploense, S.E., Barkawi, L.S., Guilfoyle, T.J., Hagen, G., Alonso, J.M., Cohen, J.D., Farmer, E.E., Ecker, J.R. and Reed, J.W (2005). Auxin response factors ARF6 and ARF8 promote jasmonic acid production and flower maturation. Development 132, 4107–4118. https://doi.org/10.1242/dev.01955
68. Wang, J.-W., Wang, L.-J., Mao, Y.-B., Cai, W.-J., Xue, H.-W. and Chen, X.-Y. Control of Root Cap Formation by MicroRNA-Targeted Auxin Response Factors in Arabidopsis. The Plant Cell 17, 2204–2216. https://doi.org/10.1105/tpc.105.033076

Key resources table

REAGENT or RESOURCE	SOURCE	IDENTIFIER
Antibodies		
Anti-FLAG M2 Magnetic Beads	Sigma Aldrich	M8823-1ML
Anti-HA-Peroxidase	Roche	12013819001
Anti-Actin (plant)	Agrisera	As132640
Anti-Actin (mammalian)	Sigma Aldrich	A3853
Anti-Rabbit IgG HRP-linked antibody	Cell signaling technology	7074S
Bacterial and virus strains		
Escherichia coli Rosetta2	Sigma Aldrich	71402
Escherichia coli DH5α	Thermo Fisher Scientific	18265017
Escherichia coli TOP10	Thermo Fisher Scientific	C404003
Agrobacterium tumefaciens GV3101	GoldBio	CC-207-5x50
Biological samples		
Chemicals, peptides, and recombinant proteins		
Isopropyl-β-D-1-thyogalactopiranoside	Carl Roth	2316.4
DTT,	Acros Organics	165680250
Pierce antiprotease EDTA free	ThermoFischer	A32965
DNAse	ThermoFischer	EN0521
fetal bovine serum	PAN	P30-3602
Cy5	Cytiva	PA55021
Agarose	Carl Roth	3810.4
Salmon sperm competitor DNA	Sigma-Aldrich	31149-50G-F
OptiMEM	Gibco	22600-134
PEI/OptiMEM	polysciences	23966-1
Gamborg's B5 basal salt powder with vitamins	bioWORLD	30630059
Plant agar	Duchefa	P1001
cellulase Onozuka R10 for protoplast assay	Serva	16419.03
macerozyme R10 for protoplast assay	Serva	28302.03
cellulase Onozuka R10 for scRNAseq	Yakult Pharmaceutical Industry	N/A
macerozyme R10 for scRNAseq	Yakult Pharmaceutical Industry	N/A
D-luciferin (Biosynth AG)	Carbosynth	FL08607
coelenterazine	Roth	4094.4
Murashige and Skoog Medium	Duchefa	M0221
Indole-3-acetic acid (IAA	Duchefa	I0901
Propidium iodide	Sigma-Aldrich	P4170
Trypan blue	Sigma-Aldrich	T8154
HAMs Medium	PAN	P04-14500
Critical commercial assays		
Klenow DNA polymerase I	NEB	M0210S
Gateway technology: LR clonase II plus	Invitrogen	12538-120
NEBNext Library Quant Kit	NEB	E7630

Single Cell B Chip	10x Genomics	PN-1000073
Chromium Single Cell 3´ library kit V3	10x Genomics	PN-1000075
phusion polymerase	ThermoFisher	F530S
NucleoSpin Plasmid EasyPure, Mini kit	Macherey Nagel	REF 740727.50
NucleoBond Xtra Midi	Macherey Nagel	REF 740410.50
Deposited data		
C- ARF10 DAP-seq data	This paper	GSE237176
scRNAseq data	This paper	GSE241573
Confocal microscopy images	This paper	10.5281/zenodo.14924818
Experimental models: Cell lines		
Experimental models: Organisms/strains		
CHO-K1 cells	DSMZ, Braunschweig, Germany	ACC 110
Arabidopsis thaliana Col-0	NASC	N1093
proIAA11::GFP	Freire-Rios et al.[41]	N/A
proIAA11Δ1::GFP	Freire-Rios et al.[41]	N/A
proARR7::mTQ2—proARR7ΔIR7::mCHERRY	This paper	N/A
proPBP1::mTQ2—proPBPΔIR7::mCHERRY	This paper	N/A
hIR8::mTQ	This paper	N/A
hER13::mTQ	This paper	N/A
hDR5::mTQ	This paper	N/A
hDR15::mTQ	This paper	N/A
hIR8::*mTQ*, *hER13::Venus*, *hDR5::mCherry*, *hDR15::LSMOrange*	This paper	N/A
hIR8/hER13::mTQ overlapped	This paper	N/A
hIR8/hER13::mTQ adjacent	This paper	N/A
hIR8/hER13::mTQ juxtaposed	This paper	N/A
hIR8/hDR5::mTQ overlapped	This paper	N/A
hIR8/hDR5::mTQ adjacent	This paper	N/A
hIR8/hDR5::mTQ juxtaposed	This paper	N/A
hIR8/hDR15::mTQ overlapped	This paper	N/A
hIR8/hDR15::mTQ adjacent	This paper	N/A
hIR8/hDR15::mTQ juxtaposed	This paper	N/A
arf1-3	NASC	N24599
arf3 - ett-13	NASC	N540513
arf5 - mpS319	NASC	N521319
arf6-1	NASC	N24606
arf7-1	NASC	N24607
arf8-3	Nagpal et al.[67]	N/A
arf19-1	NASC	N24617
arf10-2	Wang et al.[68]	N/A
arf16-2	NASC	N521448
hIR8::mTQ arf3-2	This paper	N/A
hIR8::mTQ arf5-mpS319	This paper	N/A
hIR8::mTQ arf6-1	This paper	N/A
hIR8::mTQ arf8-2	This paper	N/A
hIR8::mTQ arf19-1	This paper	N/A

hIR8::mTQ arf10-2	This paper	N/A
hER13::mTQ arf1-3	This paper	N/A
hER13::mTQ arf3-2	This paper	N/A
hER13::mTQ arf5-mpS319	This paper	N/A
hER13::mTQ arf6-1	This paper	N/A
hER13::mTQ arf7-1	This paper	N/A
hER13::mTQ arf8-2	This paper	N/A
hER13::mTQ arf19-1	This paper	N/A
hER13::mTQ arf10-2	This paper	N/A
hER13::mTQ arf16-2	This paper	N/A
hDR5::mTQ arf1-3	This paper	N/A
hDR5::mTQ arf3-2	This paper	N/A
hDR5::mTQ arf5-mpS319	This paper	N/A
hDR5::mTQ arf6-1	This paper	N/A
hDR5::mTQ arf7-1	This paper	N/A
hDR5::mTQ arf8-2	This paper	N/A
hDR5::mTQ arf19-1	This paper	N/A
hDR5::mTQ arf10-2	This paper	N/A
hDR5::mTQ arf16-2	This paper	N/A
Oligonucleotides		
Primers for cloning, see Table S6	This paper	N/A
Primers for EMSA, see Table S6	This paper	N/A
Primers for phenotyping, see Table S6	This paper	N/A
Recombinant DNA		
pPSG-IBA162	IBA Lifesciences	15613778
pCC027 (ARF10)	This paper	N/A
pJA032 chimeric ARF-HA (CHO-K1 transformation)	This paper	N/A
pDESTR4-R3 ARF (protoplast transformation)	This paper	N/A
pDESTR4-R3 ARF-luciferase-3xFLAG	This paper	N/A
pDESTR4-R3 ARF-GR	This paper	N/A
pK7m34GW *hIR8 ::mTQ*	This paper	N/A
pK7m34GW *hER13 ::mTQ*	This paper	N/A
pK7m34GW *hDR5 ::mTQ*	This paper	N/A
pK7m34GW *hDR15 ::mTQ*	This paper	N/A
pICH FASTRED *hIR8::mTQ-hER13::Venus-hDR5::mCherry-hDR15::LSMOrange*	This paper	N/A
pLok180 IR8/ER13 (overlapped, adjacent, juxtaposed)	This paper	N/A
pLok180 IR8/DR5 (overlapped, adjacent, juxtaposed)	This paper	N/A
pLok180 IR8/DR15 (overlapped, adjacent, juxtaposed)	This paper	N/A
pICH FASTRED *proARR7::mTQ2—proARR7ΔIR7::mCHERRY*	This paper	N/A
pICH FASTRED *proPBP1::mTQ2—proPBP1ΔIR7::mCHERRY*	This paper	N/A
Software and algorithms		
Cell Ranger 5.0.1	10x Genomics	https://www.10xgenomics.com/support/software/cell-ranger/
Fiji	https://fiji.sc	2.16.0

FastQC (v0.11.7)	Babraham institute	https://www.bioinformatics.babraham.ac.uk/projects/fastqc/
NGmerge	Gaspar[55]	https://github.com/jsh58/NGmerge
Bowtie2 (v2.3.4.1)	Langmead and Salzberg[56]	https://bowtie-bio.sourceforge.net/bowtie2/
MACS2	Zhang et al.[57]	https://pypi.org/project/MACS2/
MSPC	Jalili et al.[58]	https://genometric.github.io/MSPC/
MEME	Bailet et al.[59]	https://meme-suite.org/meme/
Seurat package v3.0		https://github.com/satijalab/seurat
Scanning window python script	This paper	https://github.com/Bioinfo-LPCV-RDF/TF_genomic_analysis
Correlation test script	This paper	https://github.com/BrunoGuillotin/ScRNAseq_Correlation_with_Random.git
Odd ratio test script	This paper	https://gitbio.ens-lyon.fr/ahugues/chromauxi
Random forest models script	This paper	https://github.com/govissers/ARF_Binding_2023.git
Other		

Figure 1

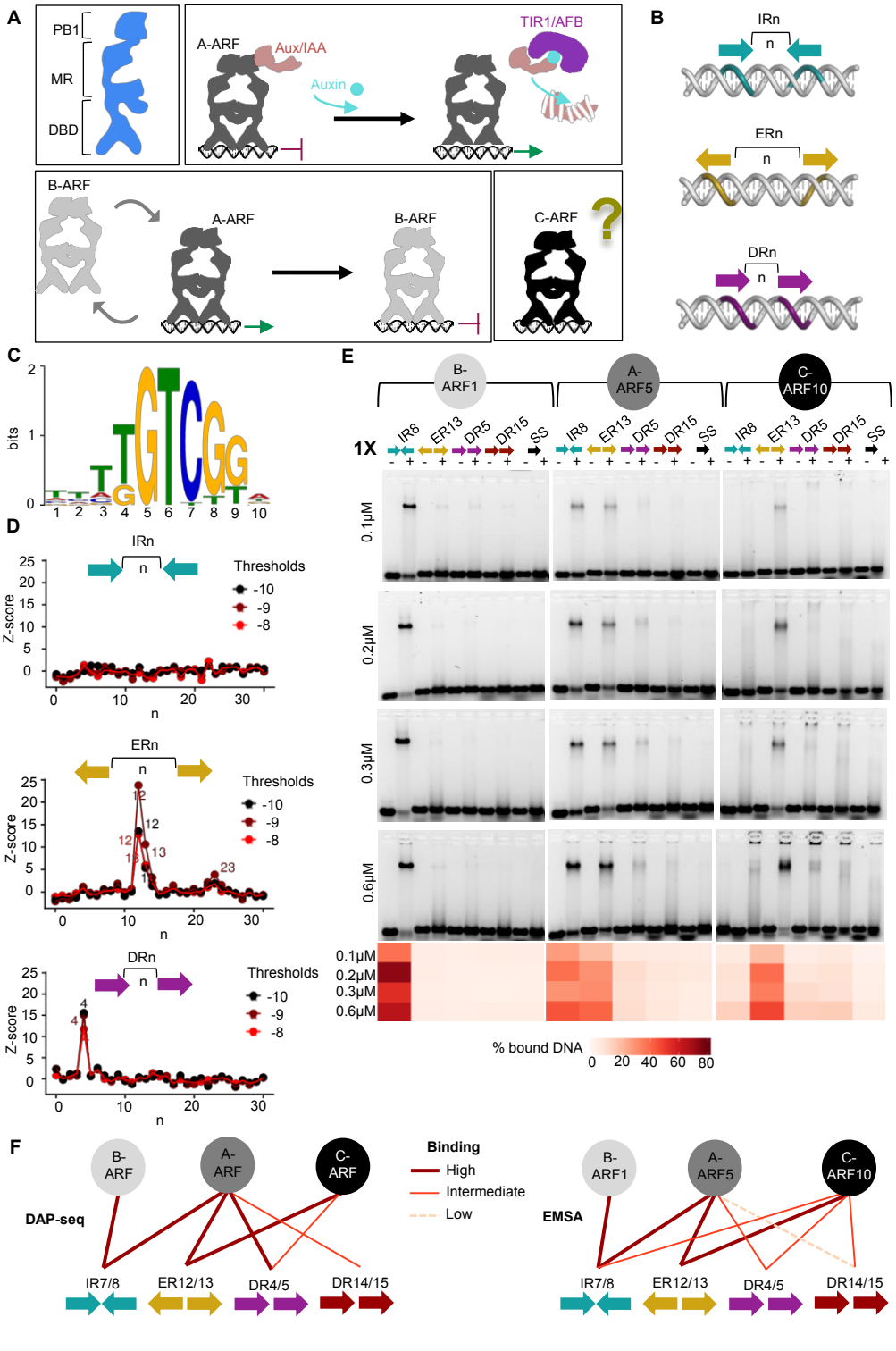

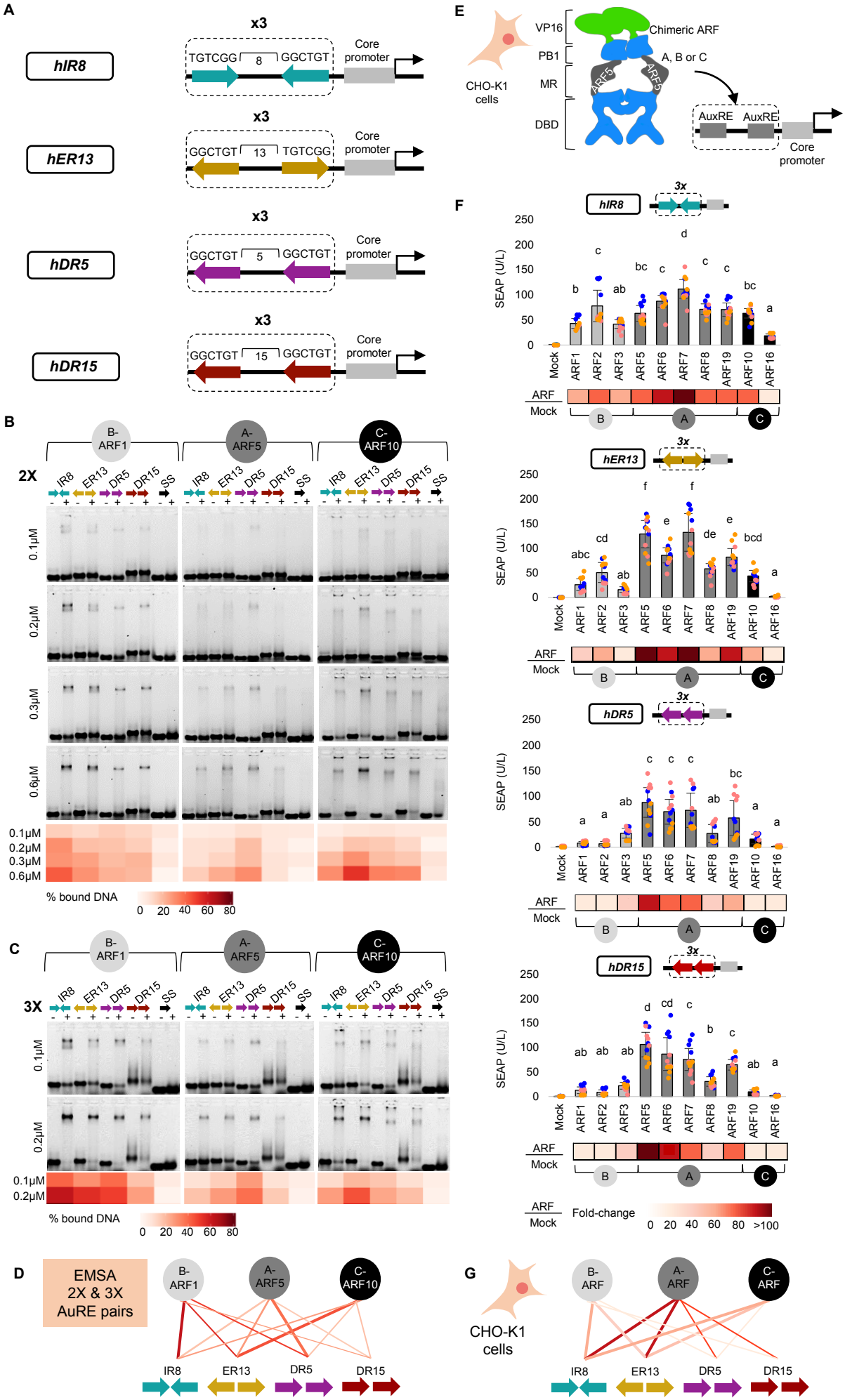
A
hIR8
hER13
hDR5
hDR15
x3
TGTCGG 8 GGCTGT
GGCTGT 13 TGTCGG
GGCTGT 5 GGCTGT
GGCTGT 15 GGCTGT
Core promoter
B
2X
B-ARF1
A-ARF5
C-ARF10
IR8
ER13
DR5
DR15
SS
0.1μM
0.2μM
0.3μM
0.6μM
% bound DNA
0 20 40 60 80
C
3X
D
EMSA
2X & 3X
AuRE pairs
E
CHO-K1 cells
VP16
PB1
MR
DBD
Chimeric ARF
A, B or C
ARF5
ARF6
AuxRE
Core promoter
F
3x
SEAP (U/L)
Mock
ARF1
ARF2
ARF3
ARF5
ARF6
ARF7
ARF8
ARF19
ARF10
ARF16
ARF
Mock
Fold-change
0 20 40 60 80 >100
G
CHO-K1 cells
B-ARF
A-ARF
C-ARF

Figure 3

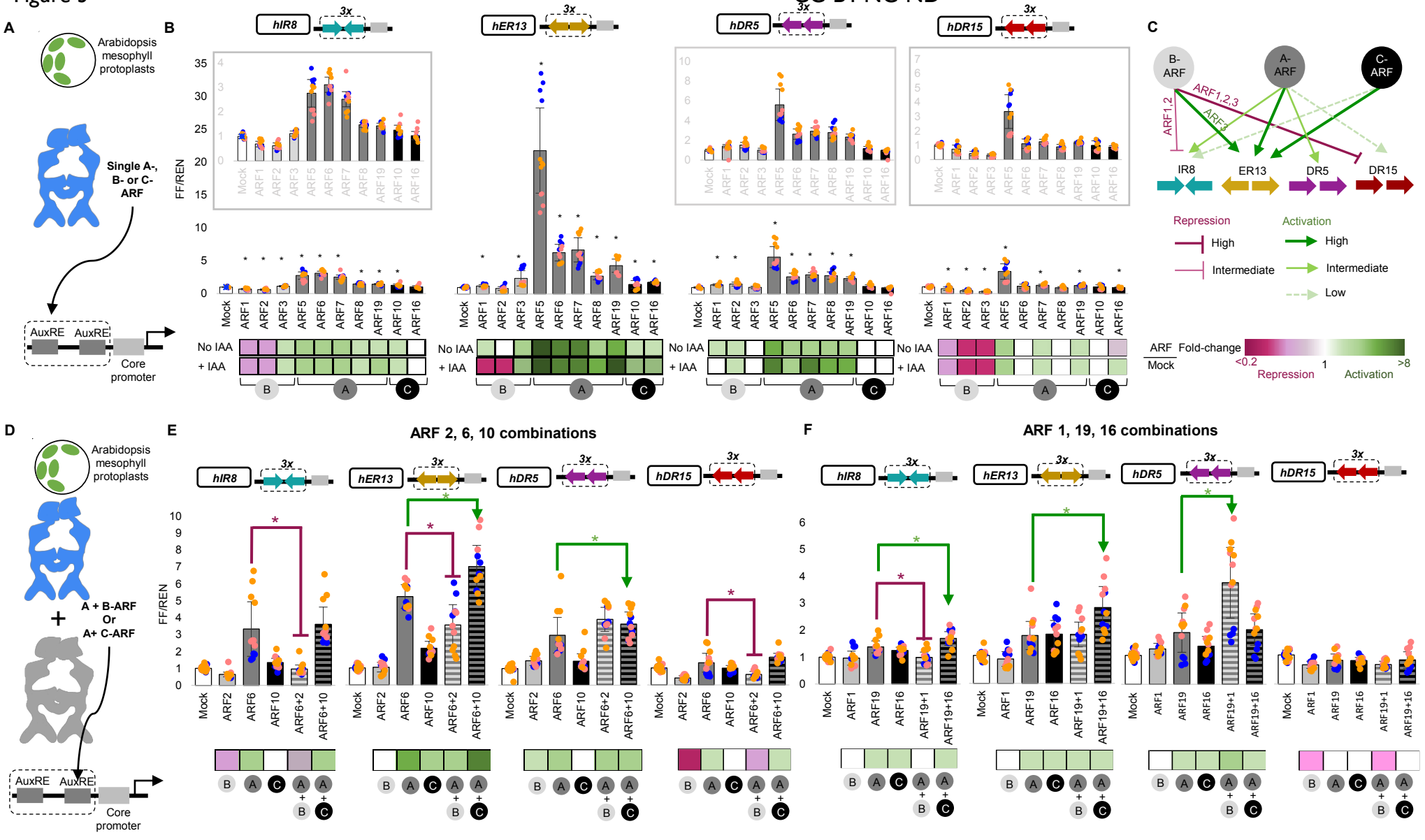

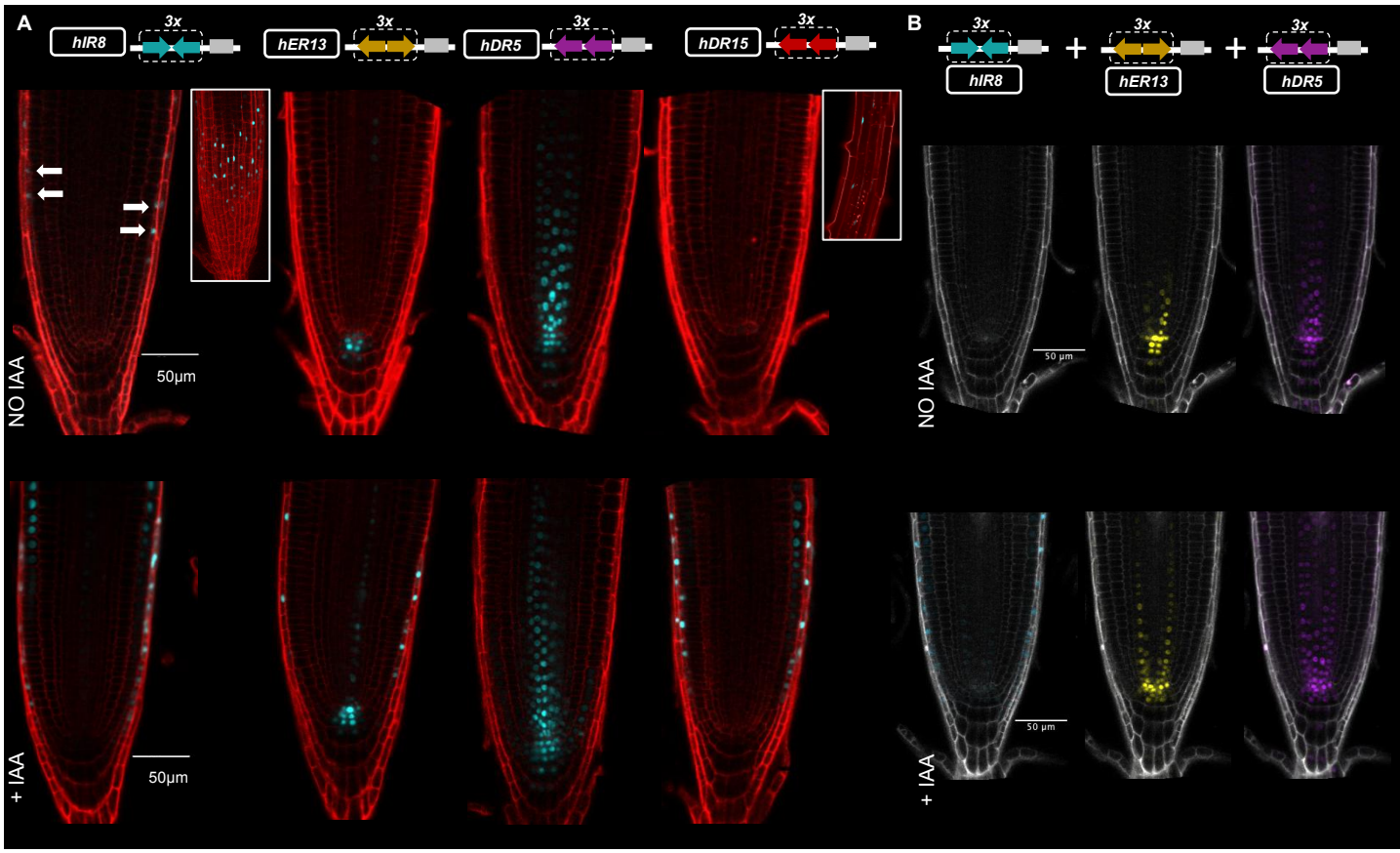

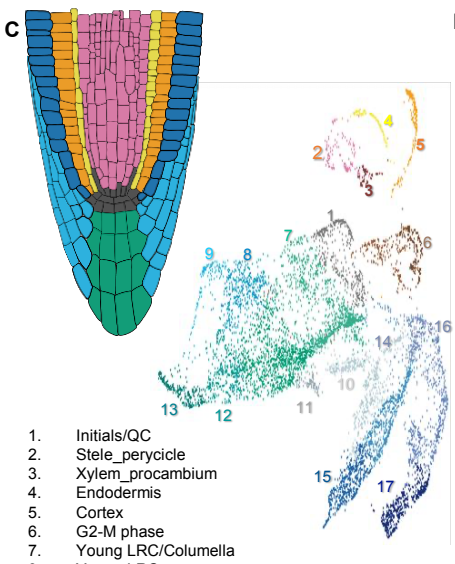

1. Initials/QC
2. Stele_pericycle
3. Xylem_procambium
4. Endodermis
5. Cortex
6. G2-M phase
7. Young LRC/Columella
8. Young LRC
9. LRC
10. Young epidermis
11. Young Columella/LRC
12. Young Columella
13. Columella
14. Young Atrichoblast
15. Atrichoblast
16. Young trichoblast
17. Trichoblast

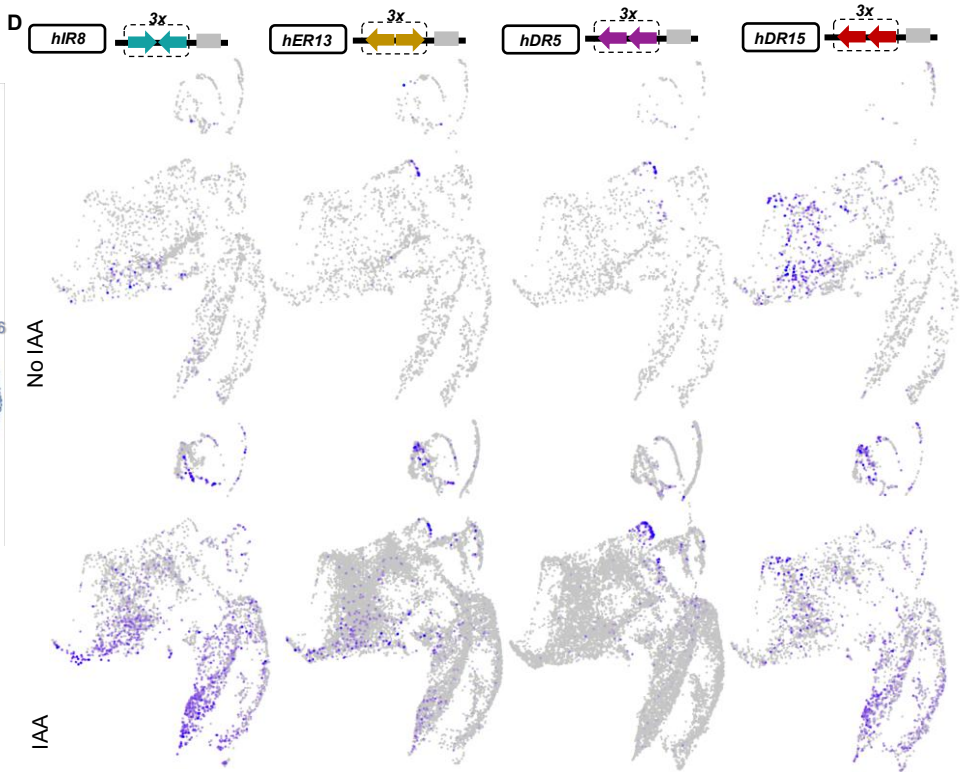

Figure 5

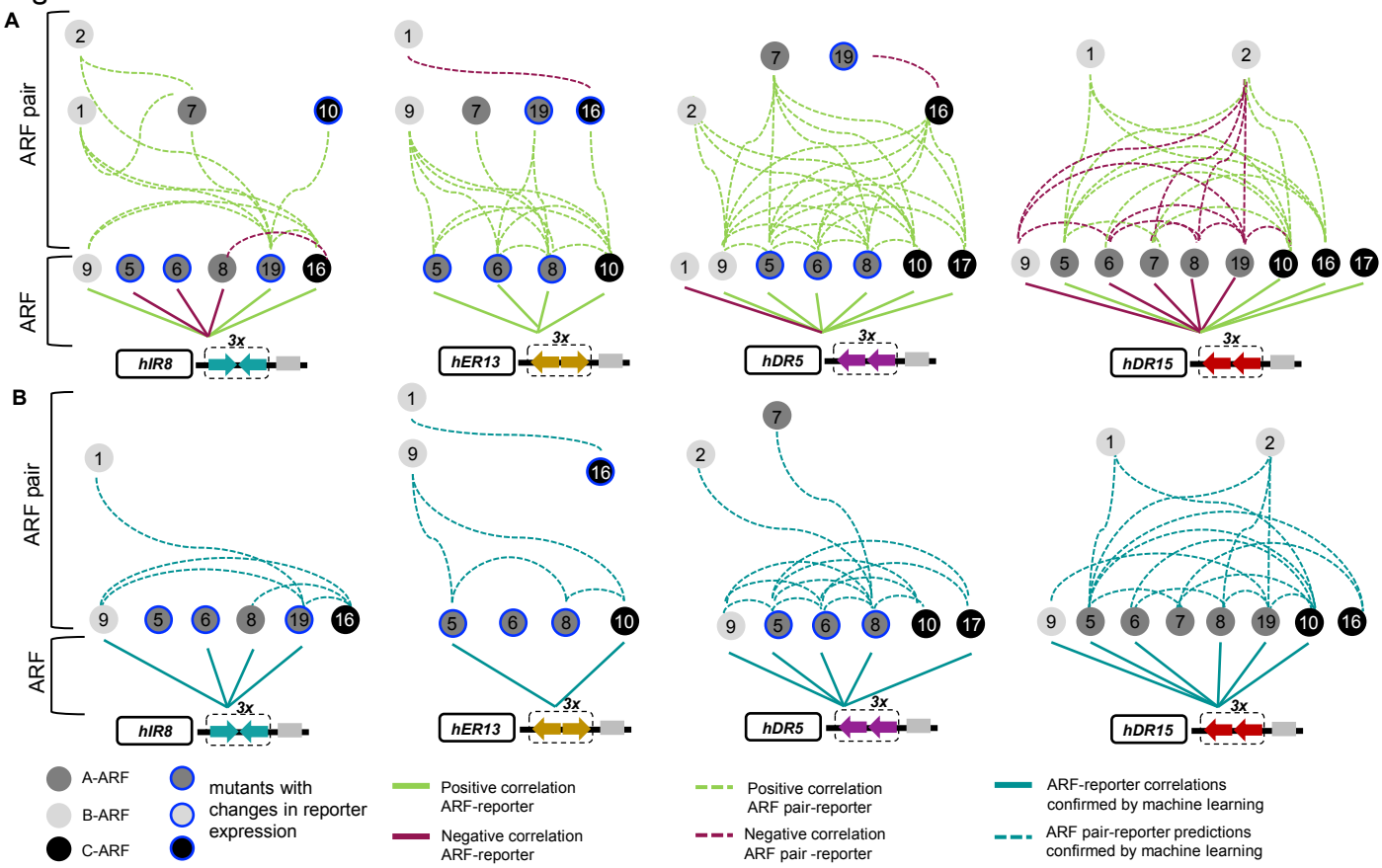

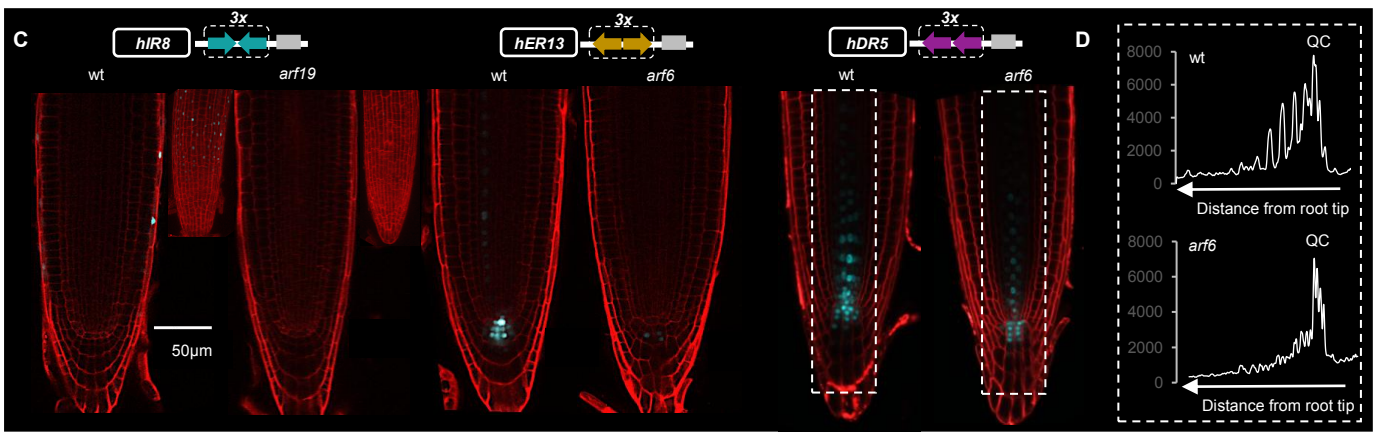

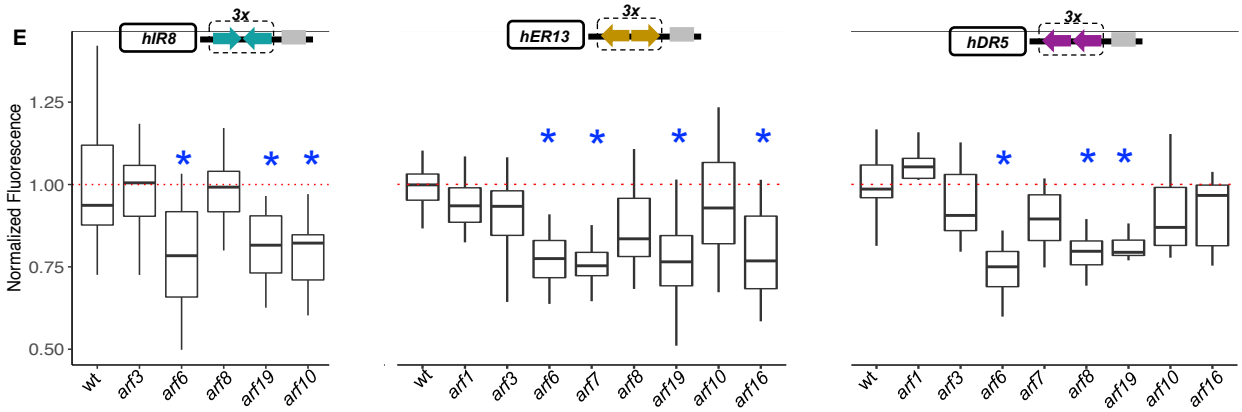

Figure 6

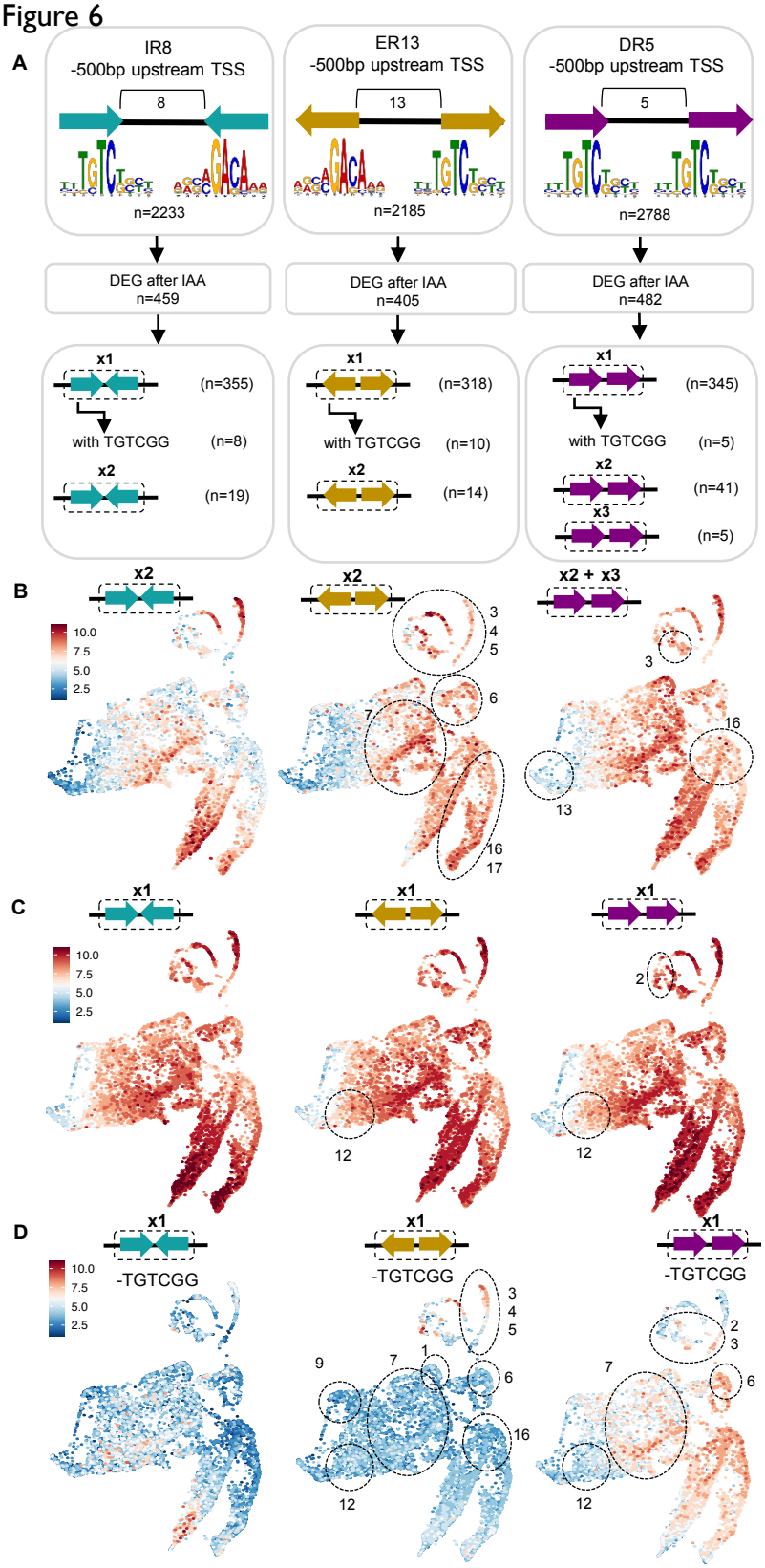

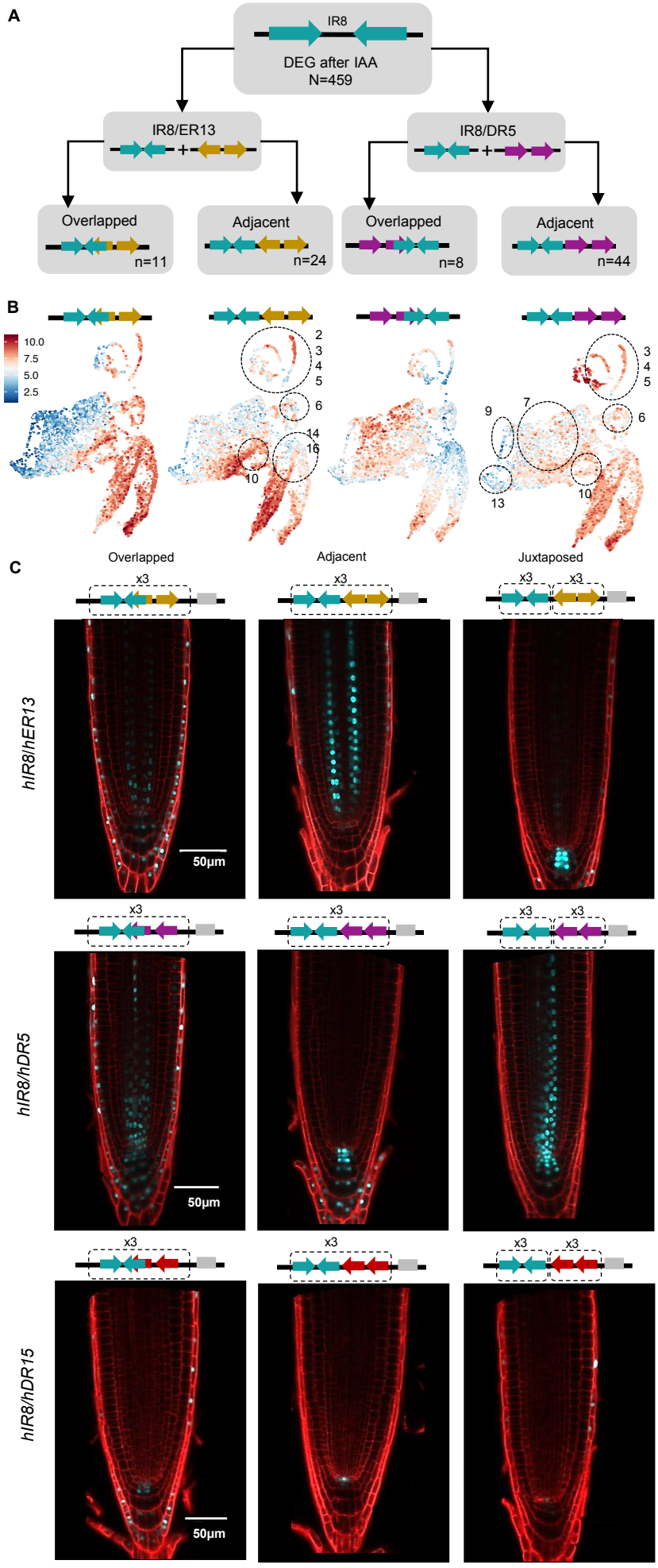
A
IR8
DEG after IAA
N=459
IR8/ER13
IR8/DR5
Overlapped
n=11
Adjacent
n=24
Overlapped
n=8
Adjacent
n=44
B
10.0
7.5
5.0
2.5
C
Overlapped
Adjacent
Juxtaposed
x3
hIR8/hER13
hIR8/hDR5
hIR8/hDR15
50µm

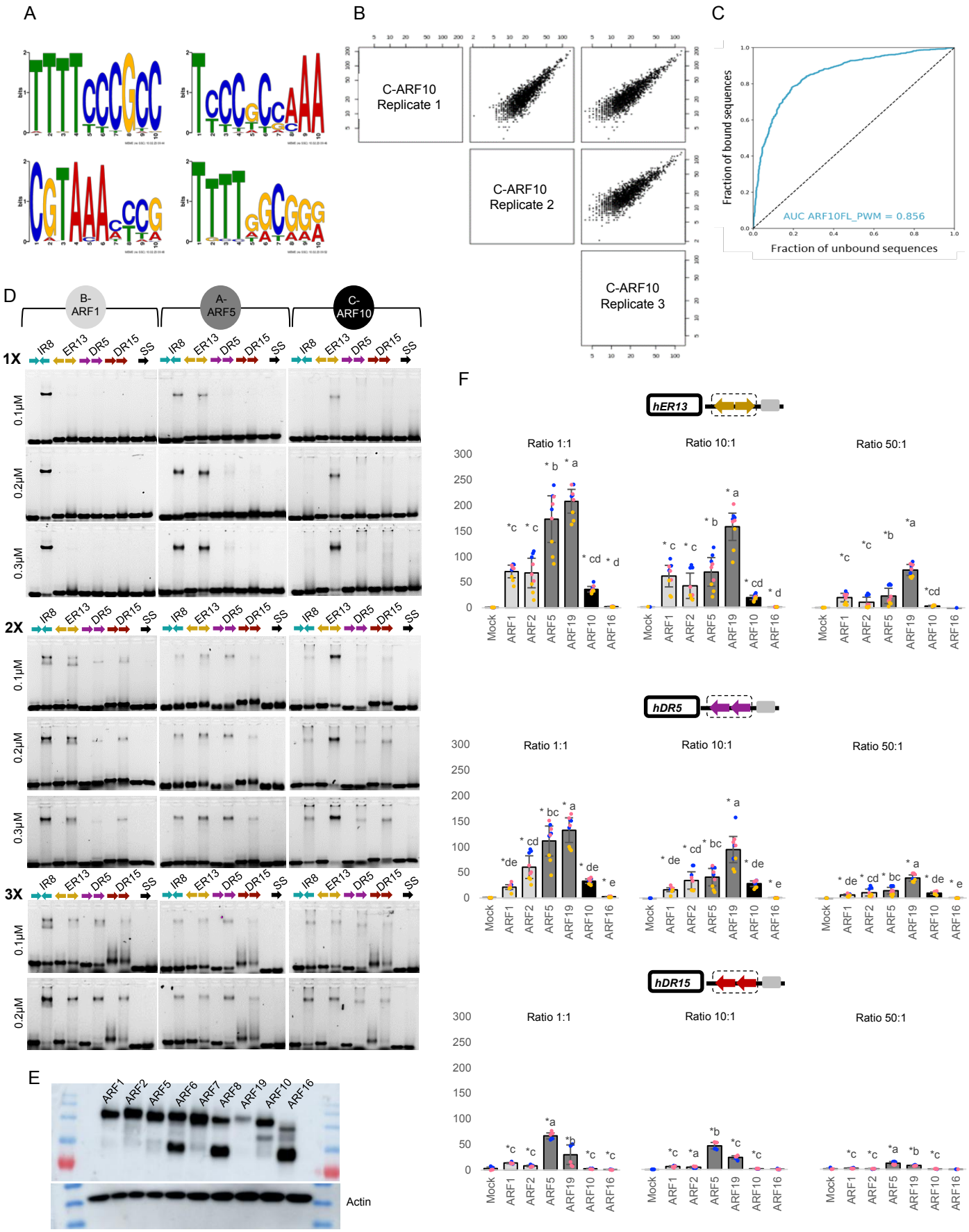

Supplemental Figure 1

Supplemental Figure 2

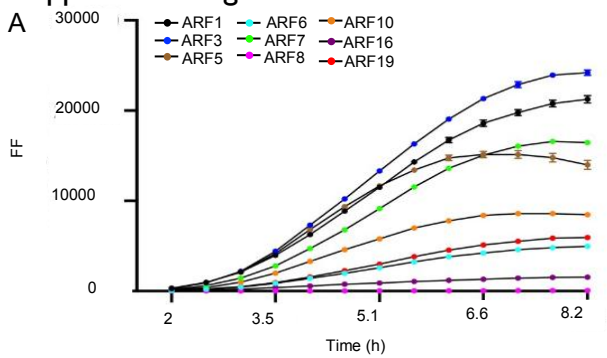

B

IAA/No IAA	Mock	ARF1	ARF2	ARF3	ARF5	ARF6	ARF7	ARF8	ARF19	ARF10	ARF16
hIR8											
hER13											
hDR5											
hDR15											

1 2 3 4 >5

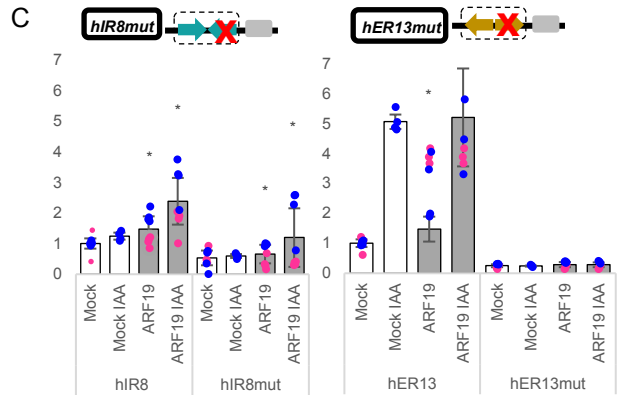

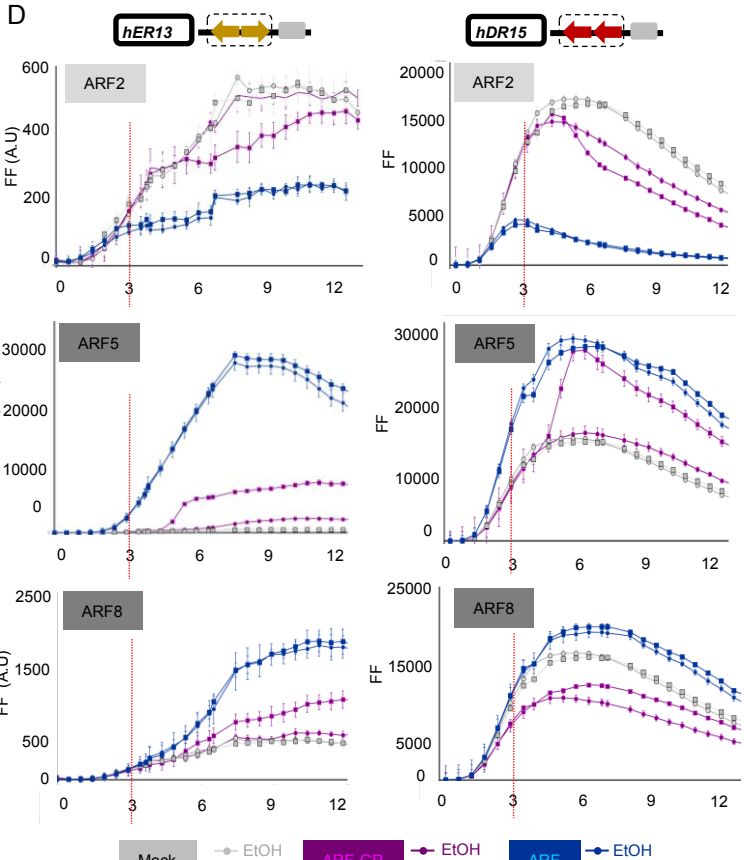

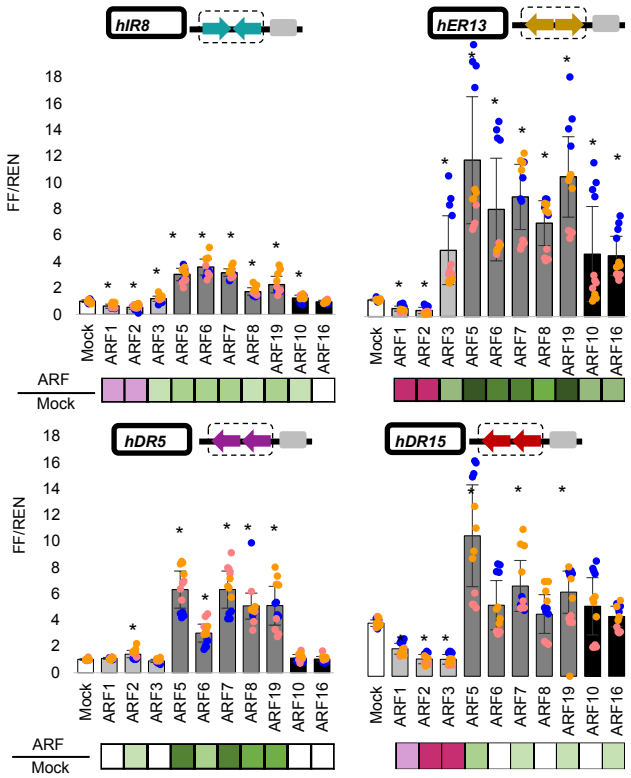

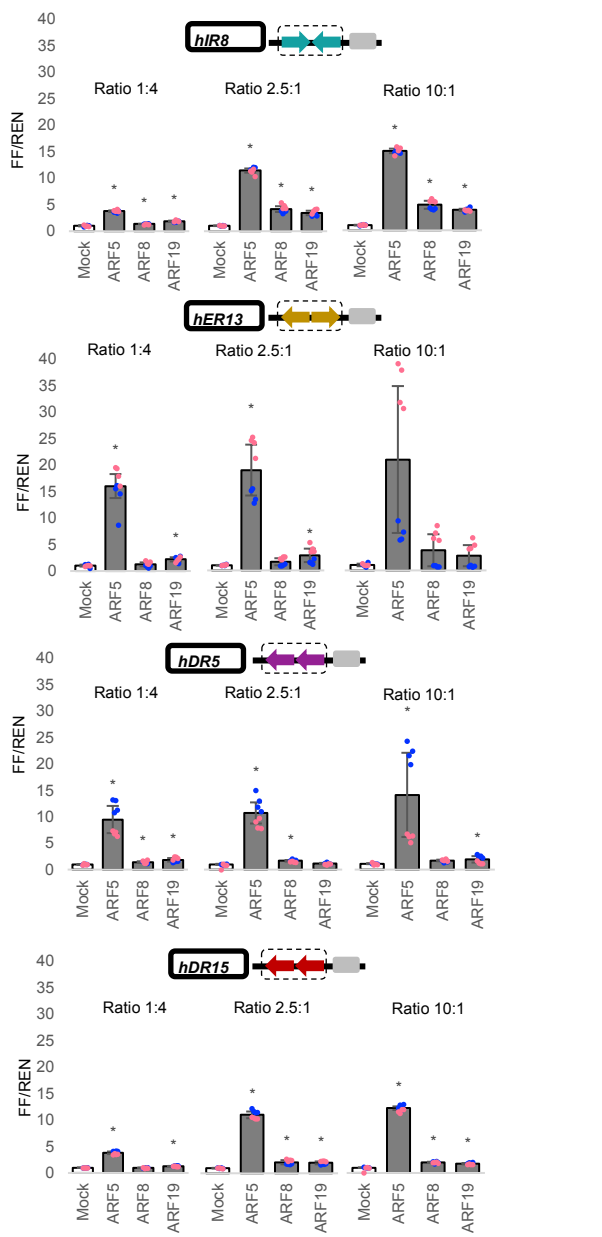

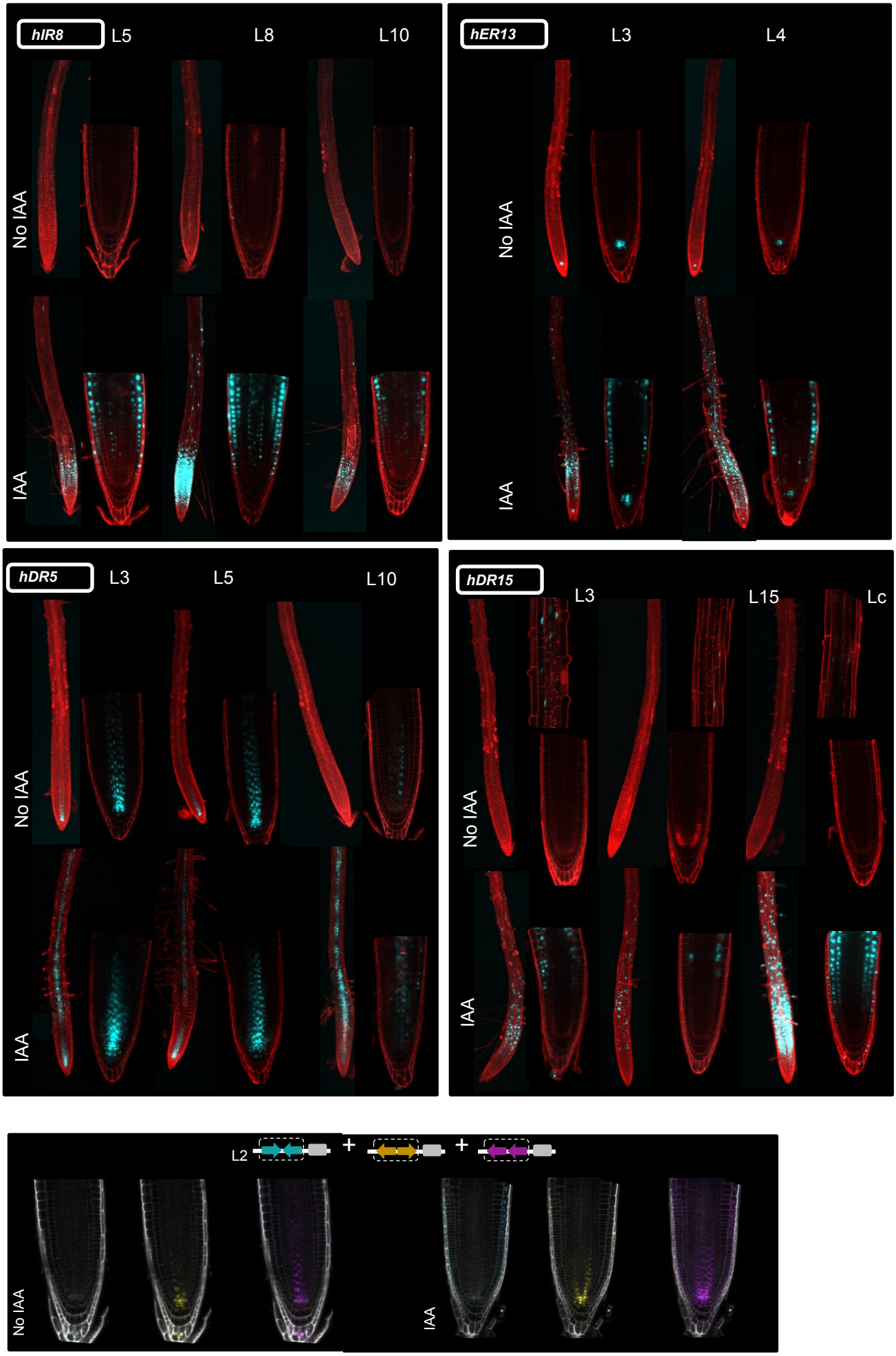

Supplemental Figure 3

Supplemental Figure 4

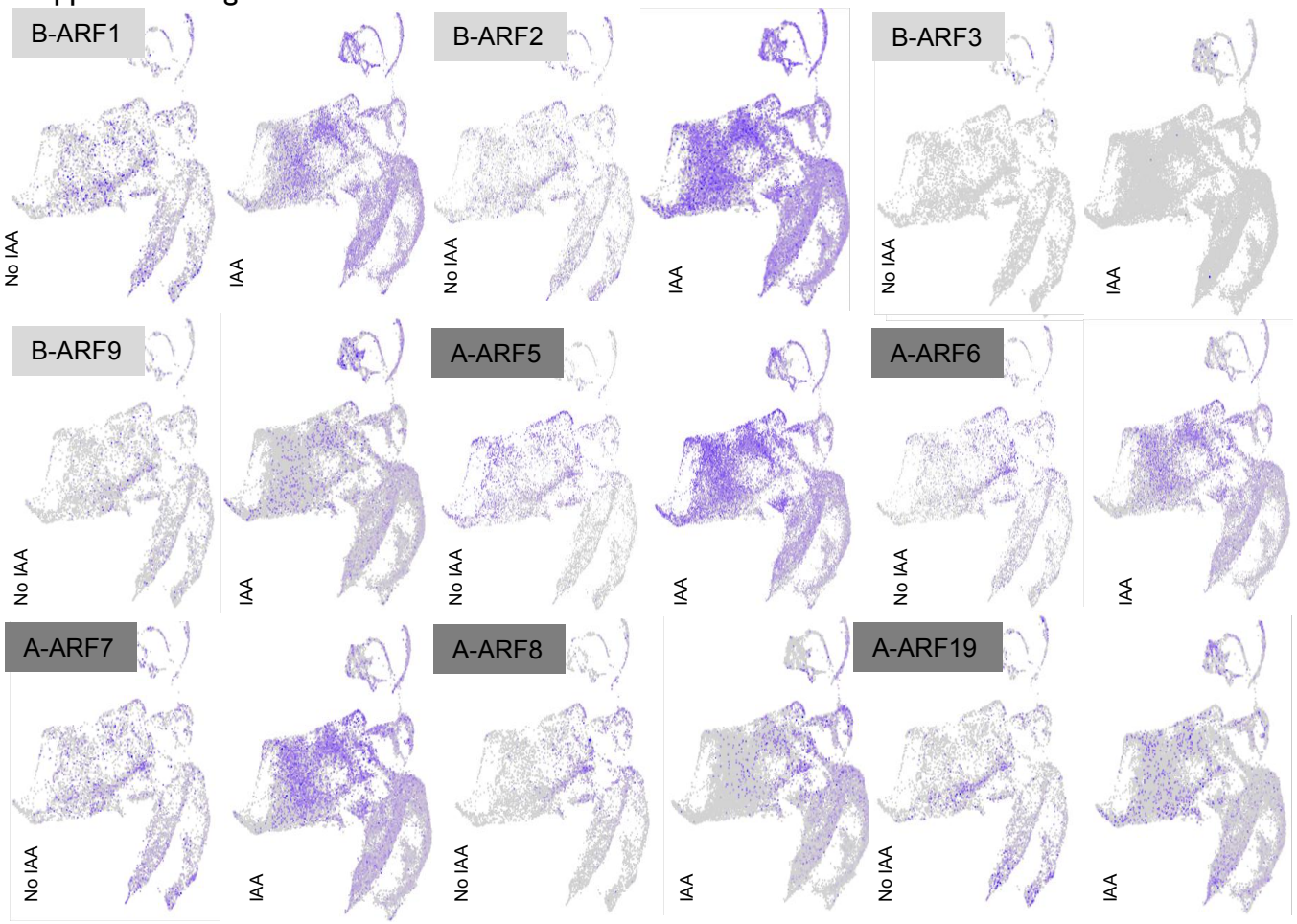

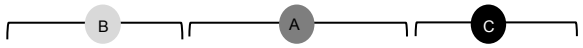

Cell type \ ARF	1	2	3	9	5	6	7	8	19	10	16	17
Atrichoblast												
Columella												
Cortex												
Endodermis												
G2_M_phase_1												
G2_M_phase_2												
Initials_Stele_QC												
LRC												
Stele_Pericycle												
Trichoblast												
Xylem_procambium												
Young_Atrichoblast_1												
Young_Columella_LRC_Histone												
Young_epidermis_Histone												
Young_LRC												
Young_LRC_Columella_1												
Young_LRC_Columella_2												
Young_Trichoblast_1												
Young_Trichoblast_2												

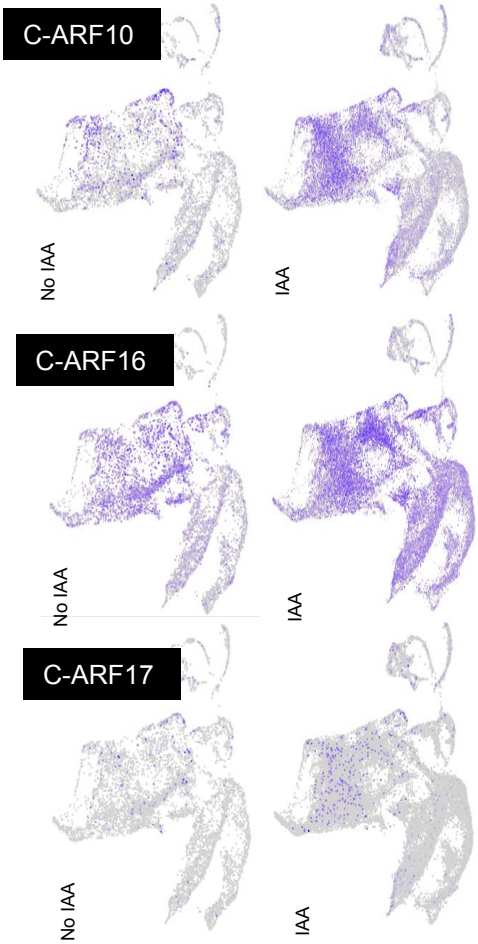

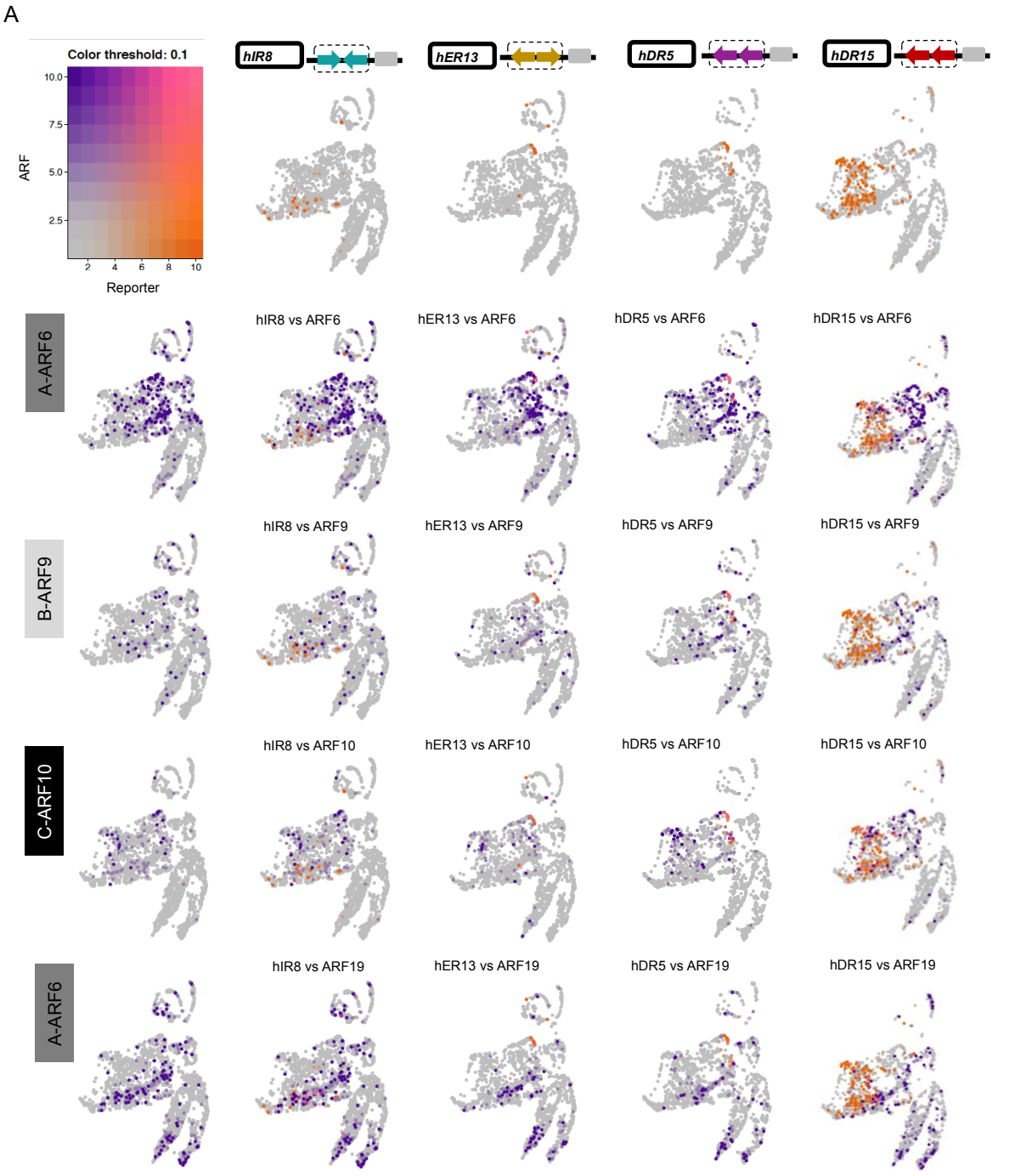
A
Color threshold: 0.1
ARF
Reporter
hIR8
hER13
hDR5
hDR15
A-ARF6
B-ARF9
C-ARF10
A-ARF6
hIR8 vs ARF6
hER13 vs ARF6
hDR5 vs ARF6
hDR15 vs ARF6
hIR8 vs ARF9
hER13 vs ARF9
hDR5 vs ARF9
hDR15 vs ARF9
hIR8 vs ARF10
hER13 vs ARF10
hDR5 vs ARF10
hDR15 vs ARF10
hIR8 vs ARF19
hER13 vs ARF19
hDR5 vs ARF19
hDR15 vs ARF19

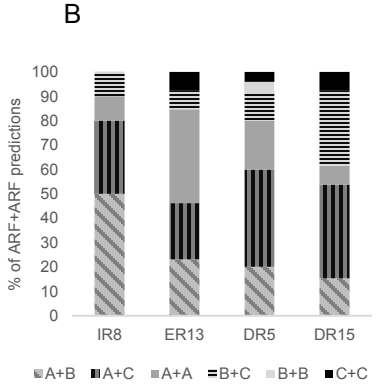
B
% of ARF+ARF predictions
IR8
ER13
DR5
DR15
A+B
A+C
A+A
B+C
B+B
C+C

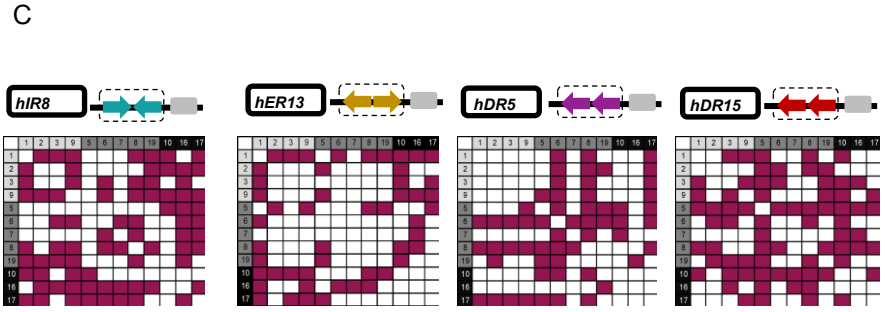
C
hIR8
hER13
hDR5
hDR15

Supplemental Figure 6

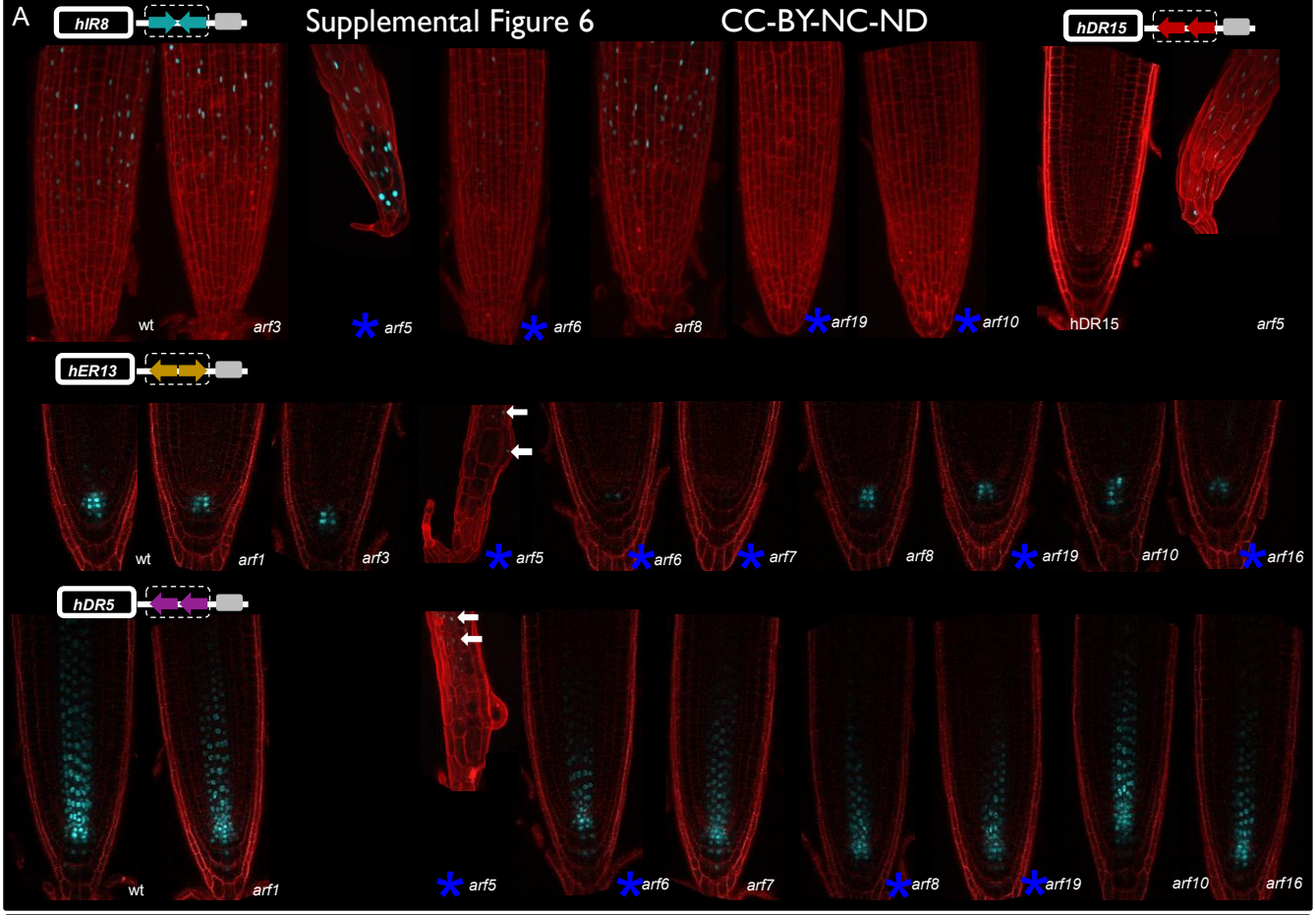

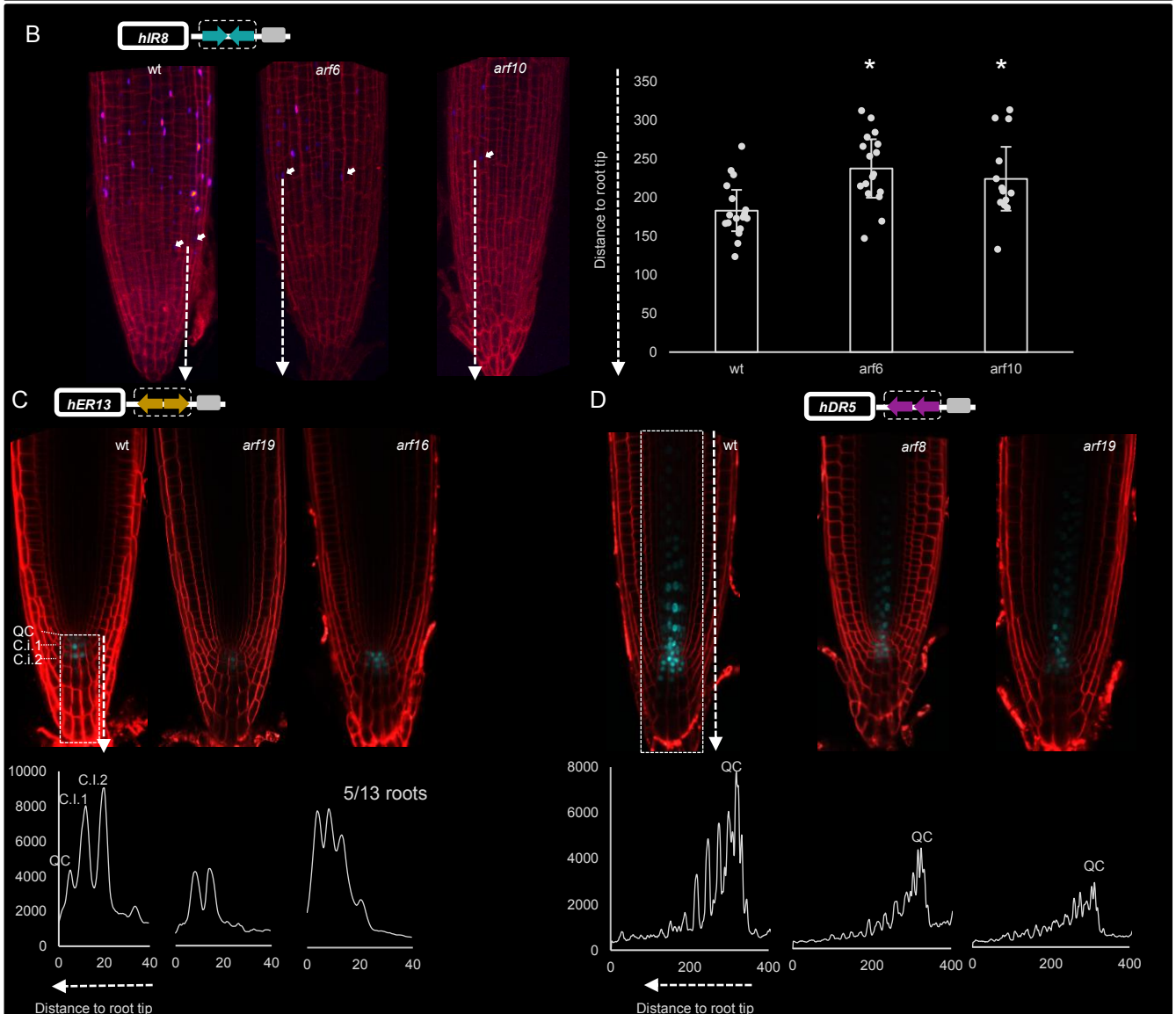

Supplemental Figure 7

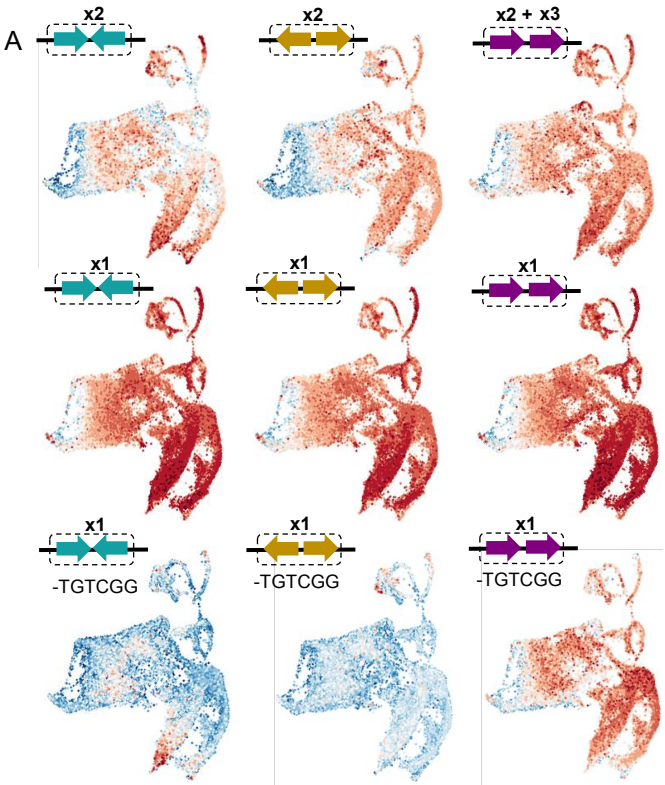

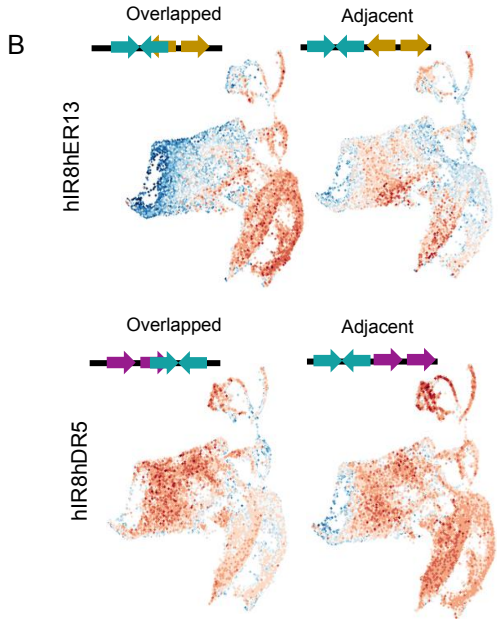

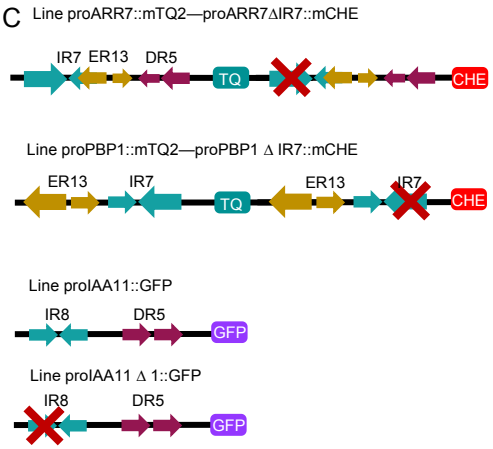

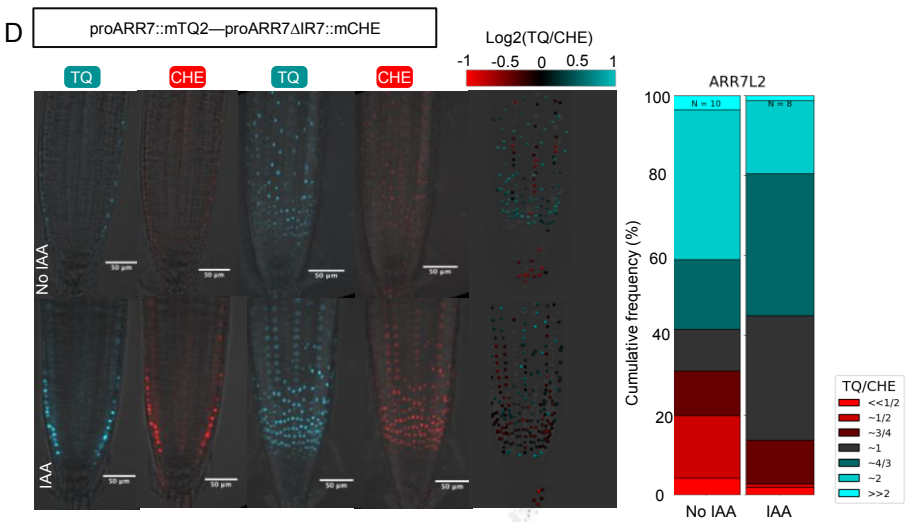

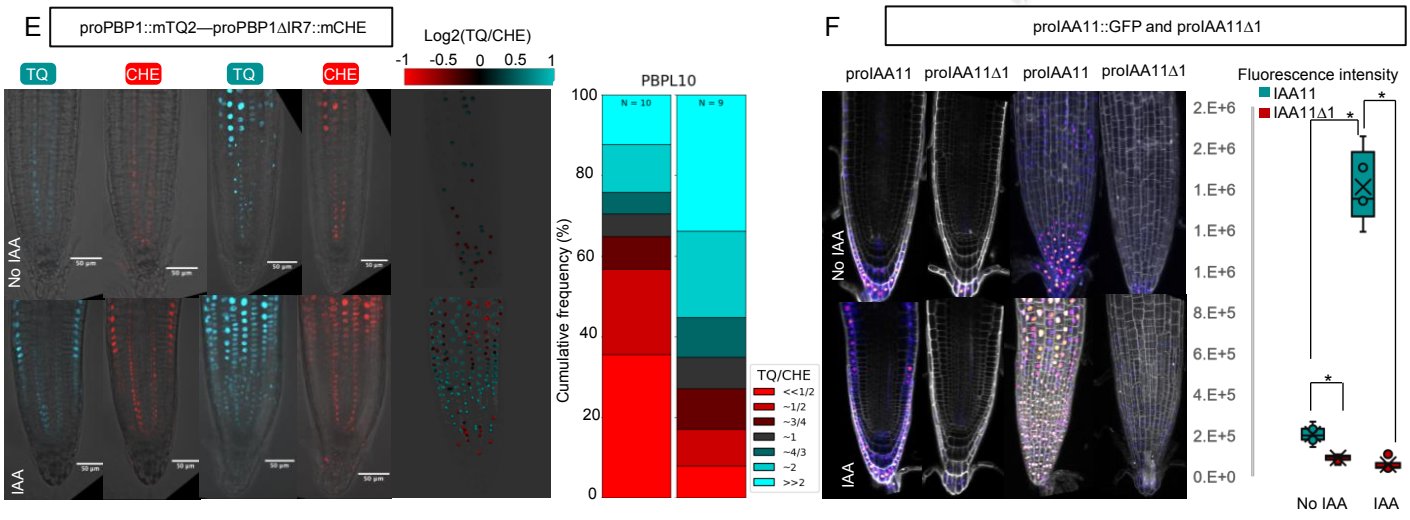

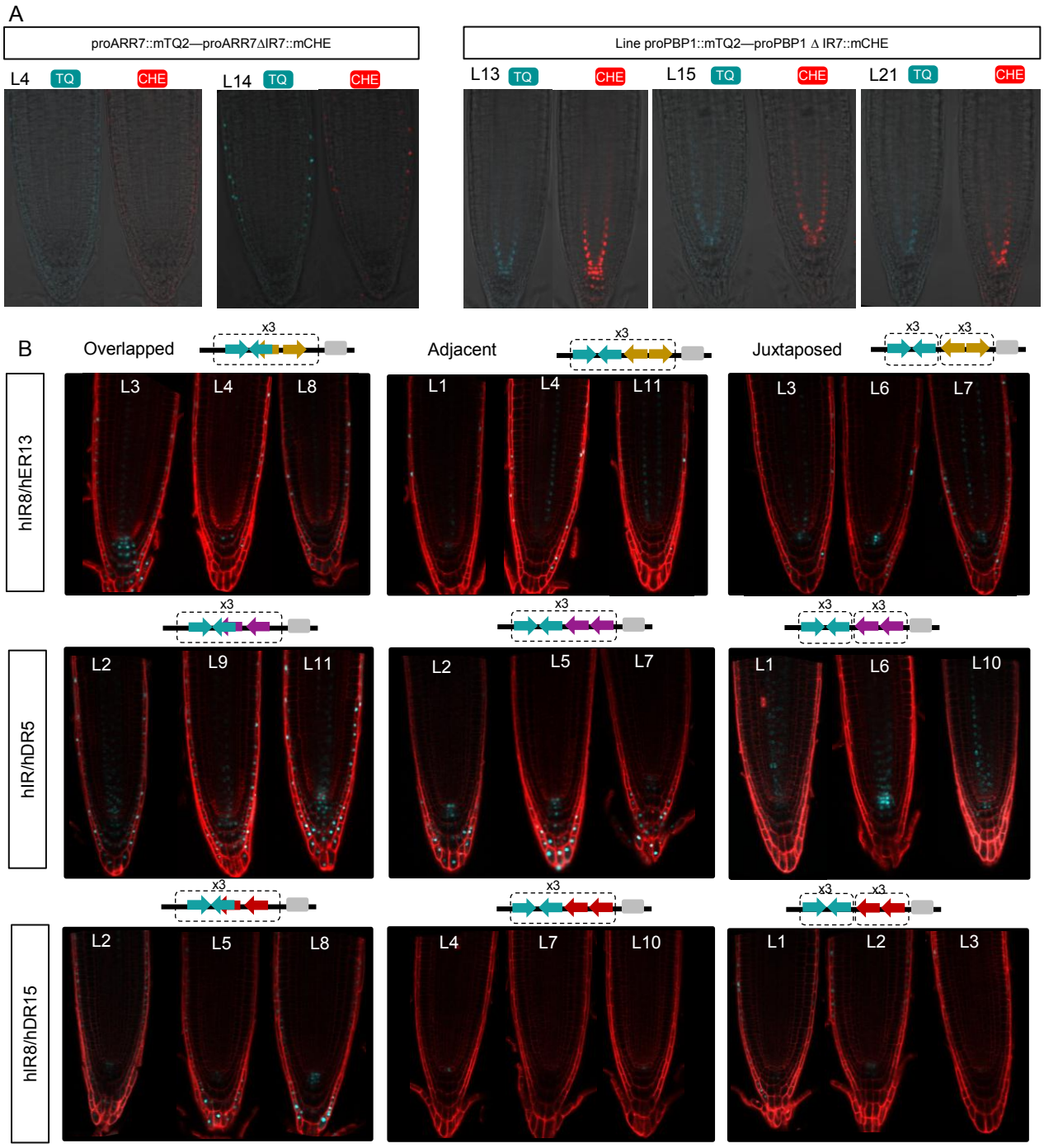
A
proARR7::mTQ2—proARR7ΔIR7::mCHE
Line proPBP1::mTQ2—proPBP1 Δ IR7::mCHE
L4 TQ CHE
L14 TQ CHE
L13 TQ CHE
L15 TQ CHE
L21 TQ CHE
B
Overlapped
Adjacent
Juxtaposed
x3
hIR8/hER13
L3 L4 L8
L1 L4 L11
L3 L6 L7
hIR/hDR5
L2 L9 L11
L2 L5 L7
L1 L6 L10
hIR8/hDR15
L2 L5 L8
L4 L7 L10
L1 L2 L3

Table S1. hIR8, hER13, hDR5 and hDR15 synthetic promoter sequences and binding sites predicted in each sequence, related to Figure 2

hIR8	GGGGACAACTTTGTATAGAAAAGTTGCCATGGACCGCTGTCGGTCATGTGACCGACAACCGCTGTCGGTCATGTGACCGACAACCGCTGTCGGTCATGTGACCGACATGCAA
hER13	GGGGACAACTTTGTATAGAAAAGTTGCCATGGACCGCCCGACAGCACCAAACTTACTGTCGGTGCCCGACAGCACCAAACTTACTGTCGGTGCCCGACAGCACCAAACTTACTGTCGGTGCAA
hDR5	GGGGACAACTTTGTATAGAAAAGTTGCCATGGACCGCCCGACAATTGACCGACAATTGACCGACAATTGACCGACAATTGACCGACAATTGACCGACATGCAA
hDR15	GGGGACAACTTTGTATAGAAAAGTTGCCATGGACCGCCCGACAATTGACAAATCTCAGCCGACAATTGACAAATCTCAGCCGACAATTGACAAATCTCAGCCGACAATTGACAAATCTCAGCCGACATGCAA

hIR8			
Predicted ARF binding sites (AuxRE pairs)			
	Spacing	Score1	Score2
DR	20	-11	-5
ER	16	-11	-5
DR	19	-5	-5
IR	8	-5	-3
DR	19	-3	-3
Er	5	-3	-5
DR	19	-5	-5
IR	8	-5	-3
DR	19	-3	-3
Er	5	-3	-5
IR	8	-5	-3
DR	11	-3	-10
ER	7	-10	-11
IR	20	-11	-11
MEME detection of other TF binding sites			
TF	Sequence	Score	
----	----	----	

hER13			
Predicted ARF binding sites (AuxRE pairs)			
	Spacing	Score1	Score2
IR	20	-11	-3
DR	16	-11	-3
ER	13	-3	-3
IR	3	-3	-3
ER	13	-3	-3
IR	3	-3	-3
ER	13	-3	-3
IR	11	-3	-10
ER	7	-10	-11
IR	20	-11	-11
MEME detection of other TF binding sites			
TF	Sequence	Score	
LFY	CATGGACCGCCCGACAATT	-10.952697385303955	

hDR5			
Predicted ARF binding sites (AuxRE pairs)			
	Spacing	Score1	Score2
IR	20	-11	-2
DR	16	-11	-2
DR	5	-2	-2
DR	16	-2	-2
DR	5	-2	-2
DR	16	-2	-2
DR	5	-2	-2
DR	16	-2	-2
DR	5	-2	-2
DR	16	-2	-3

DR	5	-2	-3
DR	11	-3	-10
ER	7	-10	-11
IR	20	-11	-11
MEME detection of other TF binding sites			
TF	Sequence	Score	
LFY	CATGGACCGCCCGACAATT	-10.952697385303955	
hDR15			
Predicted ARF binding sites (AuxRE pairs)			
	Spacing	Score1	Score2
IR	20	-11	-2
DR	16	-11	-2
DR	1	-2	-8
DR	15	-2	-2
DR	8	-8	-2
DR	15	-8	-8
DR	1	-2	-8
DR	15	-2	-2
DR	8	-8	-2
DR	15	-8	-8
DR	1	-2	-8
DR	15	-2	-2
DR	8	-8	-2
DR	15	-8	-8
DR	1	-2	-8
DR	15	-2	-2
DR	8	-8	-2
DR	15	-8	-8
DR	1	-2	-8
DR	15	-2	-3
DR	8	-8	-3
DR	11	-3	-10
ER	7	-10	-11
IR	20	-11	-11
MEME detection of other TF binding sites			
TF	Sequence	Score	
LFY	CATGGACCGCCCGACAATT	-10.952697385303955	

All sequences were ordered as synthetic DNA (Thermofisher). TGTCGG sequences in forward or reverse are indicated in blue. The synthetic promoters included these sequences followed by CMV or 35S minimal promoters for CHO-K1, or protoplast and *in planta* experiments, respectively. For each sequence we verified the presence of IR8, ER13, DR5 or DR15 repeats and of other potential transcription factor binding sites (see methods). ARF binding sites predictions provide the orientation of the two AuxREs (ER, IR or DR), the number of nucleotides in between (spacing) and the score of each AuxRE (Score 1 and score 2). IR8, ER13, DR5 and DR15 repeats are shown in blue. Sequences were optimized to avoid the presence of other AuxREs pairs with high scores (the closest to zero the higher the score is) and/or preferentially bound by ARFs according to DAP-seq data. Although other AuxRE pairs and binding sites for LEAFY transcription factor were predicted to be present in the synthetic promoter sequences, the scores for these other sites are much lower than for IR8, ER13, DR5 and DR15 sites.

Table S5. Combined synthetic promoter sequences, related to Figure 7

hIR8 hER13 Overlapped	GGGGACAACTTTGTATAGAAAAGTTGCCATGGACCGCTGTCGGTCATGTGACCGACAACCGCTAACTTACTGTCGGTGCACCGCTGTCGGTCATGTGACCGACAACCGCTAACTTACTGTCGGTCATGTGATGTCGGTCATGTGACCGACAACCGCTAACTTACTGTCGGTCAT
hIR8 hER13 Separated	GGGGACAACTTTGTATAGAAAAGTTGCCATGGACCGCTGTCGGTCATGTGACCGACAACCGCTGCCCGACAGCACCAAACTTACTGTCGGTGCACCGCTGTCGGTCATGTGACCGACAACCGCTGCCCGACAGCACCAAACTTACTGTCGGTGCACCGCTGTCGGTCATGTGACCGACAACCGCTGCCCGACAGCACCAAACTTACTGTCGGTGCA
hIR8 hER13 Juxtaposed	GGGGACAACTTTGTATAGAAAAGTTGCCATGGACCGCTGTCGGTCATGTGACCGACAACCGCTGTCGGTCATGTGACCGACAACCGCTGTCGGTCATGTGACCGACATGCAATGCCCGACAGCACCAAACTTACTGTCGGTGCCCGACAGCACCAAACTTACTGTCGGTGCCCGACAGCACCAAACTTACTGTCGGTGCAA
hIR8 hDR5 Overlapped	GGGGACAACTTTGTATAGAAAAGTTGCCATGGACCGCTGTCGGTCATGTGACCGACAATTGACCGACAATTGCCGCTGTCGGTCATGTGACCGACAATTGACCGACAATTGCCGCTGTCGGTCATGTGACCGACAATTGACCGACAATTGCCGC
hIR8 hDR5 Separated	GGGGACAACTTTGTATAGAAAAGTTGCCATGGACCGCTGTCGGTCATGTGACCGACAACCGCCGCCCGACAATTGACCGACAATTGCCGCTGTCGGTCATGTGACCGACAACCGCCGCCCGACAATTGACCGACAATTGCCGCTGTCGGTCATGTGACCGACAATTGACCGACAATTG
hIR8 hDR5 Juxtaposed	GGGGACAACTTTGTATAGAAAAGTTGCCATGGACCGCTGTCGGTCATGTGACCGACAACCGCTGTCGGTCATGTGACCGACAACCGCTGTCGGTCATGTGACCGACATGCAAcaggCCGACAATTGACCGACAATTGACCGACAATTGACCGACAATTGACCGACAATTGACCGACATGCAA
hIR8 hDR15 Overlapped	GGGGACAACTTTGTATAGAAAAGTTGCCATGGACCGCTGTCGGTCATGTGACCGACAATTGACAAATCTCAGCCGACAACAATCCGCTGTCGGTCATGTGACCGACAATTGACAAATCTCAGCCGACAACCATCCGCTGTCGGTCATGTGACCGACAATTGACAAATCTCAGCCGGACAATAGGTCGC
hIR8 hDR15 Separated	GGGGACAACTTTGTATAGAAAAGTTGCCATGGACCGCTGTCGGTCATGTGACCGACAACCGCCGCCCGACAATTGACAAATCTCAGCCGACAATTGACCGCTGTCGGTCATGTGACCGACAACCGCCGCCCGACAATTGACAAATCTCAGCCGACAATTGACCGCTGTCGGTCATGTGACCGACAACCGCCGCCCGACAATTGACAAATCTCAGCCGACAATTGA
hIR8 hDR15 Juxtaposed	GGGGACAACTTTGTATAGAAAAGTTGCCATGGACCGCTGTCGGTCATGTGACCGACAACCGCTGTCGGTCATGTGACCGACAACCGCTGTCGGTCATGTGACCGACATGCAAcattggCCGACAATTGACAAATCTCAGCCGACAATTGACAAATCTCAGCCGACAATTGACAAATCTCAGCCGACAATTGACAAATCTCAGCCGACAATTGACAAATCTCAGCCGACATGCAA